FINDING FREE PRECESSION IN PULSARS

A thesis submitted to the University of Manchester
for the degree of Master of Science
in the Faculty of Engineering and Physical Sciences

March 2006

By

Iain McDonald

Jodrell Bank Observatory

School of Physics and Astronomy

Contents

List of Tables

List of Figures

Abstract

Evidence for precession has been put forward in the case of the pulsar PSR B1828–11 by Stairs et al. (2000). However, despite some evidence for precession in, for example, B1642–03, the Crab pulsar and Her X–1, there has been no other *clear-cut* evidence of precession in other pulsars.

In this thesis, a study into pulse shape changes characteristic of precession in a number of pulsars is performed, using the Jodrell Bank profile database. This is done using two techniques: a Lomb-Scargle periodogram and a Principal Component Analysis. An attempt was made to link pulsars exhibiting possible periodic shape changes with periodicities in their timing residuals.

We have confirmed precession in B1828–11 and also present a few further interesting candidates have been identified from this study, namely B0740–28, B0144+59, B0329+54.

Declaration

The author developed the computer model from initial FORTRAN routines written by Michael Kramer, and from subroutines available in *Numerical Recipes* (Press et al. 1989). Diagrams throughout this thesis have been made using Serif Drawplus, PGPLOT and GnuPlot. No portion of the work referred to in this thesis has been submitted in support of an application for another degree or qualification of this or any other university or other institution of learning.

Iain McDonald
School of Physics and Astronomy
University of Manchester
Jodrell Bank Observatory
Macclesfield
Cheshire
SK11 9DL
U.K.

September 2005

Copyright

Copyright in text of this thesis rests with the Author. Copies (by any process) either in full, or of extracts, may be made only in accordance with instructions given by the Author and lodged in the John Rylands University Library of Manchester. Details may be obtained from the Librarian. This page must form part of any such copies made. Further copies (by any process) of copies made in accordance with such instructions may not be made without the permission (in writing) of the Author.

The ownership of any intellectual property rights which may be described in this thesis is vested in the University of Manchester, subject to any prior agreement to the contrary, and may not be made available for use by third parties without the written permission of the University, which will prescribe the terms and conditions of any such agreement.

Further information on the conditions under which disclosures and exploitation may take place is available from the head of the School of Physics and Astronomy.

The Author

The author obtained a M. Sci (Hons) degree in Astrophysics at the University of St. Andrews, graduating in 2004. In September of that year he began studying for an M. Sc. at Jodrell Bank Observatory, University of Manchester. The results of this work are presented in this thesis.

> *The number is certainly the cause. The apparent disorder augments the grandeur, for the appearance of care is highly contrary to our ideas of magnificence. Besides, the stars lie in such apparent confusion, as makes it impossible on ordinary occasion to reckon them. This gives them the advantage of a sort of infinity.*
>
> — Edmund Burke, On the Sublime and the Beautiful–Magnificence

> *Quod est ante pedes nemo spectat: coeli scrutantur plagas.*
>
> *No one sees what is before his feet: we all gaze at the stars.*
>
> — Marcus Tullius Cicero, De Divinatione (II, 13)

> *You must carry a chaos inside you to give birth to a dancing star.*
>
> — Nietzsche

Acknowledgements

I would like to thank Dr. Michael Kramer for his many efforts as a supervisor, making my job and this thesis both a lot easier and better in the process; for literally going to the ends of the Earth for the cause (and thankfully coming back again). I would also like to thank Dr. Neal Jackson for his sage advice, for helping me in and out of this course and for giving me good exam results; Prof. Andrew Lyne for use of the facilities here, and his input into my project; and Dr. George Hobbs for his timing solutions. My thanks also go out to Chris Jordan for helping me out of many a technical fuddle; Ant and Bev for computer support; and numerous visiting speakers for entertaining lectures and, more importantly, free dinners.

This thesis would also never have been completed without my fellow students, both in and out of the (Missing) Link Room — Dave, Dan, Jennie, Richard, Sarah, Hannah, Alex, Danielle, everyone at Cheshire Hunt and everyone else I don't have space to mention — for keeping my insanity at a healthy level, and to my girlfriend Genny for successfully reversing that trend. Finally, I wish to thank Virgin Trains, ScotRail, National Express and everyone who's ever given me a lift to Goostrey Station for helping make being south of the Border bearable.

Conventions and Abbreviations

The conventional abbreviations for SI units and astronomical quantities are used.

The following abbreviations have been used in this thesis:

ATNF — Australia Telescope National Facility

DM — Dispersion Measure

EPN — European Pulsar Network (and associated file type)

FFT — Fast Fourier Transform

FWHM — full-width half-maximum

MJD — Modified Julian Date

PCA — Principal Component Analysis

PSR — Pulsar

residual — residual profile: a profile with a template subtracted from it

RFI — radio frequency interference: real signal from sources other than the target

RM — Rotation Measure

r.m.s. — root mean square

Chapter 1

Introduction: Pulsars and their Emission Mechanism

1.1 Discovery of Pulsars

1.1.1 Early History

Our view of pulsars, or "pulsating radio sources", today is a result of several decades of theory and observations. We now accept that the pulses we see are beamed emission from rapidly rotating, highly magnetised neutron stars.

Baade & Zwicky (1934), first proposed that in the case of a core-collapse supernova, the stellar interior could collapse into a star "*consisting mainly of neutrons*". Detection of these stars was then thought to be almost impossible, as they would be small and not very luminescent.

Oppenheimer & Volkoff (1939) later calculated that they could have densities of 10^{14} g cm^{-3}, magnetic fields up to 10^{12} Gauss and a mass comparable to that of the Sun, yet only be a few tens of kilometres across. Even now, this is beyond anything we can create in the laboratory, hence these stars have particular scientific interest.

1.1.2 Early X-ray Observations

Despite earlier predictions they would be invisible, in 1964 two papers by Zel'dovich & Guseynov (1964), and Hayakawa & Matsouka (1964) proposed that accreting compact objects, such as neutron stars, could produce X-ray emission from their accreted 'atmospheres'.

Early X-ray observations from rocket flights found X-ray sources from the Crab Nebula, now known to harbour a pulsar; and from the source Sco X-1 (Giacconi et al. 1962), which found to have a spectrum consistent with a binary system undergoing mass loss. Since this, a number of other pulsars have been discovered with X-ray emission.

1.1.3 The Radio Discovery

Although intrinsically radio-bright sources, pulsars were not identified until 1967. This can largely be attributed to the fact that pulsar emission, at first glance, looks remarkably like interference from artificial sources. Fast sampling and repeated observations were needed to find what no-one expected — that rapidly pulsing emission was coming from a celestial source.

This discovery famously goes to Jocelyn Bell, a research student working with Antony Hewish, investigating interplanetary radio scintillation.

The pulsar, PSR 1919+21 was identified to be an extraterrestrial source due to lack of parallactic motion. Soon, three more sources were discovered. Several theories were put forward, one of which was that the pulses came from 'little green men'. Nevertheless, six months after the initial observations, a paper was published in Nature (Hewish et al. 1968) stating:

> "A tentative explanation of these unusual sources in terms of the stable oscillations of white dwarf or neutron stars is proposed."

Indeed, the pulses are remarkably stable. Precision measurements can determine periods to an accuracy of less than one part in 10^{15} (Davis et al. 1985, Kaspi 1995)

1.1.4 Linking Pulses with Neutron Stars

The connection with the observations came in the June following Hewish et al.'s announcement, in two *Nature* papers by Gold (1968) and Pacini (1968).

This is not to say that there were no other theories regarding the origin of the pulses. Prominently, theories were put forward involving emission from rotation or oscillation of white dwarfs (e.g. Ostriker & Tassoul 1968, Durney et al. 1968 and Lawrence et al. 1967).

Melzer & Thorne (1966) had showed that a rotating or pulsating white dwarf could account for pulses on a timescale of around a second, which would account for PSR 1919+21. They also found that oscillations in a neutron star would have timescales on the order of milliseconds. The discovery of the Vela (Large et al. 1968) and Crab (Staelin & Reifenstein 1968) pulsars, with periods of 89 and 33 milliseconds, respectively, proved white dwarf and oscillation theories incorrect. When combined with the discovery that the period between pulses was increasing, the logical interpretation was that the pulses were coming from rotating neutron stars.

1.2 Pulsar Formation

1.2.1 The Stellar Life Cycle and Supernovae

Young, main-sequence stars maintain their stability against gravity via the radiation pressure produced by fusing hydrogen nuclei into helium. Once the hydrogen in the core is used up, high- and intermediate-mass stars begin to fuse helium

nuclei in their cores, and hydrogen nuclei in a surrounding shell. Sufficiently high mass stars (around eight solar masses) can go on to fuse successively heavier elements, which maintain the star's stability for successively shorter periods of time. During this time, the outer atmosphere of the star expands and is gradually blown away as the star expands to become a red giant star, eventually forming a nebula around the star.

This process can continue until the star attempts to fuse iron atoms into heavier elements. At this point, more energy is required to fuse the nuclei than is obtained from the fusion process. Here, pressure support is lost and the stellar core collapses (e.g. Burrows & Lattimer 1986). The rebound wave from this produces a shock front, the emission from which is observed as a supernova. The atmospheric material from this star interacts with the inter-stellar medium (ISM), which both continue to emit radiation for many thousands of years. We see this as a supernova remnant (SNR).

1.2.2 The Birth of a Neutron Star

The core of the star continues to collapse towards the electron degeneracy limit. In white dwarfs, pressure support is restored at this point. However, in more massive stars, there is sufficient gravitational pressure to fuse electrons with and protons with the result that the star ends up composed almost entirely of neutrons, surrounded by a thin crust of heavy nuclei.

During this collapse, the angular momentum of the stellar interior is conserved, with the result that a stellar core that had been revolving on a timescale of days now revolves on a timescale of milliseconds. Magnetic flux is also conserved, so the magnetic field is also strongly intensified, hence a star with an initial field of 100 Gauss may reach field strengths of up to 10^{12} Gauss (Lyne

& Graham-Smith 1990). This magnetic field is usually misaligned to the rotation axis. Asymmetries in the supernova may also disrupt or break apart stars a binary system (e.g. Hills 1983).

1.3 Emission Mechanism

1.3.1 Magnetic and Electric Field Structure

We now know that the pulses we observe are due to the rotation of the neutron star. As the pulsar spins round, a beam of radiation, analogous to that of a lighthouse, is emitted into space. If this beam illuminates the Earth, then we observe a pulse coming from the direction of the pulsar.

Figure 1.1 shows a simplification of our understanding of the magnetic dipolar field of a pulsar.

A quick calculation shows that, for charged particles, the magnetic force accelerating particles out of the star vastly exceeds the gravitational binding force. For an electron in a typical pulsar with $g = 10^{12}$ Nkg^{-1}, $B = 10^12$ G, $r_{ns} = 10$ km and $P = 33$ ms (i.e. the Crab pulsar period), and for electronic mass m_e and charge q_e (c.f. Lyne & Graham-Smith 1990, section 2.4):

$$F_g = m_e g \approx 10^{-18}\text{N}, \tag{1.1}$$

$$F_B = \frac{B q_e r_{ns}}{P} \approx 3 \times 10^{-5}\text{N}. \tag{1.2}$$

Clearly, the magnetic field dominates for electrons and most other charged particles by many orders of magnitude, hence the distribution of particles near to the star is governed by the magnetic field and the quadropole electric field that is also set up, shown in Figure 1.2.

As a result, plasma is stripped from the neutron star and forced along the field lines. Even at comparatively large distances from the pulsar, the particles remain tied to the magnetic field lines, hence they co-rotate with the star.

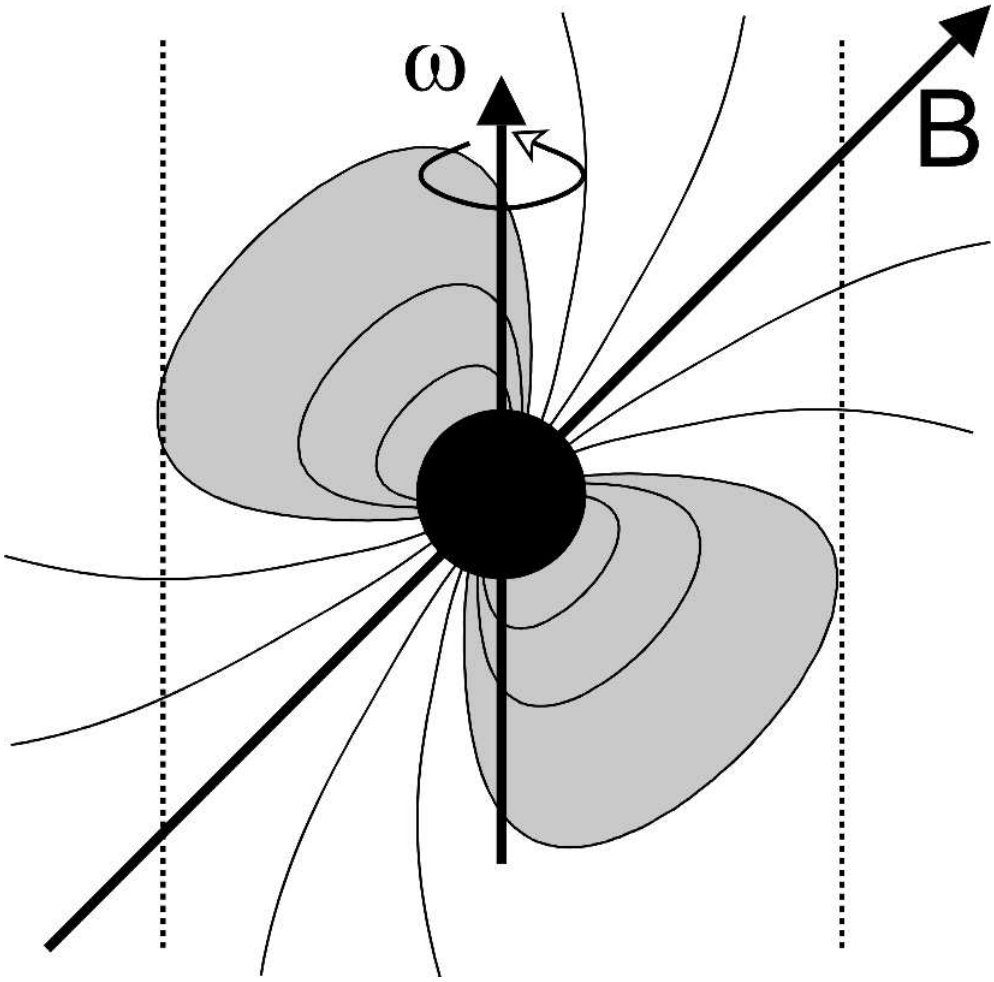

Figure 1.1: The magnetic field structure of a pulsar. Here, the magnetic field axis **B** is inclined to the rotational axis ω. Charged particles are tied to the magnetic field lines shown and co-rotate with the neutron star. The dotted lines denote the velocity-of-light cylinder, where the co-rotation velocity equals the speed of light. Highly relativistic particles can thus escape on magnetic field lines lying outside the shaded area.

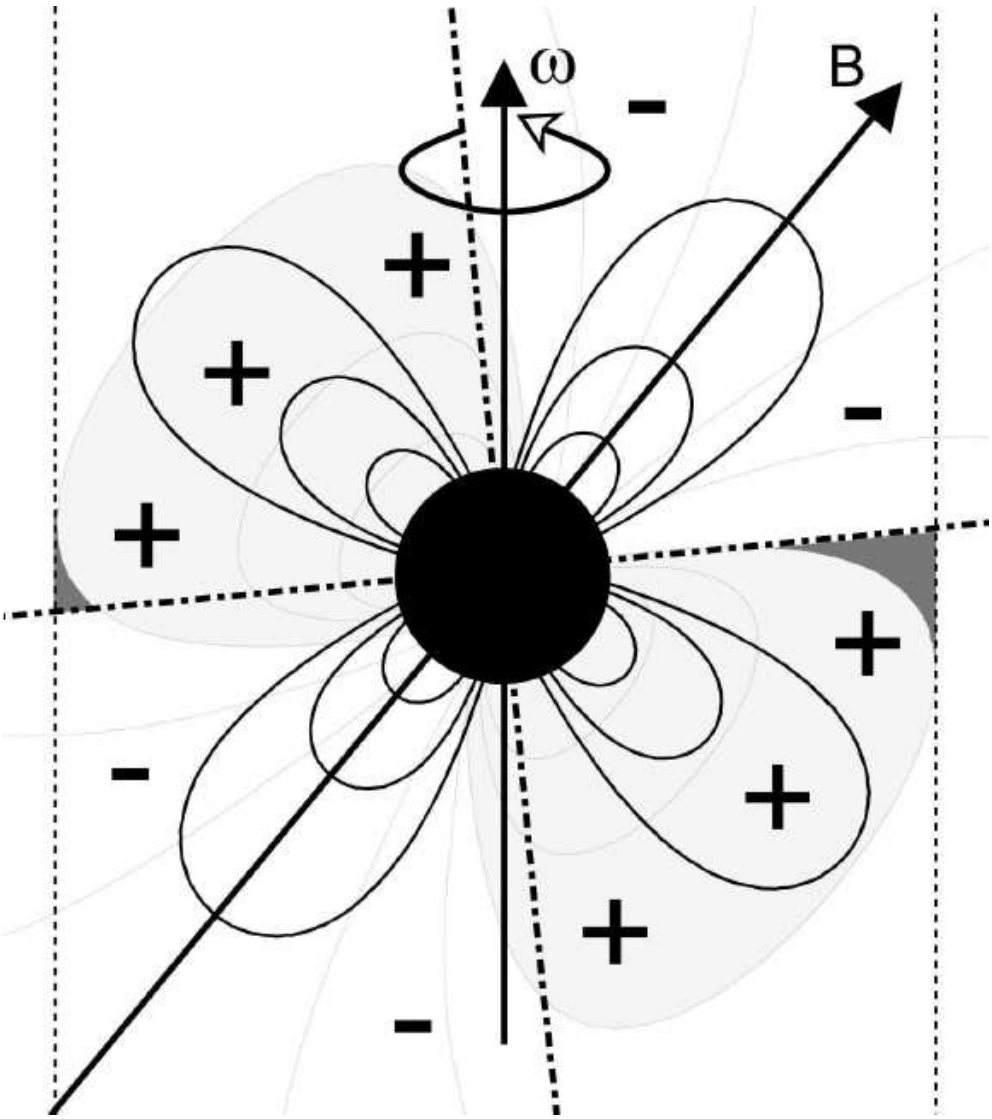

Figure 1.2: The electric field structure of a pulsar. The quadropole structure of the field leads to a plasma of positrons and electrons tied to the magnetic field lines in quadrants as indicated by the plus and minus signs. The dark grey boxes denote the outer magnetospheric gaps (see e.g. (Lyne & Graham-Smith 1990), section 16.1), thought to be a source of high-energy emission.

1.3.2 The Polar Cap

The fate of the particle largely depends on which field line it is on. We can define the radius of the "velocity-of-light cylinder"

$$r_{lc} = \frac{c}{\omega_{ns}} \tag{1.3}$$

for a pulsar with angular velocity ω_{ns} where the co-rotation radius reaches the speed of light. Particles on lines which close within this radius remain trapped and we can essentially define a stable area of plasma running in a loop from the star (shaded region, Figure 1.1).

Particles traveling along field lines not closing inside the velocity-of-light cylinder cannot co-rotate with the star and must therefore decouple from the field lines. The field lines on which this happens defines the 'polar cap'.

Observational evidence suggests that the emission we receive comes from this region, producing a circular ring of patchy emission (see Figure 1.3), whose frequency depends upon the height above the pulsar's surface from which it is emitted (see e.g. Rankin 1983b, Rankin 1983a, Rankin 1993, Mitra & Rankin 2002), with higher-frequency emission thought to emanate from closer to the surface. The precise mechanism for this emission is unclear, as the magnetic field strengths in this region are too strong for synchrotron emission to occur.

1.3.3 Polarisation and Determining the Shape of the Cone

Studies of polarisation data from pulsars have found that the angle of polarisation largely depends on the impact parameter β and the angle of inclination of the magnetic axis to the rotational axis α (see Figure 1.4). The angle of polarisation lies parallel to the magnetic field lines, which, when looking towards the magnetic pole, appear to radiate from the centre of the pulsar beam (e.g. Radhakrishnan & Cooke 1969). A generalisation of the variation in polarisation of a pulsar

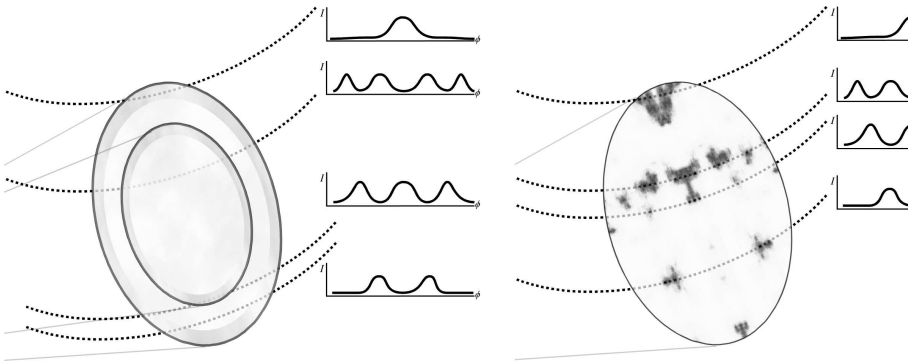

Figure 1.3: Theoretical models used to interpret pulse profile shapes, based on a figure from *Handbook of Pulsar Astronomy* (Lorimer & Kramer 2004). Left: Nested cone structure (Rankin 1993; Gil et al. 1993). Right: Patchy beam structure (Lyne & Manchester 1988).

over a pulse can be seen in Figure 1.4. We can see that there is a rapid switch around the centre of the pulse. The rate of this switch and the difference between polarisations points T and S can tell us information about β and α, the offset of the magnetic axis from our line of sight.

The phase angle of the points T and S (often defined by peaks in intensity) can tell us about the width of the beam. Hence, by observing how these change with frequency (remembering that higher-frequency emission occurs closer to the pulsar), we can determine the shape of the emission beam. Studies such as Phillips & Wolszczan (1992) have shown this to be funnel-shaped, which is consistent with the model shown in Figure 1.1.

Another feature that is observed is the circular polarisation. This polarisation sometimes changes hand (from clockwise to anti-clockwise, or *vice versa*), often near the middle of the pulse. As we expect the field strengths here to be too high to produce synchrotron emission, there is difficulty in producing a working model to account for this attribute. One theory that may account for this is that there is some intervening birefringent media which converts linearly polarised light into partially circularly polarised light (e.g. Melrose 1979).

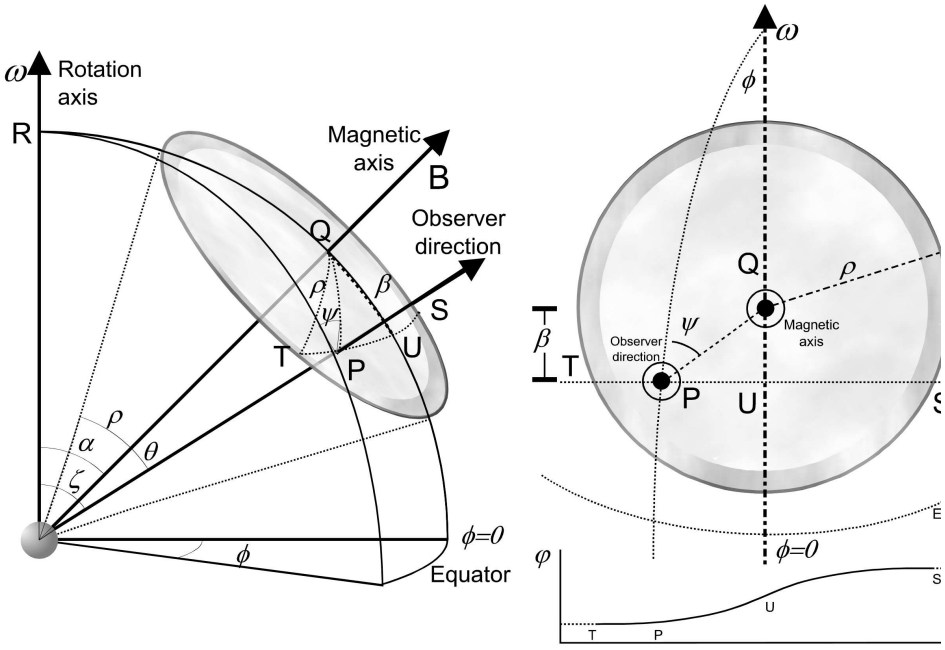

Figure 1.4: A view of the pulsar emission cone from an arbitrary angle to the pulsar (left) and looking down the magnetic axis (right). The pulsar rotates, bringing the observer's line of sight through the arc TPUS. The polarisation angle, φ (shown at the bottom-right) thus varies with the impact parameter β. (Left-hand figure largely reproduced from *Pulsar Astronomy*)

1.4 Uses of Pulsars

The possible uses of pulsars are varied. Their most striking property is that they represent the most accurate natural clocks in the Universe (Davis et al. 1985, Kaspi 1995). If we intend to use them as such, it is therefore necessary to observe timing variations in these pulsars, caused by effects such as precession.

Due to the nature of their birth, we can also use pulsars to study supernovae. Details of neutron star make-up, the angle between the magnetic and rotational axes and the proper motion of pulsars can tell us about the structure and asymmetries present in supernovae. Studying the ages of pulsars (assumed from their 'spin-down' rate) can determine the rate of supernovae, and hence the history of massive star formation in our galaxy.

Pulses also exhibit a frequency-dependant delay in arrival time due to scattering interactions with electrons in the inter-stellar medium (ISM). We can define a Dispersion Measure (DM) as the integrated column density of electrons between the pulsar and our telescope (Lorimer & Kramer 2004, pp. 86–87). By observing these DMs for a range of pulsars, we can also infer details about the ISM, such as the density of the ionised component.

As previously stated, pulsars offer a unique view into ultra-dense matter. The densities and pressures in the pulsar interior far exceed those creatable in our laboratories, so studying these pulsars can give us an idea of how matter behaves under extreme conditions. In particular, it has implications for the behaviour of superfluids and superconductors, as we surmise that the neutron star interior consists of a superfluid of neutrons infused with 5–10% of superconducting protonic fluid.

Perhaps more topically, pulsars, especially millisecond pulsars, can be used as detectors of phenomena such as gravitational waves (Bertotti et al. 1983) and possible changes in the gravitational constant (e.g. Kaspi et al. 1994).

A final, very important use of pulsars is in testing General Relativity. A comprehensive view of this is given in (Stairs 2003), which discusses the use of pulsars for tests of equivalence principle violations and tests in strong-field gravity cases.

Chapter 2

Free Precession

2.1 An Introduction to Free Precession

2.1.1 Causes of Free Precession

The concept of precession can perhaps most readily be understood in terms of a spinning top. When a spinning top is allowed to rotate on a surface, its rotational axis will trace out a circle. This is due to the misalignment between its angular momentum vector and its symmetry axis. As a result, the rotational axis will also be misaligned from the angular momentum vector. Both the symmetry axis and the rotation axis will therefore precess around the angular momentum vector. Specifically for a magnetic object, such as a pulsar, the magnetic moment vector will also precess around the symmetry axis. This is shown diagrammatically in Figure 2.1.

2.1.2 Effects of the Pulsar's Structure

In order to understand precessional effects in neutron stars, we must take into account that the neutron star is not an infinitely-rigid, solid object. Figure 2.2 shows the model cross-section of a typical neutron star.

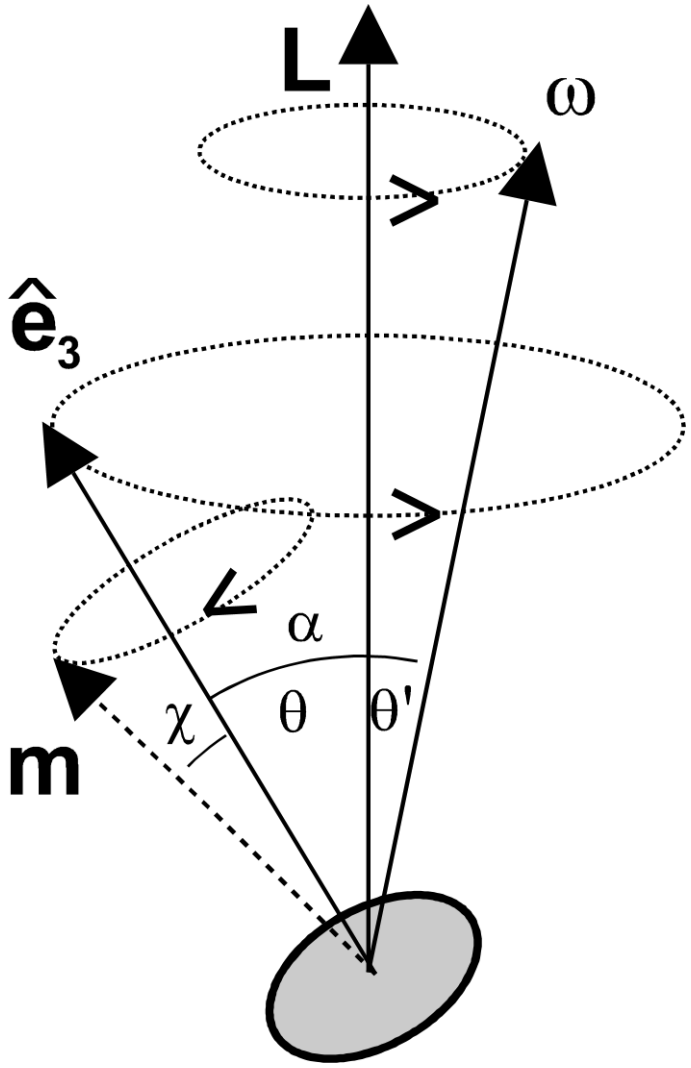

Figure 2.1: Geometric precession of a biaxial neutron star in the inertial frame. Reproduced from Link & Epstein (2001), who provide the following description: *The body's symmetry axis is denoted by $\hat{e}_3$, the angular momentum by L, and the angular velocity by ω; the three vectors always span a plane as shown. The angle θ, θ', and α are constant, with $\theta' \approx \epsilon\theta \ll \theta$ for small oblateness ϵ. The vectors $\hat{e}_3$ and omega rotate about L at nearly the spin frequency ω. A dipole moment m fixed in the body, and taking an angle χ with respect to $\hat{e}_3$, rotates in a retrograde sense about $\hat{e}_3$ at frequency $\approx \epsilon\omega$.*

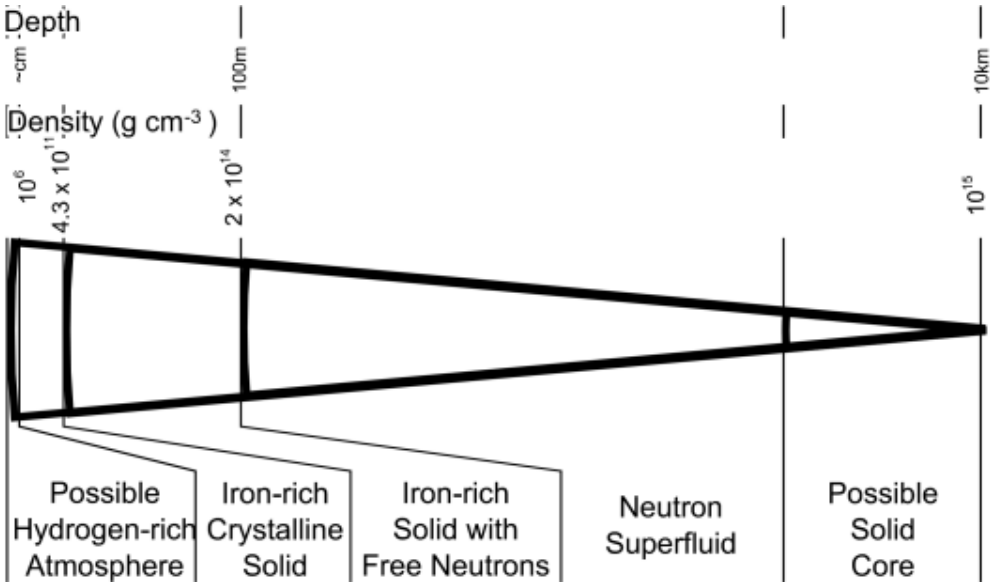

Figure 2.2: Typical cross-section of a neutron star, reproduced largely from Lyne & Graham-Smith (1990) with additions from Pasachoff (1977). Note that the atmosphere is most likely only present on accreting neutron stars, and the solid core may not be present and the outer layers more extended in low-mass neutron stars.

As was illustrated in Figure 2.1, a rotating superfluid neutron star will adjust its shape into that of an oblate spheroid, as will any freely rotating fluid object, with an ellipticity dependant on its angular frequency (discussed in Chapter 6).

What is of key importance here, as in many other aspects of pulsar astronomy, is the amount of pinning that occurs between the superfluid vortices in the pulsar's 'mantle', the solid core and, more particularly, the solid crust. The superfluid cannot precess, hence the amount of pinning will determine the amount by which the precession is damped.

The problem comes in working out the timescale of this variation. Shaham (1977) noted that precession would occur on timescales of order of milliseconds and that it was expected to damp away within a hundreds or thousands of precessional timescales, assuming the crust and 'mantle' were perfectly pinned. Later work by Sedrakian et al. (1999a) showed that when pinning is strong, but imperfect, both the period of oscillation and the damping timescales were considerably

increased, but were still damped away eventually.

2.1.3 Observational Evidence

There has always been a large amount of tentative evidence that appears to point to precession-induced oscillations in the pulse arrival time of several pulsars. The best known is the apparent 35-day quasi-sinusoidal oscillations in the timing residuals of Her X-1 (e.g. Brecher 1975). Her X-1 is in a binary system and it has been theorised that matter accreted from the companion star has excited precession in the pulsar. It is undetermined whether this is free precession, or whether it is geodetic precession — a precession of the rotational axis due to relativistic spin-orbit coupling in a binary system.

However, the only substantial evidence for free precession in an individual pulsar is that of PSR B1828–11 (e.g. Stairs et al. 2000). Here, sinusoidal oscillations are seen with periods of order 250, 500 and 1000 days, which we surmise are due to precession in an asymmetric pulsar (see Figure 2.3).

Scientifically, we are left with a problem: if PSR B1828–11 is the only pulsar to exhibit free precession, why is its case so special, and if it is not the only precessing pulsar, why have we not detected precession before?

This question underlines the need for a review of the timing and profile histories of all known pulsars in an attempt to find precessional effects in historically recorded data, in order to find these missing 'precessing pulsars'.

2.2 Detecting Precession

2.2.1 Visible Effects

The observed effects of precession in solitary pulsars could only come from what is presently our only observable information source — changes in the radiation

we receive from the emission cone.

The changes we would expect to observe are changes in both the shape of the observed profile and the time of arrival of the pulses. Changes in the shape of the profile would be expected as the impact parameter β shown in Figure 1.4 changes, meaning a change in the cut our line-of-sight makes across the emission cone. Changes in the time of arrival of the pulses reflect changes in the rotation period of the neutron star, determined by changes in the spin-down torques produced by the precessional effects. Thus, for us to be able to say that precession occurs, we should see changes in both features, otherwise it is likely that some other process is occurring.

2.2.2 Measuring Changes

2.2.2.1 Changes in Period

Finding changes in period is a comparatively trivial one. Although individual pulses from pulsars are quite varied, average profiles, summing over a few hundred pulses yields remarkably consistent results. For each observing run, we can therefore identify the precise arrival time of the pulse peak and find its deviation from a recorded ephemeris, using a given period, P, and spin-down rate, $\dot{P}$.

Deviations from this can be quite clear. In the case of PSR B1828–11 (see Figure 2.3), the accumulated pulse time offset over a complete precessional period amounted in 1995 to around 20–50 ms and was quite clear from the observations. Changes in the rotation period, or spin-down rate, could be accurately calculated to within a nanosecond, with good fitting. Changes in this spin-down rate themselves were also identified, and a reasonable fit could still be made to the observations.

Given how clear-cut these period changes are, they should be observable in any bright pulsars that exhibit them, provided they are not obscured by other

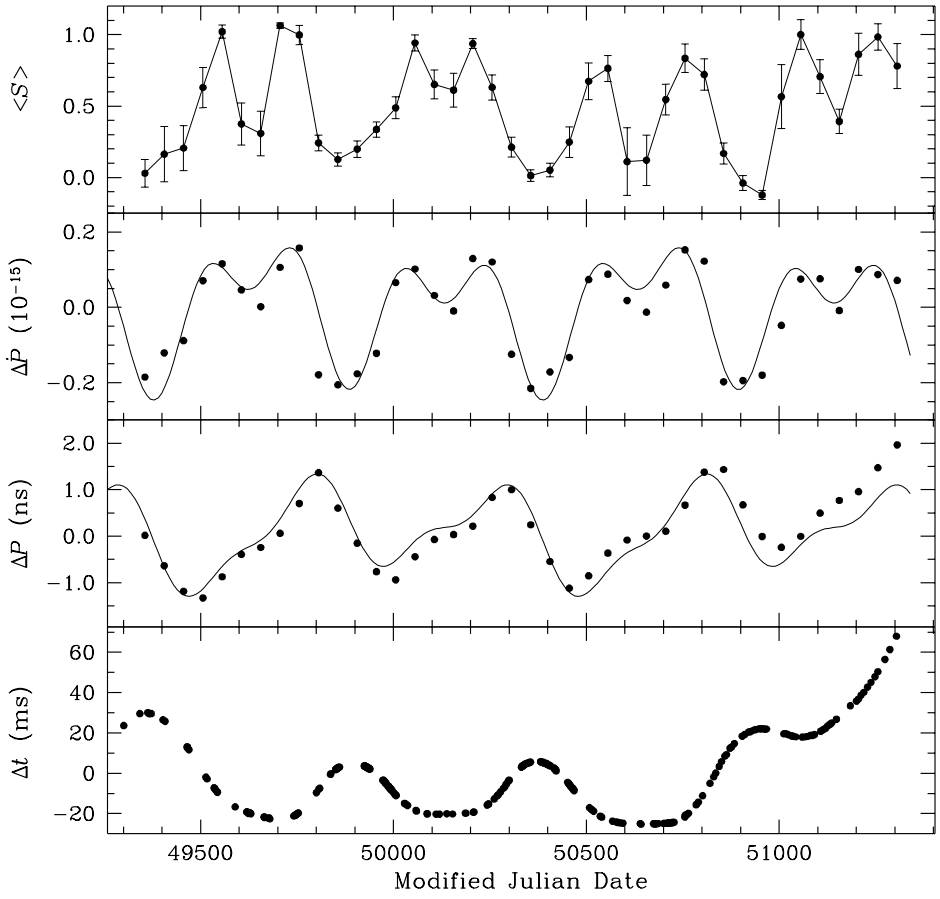

Figure 2.3: The change in arrival time, Δt, change in period ,ΔP, change in period derivative $\Delta \dot{P}$ and "shape parameter", $< S >$, for B1828–11, reproduced from Stairs et al. 2000, showing clear pseudo-sinusoidal variations coherent with a model of a precessing pulsar.

factors.

2.2.2.2 Changes in Pulse Profile

Quantifying changes in pulse profile is a much more difficult task. For these, we lack a single, quantifiable number with which to represent changes in the profile we observe. For example, we could expect to see changes in the phase difference between the two conal components, changes in the relative amplitudes of both the core and conal components, changes in the overall brightness of the pulsar,

along with a myriad of other effects.

The advantage of using a single parameter is that it makes finding periodicities in changes in the profiles far easier. Using multiple parameters would require coherently finding periodicities in some or all of these, making it more difficult to determine whether the periodicity is noise or inherent change. With a single parameter, however, a simple power spectrum of periodicities in the data can be made, and any strong periodicities found easily from this.

Several methods could potentially be used in order to determine an absolute value for shape changes in a pulsar. These methods can either take into account some or all of the inherent variables. Models which fail to take into account all the variables could miss variations which are important. Models which take into account all the variables risk where two variables can cancel each other out risk missing the identification of profile changes.

2.2.2.3 Single-Variable Profile Analysis

Using a single parameter to model changes in the complex profile of a pulsar pulse can be achieved to varying degrees of success by using a number of models. Some possibilities are listed here.

Firstly, we could investigate the variation within a model. Simple models using this could investigate changes in the separation of the profile components. Observed changes in these are quite readily identifiable, given sufficient enough time resolution, but could be confused with other phenomena, such as mode switching, or variations of sub-pulses (see later).

Another more advanced approach would be to assume a model of cone emission, likely based on a ring of emission and a central component, and try to fit changes in the profile to different cross-sections through this model. This would

have the danger of using a model to fit the data, which may completely misrepresent the emission cone in reality.

A different method would use an observed parameter change which is not necessarily expected to change, such as changes in the ratio of the amplitudes of the conal components. As with most other simple attempts to identify variations, this could also be confused with other phenomena, such as mode switching (see e.g. Backer 1970).

Taking this model a step further, two different pulse profiles, each representing two extremes of variation, could be used and matched to other observed profiles using a weighted, scaled addition of the two extremes. By doing this, we are effectively placing each observation on a scale between one extreme and another. This approach encounters difficulties if the modulation is more complex, or the change is highly non-linear.

2.2.2.4 Multiple-Variable Profile Analysis

A more comprehensive analysis of profile changes would seek to incorporate every variability in the data, then reduce the observed changes down to a single quantity. This approach tends to bring about other problems, however.

Perhaps the easiest approach would be to use some combination of the above techniques and either sum their results, either directly, or summing their squares. Firstly, the problem then arises of how and if we should attach weights to these parameters. A second problem is that this should work well if we are looking for deviations from an equilibrium position (which may still be applicable here), but is not particularly satisfactory when it comes to analysing changes between one state and another, where one quantity may increase and one simultaneously decrease.

A similar situation is encountered using the more complex method of principle component analysis. This involves representing each observed profile as a weighted sum of constituent profiles. These constituent components could be as complex as entire profiles or as simple as Gaussian peaks. The difficulty comes once the weights of each component have been determined. How do we reduce this set of weights into a single number?

Traditional principle component analysis methods would then reduce the number of variables by identifying linear relationships between two variables and reducing them to one number representing the coefficient of the relationship. Thus this process can reduce the parameter set down to one number.

The problem with this method is that situations can again occur when the effect of one change cancels out another, hence variability could occur but not be observed. Practical tests carried out by Michael Kramer [private communication] found that this traditional method is not particularly effective in the case of PSR J1022+1001.

2.2.3 Other Factors Mimicking Timing Changes

2.2.3.1 Data Pre-processing

It is important to remember that a lot of data pre-processing is done automatically before timing residuals are found. The details of this can be found in Lyne & Graham-Smith (1990) (p.165–167). This pre-processing removes the effects of dispersion introduced by the ISM by determining a DM; a constant time derivative, $\dot{P}$; and classical and relativistic effects of the Earth's rotation and (elliptical) orbit around the solar system barycentre.

This is a well-practiced science, and for many pulsars with good signal-to-noise this can be done with great accuracy. However, if $\dot{P}$ changes for any reason, a parabolically increasing offset will be introduced to the timing residuals.

It has also been found that, for an average pulsar, the dispersion measure ('DM') can change by $\Delta DM \approx 0.0002\sqrt{DM}$ cm^{-3} pc yr^{-1} (Hobbs). For a fast-moving pulsar in a clumpy region of the ISM, this could introduce small timing errors.

Both of these errors should produce non-repeating changes in timing noise. Changes in $\dot{P}$ will not affect the pulse shape at all, and changes in DM are unlikely to affect it to any great extent. Hence, we are not greatly concerned about the effects these could have on our data.

2.2.3.2 Orbiting Bodies

If a pulsar is in an orbit with another body, motion along the orbit will lead to variations in the arrival time of pulses, both due to Doppler and relativistic effects. An orbiting body could be a normal star or neutron star, such as in the case of PSR B1913+16 (Weisberg & Taylor 1984), or another pulsar, such as PSR J0737–3039; in both cases gravitational radiation must also be taken into account, which will slowly decrease the period of the orbit.

Alternatively, the pulsar could be orbited by planets, as with PSR B1257+12 (Wolszczan & Frail 1992; Rasio et al. 1992; Wolszczan 1994), which would give a sinusoidal variation similar to that seen with precession in PSR B1828–11 (Stairs et al. 2000); however, in the case of a precessing pulsar, we expect to see regular profile shape changes as well, which are not observed in B1257+12, and are only likely to occur if precession is taking place, or, perhaps, if the orbiting body interacts with the pulsar's magnetosphere.

2.2.3.3 Timing Noise

Another major complicating factor in determining precessional effects is distinguishing them from timing noise present in pulsars. Timing noise is thought to

arise from irregularities in the pinning of the crust to the neutron superfluid below it. This results in phase jitter, slow variations in the pulsar's period and period derivative, etc., occurring over on a timescale of months to years.

Timing noise can often create signatures in the timing residuals which look remarkably like precessional effects (e.g. Helfand et al. 1980). The amplitude of this noise correlates fairly well with pulsar age, with older pulsars showing less of an effect (Cordes & Helfand 1980). Well-timed pulsars can exhibit deviations on the order of milliseconds, and less-well-timed pulsars on the order of tens of milliseconds (Gullahorn & Rankin 1982, (Hobbs 2002)). We can discriminate most easily between the two by looking again at the pulse profiles: timing noise should not produce any profile changes, but precessional effects should.

2.2.3.4 Glitches

Glitches are readily identifiable in timing residuals as a sudden jump in period (e.g. Radhakrishnan & Manchester 1969, Reichley & Downs 1969), which will correspond to a rapid increase in timing residuals. These are usually followed by a fairly exponential recovery (e.g. Krawczyk et al. 2003a). Looking at the data, it is clear that a glitch is not attributable to precession (again, it does not create any profile changes), but if we look for periodicities in timing data, if a glitch were to occur in a precessing pulsar, the periodicity of the oscillations would not necessarily be picked up.

2.2.3.5 Tkachenko Oscillations

Tkachenko oscillations are oscillations set up in a rapidly rotating superfluid (Tkachenko 1966). For a typical neutron star, these are theorised to be on a timescale on the order of months (Stairs et al. 2000) — the same timescale we would expect precessional effects to occur on. Being stable oscillations, these

should produce well-defined sinusoidal variations in the timing residuals, but again these should not affect the pulse profile, so by examining both we can rule out this effect.

2.2.4 Other Factors Creating Profile Changes

2.2.4.1 Mode Changing

Mode changing occurs when a pulsar switches from one meta-stable mode of emission to another meta-stable mode. Pulse profiles of pulsars in which this is observed show two or more distinct profiles, with the pulsar switching between them in an largely unpredictable fashion. This is discussed extensively by Rankin (1986). Profile changes appear to occur mostly in pulsars with triple or multiple profile components, although this could be due to the fact that this makes it easier to see profile changes, as in a single component system, one may not see more than a brightness change. Rankin also stresses that, although previously it was thought that mode changing occurred in older pulsars, a larger sample of objects does not support this conjecture.

Mode changing has the complicating effect of producing pulse profile changes in pulsars. However, these changes are, for our purposes, instantaneous. This should theoretically make them easy to separate from the gradual changes in profile we would expect from precession.

Mode changing can also affect the timing results, as different components can become dominant, or an addition of one component to a noisy profile could make changes in the way a cross-correlation function would fit a template to the data. It does not affect the actual rate of rotation of the pulsar itself. Again, due to the sudden change between modes, this should be easy to separate from gradual changes in timing residuals due to precessional effects.

2.2.4.2 Sub-pulse Drifting

Sub-pulse drifting is also considered by Rankin (1986). In pulsars in which this occurs, small pulses within the conal emission of the main pulse drift either forwards or backwards in pulse phase. The pulse profile will, accordingly, reflect this change. As with any change in pulse profile, this can lead to a small change in pulse timing, as fitting the cross-correlation function to the data accurately relies on a reasonable pulse profile match.

It is not thought that sub-pulse drifting will affect any searches for precessional effects. The reason for this is that this drifting appears to occur on timescales of between 2 and 100 times the pulse period — i.e. on the timescale of seconds to minutes. On a sufficient timescale (Helfand et al. 1975), these sub-pulses will 'smear out' over the profile and any variability will be lost. This limits the time resolution with which we can search (this limit is well below the Nyquist limit imposed by our data), but given the timescales of 250 days for PSR B1828–11 (Stairs et al. 2000) we do not expect to have to use timescales of this length anyway.

2.2.4.3 Pulse Nulling

Also covered by Rankin (1986) is pulse nulling. Here, all pulsed emission from the pulsar either completely ceases, or is reduced to an insignificant fraction ($< 10^{-3}$) of its average power. It was previously suggested (e.g. Ritchings 1976) that this was a precursor to the pulsar 'switching off', but Rankin argues that it is a phenomena observed in pulsars of all ages and is instead a feature of pulsars with conal elements to their profile.

Hesse & Wielebinski (1974) split nulling profiles into three groups according to their power histograms: type I, showing a distribution of power around a value ('always on'); type II, showing an exponential distribution; and type III, showing

a bimodal distribution, combining types I and II.

The nulling process appears to represent the shutdown of the magnetospheric production of radiation. Rankin's review shows this nulling can occur on any timescale up to several minutes or hours.

The effect of nulling on discovering precession is minimal, although it could add some noise to the data. Nulling does not appear to affect either the pulse profile or the timing residuals. Any variations due to switching on or off as we observe the pulse will be averaged out, as we are dealing with average profiles. At most, this process is expected to represent partial loss of data during an observation, or perhaps the complete loss of the occasional data point. This should not have any great bearing on our results.

2.3 Discussion

From the previous section, the main observing tolerance on detecting precession in timing residuals appears to be timing noise, although the other effects may be important. Detecting changes in the profile shape remains a difficult task, with no single completely satisfactory means of quantifying the profile shape in a general way.

The data for B1828–11 shows clear variations in the timing data, which should be easily detectable above timing noise, even in poorly timed pulsars. Variations in the shape parameter do indicate periodicities, but they are much less clear. A key problem, therefore, is to find a suitable method of identifying changes in profile shape.

The remaining question is whether there are changes out there to be observed. We must ask what would cause a misalignment between the axes, and as to whether B1828–11 is special in this case. For example, we could hypothesise that precession is linked to core-crust coupling in some way, perhaps through

glitches, in which case we would expect many more pulsars to be precession. Alternatively, we could envisage a more unlikely scenario, perhaps precession could be excited if B1828–11 was hit by another body, causing chaotic motion, in which case we would not expect to find precession in many, if any, other pulsars. Another possibility is that the periodicities we see due to some effect other than precession, such as orbiting bodies or an orbital disc interacting with the magnetosphere. The archives at Jodrell Bank Observatory contain a history of pulsar data stretching back to 1970, so there is sufficient data for us to find precession in most other pulsars that we have discovered if they precess on timescales (and width amplitudes) comparable to B1828–11.

As described in, e.g., Jones & Andersson (2001), the amplitude of any precessional variations will depend on the amount of deformation the neutron star has undergone. These deformations are distinct from centrifugal deformation, and must be non-axisymmetric, 'mountainous' deformations on the crust in order to induce precession.

Precession in pulsars with small deformations will be more difficult to detect, as there may not be sufficient data to find strong enough periodicities in recently discovered pulsars, although it remains to be seen what the effects of precession on a completely triaxially symmetric star would be (Link & Epstein 2001).

We must accept that until more definite evidence for other precessing pulsars is found, B1828–11 remains the one pulsar among hundreds that shows precessional effects. Finding only one object in such a large dataset with these properties is of concern. It may be that B1828–11 precisely satisfies some conditions that allow either precession or an effect with very similar visible identifiers. Thus we can imagine that one of the following scenarios could be true: firstly, that precession exists, but has not been identified; secondly, that the scales or methods with which we look for precession are unsuitable (c.f. the unexpected finding of numerous

'Hot Jupiters' instead of 'Cold Jupiters', e.g. Schilling 1996); or thirdly, that precession exists, but is masked from detection by some other feature.

In conclusion, we have strong evidence for precession in the case of B1828–11. The task ahead is therefore to find if this behaviour is repeated in other pulsars, and if not, why not. For precession to be identified, regular, sinusoidal changes in both pulse shape and pulse timing ought to be identified. If B1828–11 is a typical example, then there should be sufficient good data to find this effect in other pulsars, if it exists.

Chapter 3

The Computer Software

3.1 Introduction and Principals

As part of this thesis, it was required to produce software capable of detecting changes in profile shape that could be attributable to precession. This chapter describes how this software works and its limitations.

The software is designed such that it can run independently of machine and with minimal user input, yet retain complete functionality and versatility. All the software was written in FORTRAN 77 and consists of the following modules: *READDB*, which reads in the profiles as EPN files (Lorimer et al. 1998); *MAKEPROF*, which alternatively creates artificial profiles using a cone model; *DORESID*, which subtracts the template from the profiles to produce 'residual' profiles; *LOMBPERIOD*, which performs a Lomb-Scargle Periodogram on the residual profiles; and *PCATEST*, which runs a Principal Component Analysis on the residual profiles.

The program is designed to be run as a single unit, with components that can be switched and off, and parameters that can be altered, as the user requires. This is done in one of two ways. Firstly, the user can edit the parameter file. This is a permanent file containing the parameters for the entire program, and

allows semi-permanent changes to be made to the way the program runs, which is useful for setting up global parameters for a run through a database using a script. Secondly, the user can enter parameters from the command prompt, allowing changes to be made for that run only, allowing scripts to run through a catalogue of pulsars, or explore how varying a set of parameters alters the program output.

Global parameters set in the parameter file include the activation state of each stage (i.e. whether to run a particular module or not), which plots to display at runtime and which directories the input and output files are to be contained in.

3.2 READDB

3.2.1 Function and Parameters

The function of the *READDB* subroutine is to read data from an EPN archive file. The EPN standard (Lorimer et al. 1998) was chosen to allow portability between archives. EPN filetypes are easily created from the Jodrell Bank archive using the PSRPROF software package.

The *READDB* subroutine contains a number of parameters. Most obviously, the input file can be changed, along with the messages file. There is also an option to set the template. More on the generation of templates is discussed later. Additional parameters can be changed, namely the allowed range of frequencies, the signal-to-noise rejection level, the method of template generation, the seed template (see below) and the date range of profiles to accept.

3.2.2 Method

READDB works as follows: firstly, the EPN header is read from the database input file. The profile length is then set to one pulse period, based on the parameters contained in the header. The program then begins a loop in which it reads in the profile, first by scanning the header for the relevant timing and frequency information, then it reads in the profile data. The profile is then accepted or rejected based on a frequency and an optional signal-to-noise test (discussed in Chapter 4). The frequency test checks whether the observation falls within the specified range of frequencies. The signal-to-noise test compares the peak intensity with an iterative, sigma-clipped median[1] of the profile, and rejects it if the ratio is too low. If the profile is accepted, it is written out to a file and the observation time recorded.

The frequency test is necessary as the profile from any particular pulsar is liable to dramatic changes in shape and amplitude between frequencies (e.g. Rankin 1983b, Rankin 1983a). The signal-to-noise test allows more careful selection of the quality of input to be controlled. This comes as a mixed blessing. On the one hand, it is possible to completely remove profiles where the signal is not detected, or only weakly detected. This works to our advantage when data weighting is not possible, such as when performing Fourier analysis. However, one can envisage a scenario where precession is causing the beam to be brighter and dimmer as our line of sight cuts through different parts of it. In this case, a signal-to-noise cutoff which is too severe could result in the fainter profiles being dropped, hence variations in pulse shape not being detected. Therefore, care must be taken when setting the signal-to-noise cutoff that it is significantly lower than the signal-to-noise of the clearest pulses.

[1]This process calculates the median of the data, removes all data lying more than a user-specified number of standard deviations away from the median (here the default is 3), then iterates a user-specified number of times (here the default is 8). This is used here as it allows RFI and any pulsed emission outside of the pulse window to be removed to find a true baseline.

3.2.3 Template Generation

Once the profile database has been read, the program creates its own template using a variety of different methods, selected using the *tempmethod* parameter, which can range from 0–8. Part of this generation occurs within the *READDB* subroutine, and part in the main module. Regardless of *tempmethod*, once *READDB* has read the profile database, it estimates the full-width half-maximum (FWHM) of each template as the number of bins above the half-maximum intensity level.

For the *tempmethod* = 0 option, the program keeps the template it had previously been using. For *tempmethod* = 1, a profile is read from a database file using the same method described above, with the profile's position within the file given by the *templateno* parameter.

Option *tempmethod* = 2 creates a template using an average of all the profiles in the dataset. It cross-correlates each profile against this average using the *DORESID* subroutine, then creates an average of the cross-correlated profiles. This method only works if the timing model is sufficiently accurate that the timing residuals (which determine the phase of the pulse peak of a profile in the database) are of the order of the width of a phase bin, which is not the case for many pulsars. Consequently, this option is largely redundant and was superseded towards the end of coding by the *tempmethod* = 7 option (see below).

Option *tempmethod* = 3 takes a user-supplied Gaussian pulse profile and fits it to the data. Here, the user can control the FWHM and location (in phase bins) of the Gaussian using the *tempgaussian* parameter. Options *tempmethod* = 4–6 also use this method, but centres the pulse in the profile and use the maximum, minimum and average FWHM found by *READDB*, respectively. While these

methods, and in particular *tempmethod* = 6, work for pulsars with Gaussian-shaped profiles, the majority have distinctly non-Gaussian profiles, or with profiles with multiple components, that cannot be modelled, or are inaccurately modelled by this technique.

We found *tempmethod* = 7 to be the most effective method of creating a template in this program in terms of results and processing power. To begin with, it runs as does the *tempmethod* = 6 option, producing a Gaussian template based on the average FWHM of the profiles read from the database. The program then cross-correlates the profiles with this Gaussian profile using *DORESID*. Having done this, it then creates an average of these profiles and uses this as the template. This allows a representation of the pulsar's intrinsic profile to be used as a template.

There are scenarios where the above method will not work — for example, where there are two unresolved components and a third, resolved component. Variations in the unresolved components would upset the cross-correlation and hence smear the template out. This can be minimised by running the above process iteratively, as is done in the final method — *tempmethod* = 8 — but this greatly increases the processing power needed and tests on both real and fake datasets suggest that there is not much room for improvement on *tempmethod* = 7. As a consequence, *tempmethod* was set to seven in all our data tests. Possible effects of this will be discussed later.

The template generation routines also estimate the on-pulse window. This is done by moving outwards from the pulse peak, and setting the limits of the on-pulse window to be the first bin in the template to the left and right of the peak which falls below a threshold value, set by the user (for our analysis it was set to 10% of the peak intensity). This is not always ideal, as there are pulsars with multiple components with near-zero emission between the components; however,

for most bright pulsars, setting a sufficiently low threshold value will pick out the pulse window well. The pulse window is mostly used for off-pulse noise calculations.

3.3 MAKEPROF

3.3.1 Function and Parameters

The *MAKEPROF* sub-package is designed to test the detection software and allow modelling of the pulsar profile changes. It comprises of two main sets of software: *MAKEPROF* itself, which is modified from code developed by Michael Kramer, and *MAKEMODEL*, which is a related piece of software based on the same code. The purpose of both subroutines is to create fake profiles based on a set of input parameters; the difference between them being that *MAKEPROF* relies on a set of Gaussian peaks with randomly changing position, width and amplitude, whereas *MAKEMODEL* relies on a set of pseudo-Gaussians produced by taking a slice through a cone model, as described below.

User-defined controls in this section are: the number of profiles to create, the fractional level of artificial noise to add onto the profiles and the number of phase bins in each profile. *MAKEPROF* also has the additional choice of the input file containing the initial Gaussian components that make up the simulated profile.

By its nature, *MAKEMODEL* requires a number of extra parameters. These are the radii, full-width half-maxima, amplitudes and angle offsets of the cones used (r, w, a, x and y as defined in Figure 3.1); the variation and mean value of the impact parameter (β and σ_β in Figure 3.1); the period of this variation and the sampling timescale (t_{var} and t_{samp}).

There is also the option to use the observation times of the previous dataset. This is useful in determining whether an object is real, or an artifact created by

the sampling of the observations.

3.3.2 Method: *MAKEPROF*

MAKEPROF begins by loading a template from a pre-existing, user-specified file containing the widths, amplitudes, and positions of Gaussian components. It then produces a profile by adding those components, which it normalises. A user-specified level of Gaussian-distributed noise is then added. The profile is written to a file, then the widths, amplitudes and positions are modified by multiplying them by a random variable taken from a Gaussian distribution. This process is carried out iteratively for each profile.

3.3.3 Method: *MAKEMODEL*

The *MAKEPROF* subroutine is not suitable for simulating precessing objects, as no periodic variations can be induced. It was therefore decided to create a subroutine that would simulate the profiles observed from a precessing object. To do this, it was necessary to assume a two-dimensional model for the emission from the pulsar, as the impact parameter, β, would vary depending on the phase of the precessional cycle.

For this process, it was decided to base our model on the nested cone structure of Rankin (1993) and Gil et al. (1993), partly since it is easier to simulate, and partly because the results are more meaningful in this context. Using the parameters file, the user inputs the parameters required to make up emission cones as shown in the left panel of Figure 1.3. These parameters are defined in the above section and in Figure 3.1.

MAKEMODEL works in much the same way as *MAKEPROF*: the cone parameters are read in by the main module and passed down to it. It then creates a profile based on these parameters, which it normalises and adds noise to. The

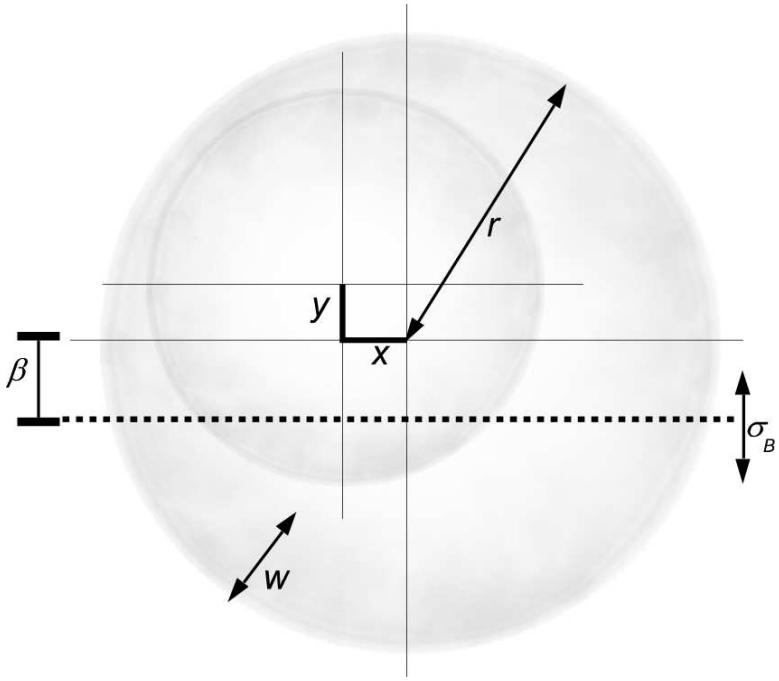

Figure 3.1: The cone model used to create profiles in the *MAKEMODEL* subroutine, showing the inputs to be given by the user. The emission is modelled as a number of cones, with axes perpendicular to the line of sight, modelled by the radius r, half-maximum width w, amplitude a, and offset (x, y) from the emission centre. Our observed profile is a slice taken a distance β away from the origin, which varies by σ_β over the precessional cycle.

profile is written to a file, the observation time advanced, and the process begins again for the next profile.

The calculation of the profile, $\mathbf{v}$ is performed as follows. The line-of-sight cut through the beam can be represented as a horizontal line through an X-Y plane, such that, for any particular phase bin i:

$$x_i = 2\pi \frac{i}{M} \tag{3.1}$$

$$y_i = \beta + \sigma_\beta \sin\left(\frac{t_{obs}}{2\pi t_{var}}\right) = \text{constant}, \tag{3.2}$$

where M is the number of phase bins in the profile and t_{obs} is the observation time, given by Nt_{samp}, where N is the profile number.

Assuming a flat beam (in reality the beam will be a section of a sphere, but this difference is not important here), the distance, d, of a particular phase bin,

i from a particular emission cone, n, can be given by:

$$d_n^2 = \left(r_n - \sqrt{(x_i - x_n)^2 + (y_i - y_n)^2} \right)^2, \tag{3.3}$$

for a cone centre offset of x_n, y_n.

Thus, the profile amplitude, v_i, for phase bin i will be:

$$v_i = \sum_{n=1}^{N} a_n \exp\left(-\frac{d_n^2}{2w_n^2} \right), \tag{3.4}$$

for N emission cones.

3.4 DORESID

3.4.1 Function and Parameters

The *DORESID* function has two main, related purposes. The first is to cross-correlate the observed profiles from the database with the template, which allows it to perform its second task of producing residual profiles.

The above processes are fairly intuitive procedures, therefore the only parameters required are the output filenames. An option is provided to smooth the data in phase to remove white noise, but this was found to have a detrimental effect on the data and is retained only to be used should the subroutine be required for other purposes — it is not used in any of the results of this thesis.

3.4.2 Cross-correlation

Arguably one of the more important routines in this analysis is the cross-correlation routine. Any precession hitherto undiscovered is likely to involve very small changes in profile shape, thus a very accurate fit is required. Our data is binned to 400 or 512 bins per profile, with the pulse window corresponding to only a few bins. To obtain a sufficiently accurate fit, we must therefore have a cross-correlation routine capable of working in fractions of a bin. For this reason, we

use the routine *LINEUP*, provided by Michael Kramer, to 'rotate' the phase of the observations until the profile peak aligns with the template peak. *LINEUP* takes an input offset, rotates the data by an integer number of bins, then uses a spline function to interpolate the data to rotate the data in by a fraction of a bin.

Of course, the key value here is the input offset. In the course of this investigation, we used a number of different methods to best determine this. We found that, while simple test profiles with low signal-to-noise were successfully lined up using all the routines tested, more complex profiles taken from our database were not able to be lined up successfully.

First of all, a frequency-domain fit was implemented, using the *FFTFIT* subroutine (Taylor 1992). This was found to be inadequate, as the profiles we were using did not have a sufficient number of bins for frequency-domain fitting to work well. A simple time-domain search was then implemented, using a parabolic fit to a chi-squared minimum to find the offset to a fraction of a bin. Again, this was deemed unsuitable, as multiple-peaked and 'square'-shaped profiles could not be fit well. After extensive experimentation, a time-domain fit was used in the final analysis. Rather than cross-correlating the profile and template directly, a modification was made to cross-correlate the third power of the derivative of each.

This approach reduces the problems caused by low-frequency noise in the data, which can occur when white noise is interpolated. The majority of pulse peaks have at least one well-defined edge and usually two. Taking the derivative allows the edges of the peak to be lined up, while taking the third power accentuates the main peaks, while reducing peaks due to noise on profiles of sufficiently high signal-to-noise.

3.4.3 Method

DORESID begins by reading in the template, produced/read above, from a file. It then smooths this template if required (see above), then performs an FFT on the template to prepare it for the cross-correlation subroutine. *DORESID* then begins a loop over the database profiles, reading each one in turn; smoothing it, if required; cross-correlating it with the template as described above; lining up the profile with the template using *LINEUP* (also see above); scaling and removing the template, if set to create residual profiles; zeroing the resulting profile and normalising the peak intensity to unity; and writing the profile out to a file, plotting a graph of the profile if requested.

The penultimate stage — the zeroing and normalising — is done to avoid DC offsets and unfair biases when it came to processing the results. This is done by calculating an iterative, sigma-clipped median, using the same subroutine as in *READDB* and subtracting it from the profile. The profile is then normalised by dividing it by the maximum value in the profile.

3.5 LOMBPERIOD

3.5.1 Function and Parameters

The *LOMBPERIOD* subroutine is the first of the two main analysis sub-packages included in the software. Its purpose is to perform a Lomb-Scargle periodogram on the data, using the *Numerical Subroutines* subroutine *FASPER* (Press et al. 1992).

LOMBPERIOD allows a number of options to be set, aside from the standard naming of the output files. Firstly, it can be run on either the cross-correlated profiles, or the cross-correlated residual profiles (hereafter 'profiles' and 'residuals') created in *DORESID*. Secondly, the data can either be smoothed or re-binned,

depending on the user's preference (although these have not been used in our analysis). Also set are the *hifac* and *ofac* parameters in *FASPER*, discussed below. Thirdly, the number of bins used in the histogram and the tolerance with which the program finds the probability factor, m, (also discussed below) can be set. Fourthly, a number of plotting options can be set; and finally, the statistical output can be limited to periods less than a value proportional to the range of observations.

As with *DORESID*, it is advised that smoothing is turned off for the intended purpose of the program. Binning can be used to condense the dataset to reduce running time, but is primarily useful in finding periodicities, especially in weak pulsars, that occur over a wide bin range.

An advantage of the Lomb-Scargle periodogram is that the data can contain, in principle, any number of bins and any number of profiles, subject to memory constraints. This is not the case with the Principal Component Analysis subroutine *PCATEST*, as described below.

3.5.2 Method

Due to the complexity of options involved, *LOMBPERIOD* is quite a complex program. It also requires a significant amount of memory in order to run at a reasonable speed.

LOMBPERIOD works as follows. First, the program reads in the observation times for the profiles from disk. It then reads in the profile data into a two-dimensional array, with an element for each phase bin of each profile. Having done this, it begins a loop over the range of bins specified, re-binning or smoothing the data as required as it goes. The data for the working bin is then passed through the *FASPER* subroutine, which performs a Lomb-Scargle period analysis (Press et al. 1992) and returns a list of powers over a range of frequencies. This

power spectrum is optionally plotted, then written to file. Once this has been calculated for all bins in the range, the program calculates the probability factor m using the *GETM* and *FINDM* subroutines (as explained below), and draws a two-dimensional grey-scale plot of the power as a function of pulse phase (bin number) and frequency.

Once the plotting subroutine has been called, the plot size is adjusted, either as defined in the user settings, or reduced to a 512×512 pixel array, in order to avoid overflows in the *PGPLOT* subroutines used for plotting. Each bin can then be normalised with respect to its maximum value, and/or presented on a log-scale, with a user chosen base, in order to improve clarity. Depending on whether the user has chosen to pause the program when a graph is output, the plot is halted, allowing the user to output a GIF or PS file, or zoom in on a specific region of the plot.

Having created a plot, the program then calculates the r.m.s. of the power array, then sorts the array by power in descending order, to determine the bins and frequencies showing a maximum in power, which corresponds to a strong periodicity. It writes the first 1024 records out to a file for viewing or plotting.

3.5.3 The *FASPER* subroutine

The *FASPER* subroutine is one of the *Numerical Subroutines* subroutines (Press et al. 1992). It allows a spectral analysis to be performed on data with uneven sampling — as is usually the case with observational data. Aside from input arrays of data and observation times, it requires two parameters: *ofac*, an over-sampling factor, and *hifac*, the high-factor ratio. Details on the use of these are both included in depth in the *Numerical Subroutines* documentation. They combine to give the number of frequencies output from the subroutine. Typically, these are set to 4.0 and 0.99 for our purposes, although *hifac* can be increased

to allow sampling at frequencies greater than the Nyquist frequency of the data, which is possible since our data are significantly unevenly sampled.

FASPER also returns an estimated probability for the data, but this critically depends on the factor, m, found using the method below; hence the probabilities given directly by *FASPER* are not used.

3.5.4 Signal Significance

It is obviously important that we establish whether any results from *FASPER* are significant. The probability, P, that a periodicity of a given power, z, is due to noise is given by (Press et al. 1992):

$$P(> z) = 1 - (1 - \exp(-z))^m \tag{3.5}$$

where the power m depends on the number and regularity of the sampling of the data points. m can be found through Monte-Carlo simulations. However, we can obtain an independent estimator of m from our off-pulse data, which is of the same sampling and should be entirely composed of noise. Having found this m, we can therefore estimate the likelihood that a periodicity detected in due to noise or a real signal.

Finding m from our off-pulse data is comparatively simple, as the pulse window is defined using the template creation method described under *READDB*. Taking the periodicity with the highest power for each bin, *GETM* then forms a cumulative histogram of power for the entire off-pulse data, then *FINDM* fits a value of m using equation 3.5.

For evenly sampled data, m should be equal to the number of data points. However, as the data points become more and more 'clumped' in time, m decreases. We find that, for a typical sample of 400 profiles, m tends to be roughly 100.

3.5.5 A Note on Memory

The *LOMBPERIOD* sub-package requires a considerable amount of memory to run. An intrinsic problem of Fortran 77 is the lack of re-allocating memory to an array that has already been declared in order to change the size. Certain compilers also have issues with allocating an amount of memory that is found during run-time to an array. This practice has been kept to a minimum, but is required for certain arrays to conserve memory. If this step had not been taken, the amount of memory required for a full analysis would run into several gigabytes. We therefore have limited the number of processable profiles to 4096 throughout the program, each with a maximum of 4096 bins. Therefore, to store our input data alone, we require 128MB of memory for an eight-byte REAL array. The size of the frequency and power arrays calculated by *FASPER* is given by:

$$n_{dim} = 2 \cdot n_{freq}, \tag{3.6}$$

where n_{freq} is the power of two immediately greater than n_{freqt}, which is given by:

$$n_{freqt} = \frac{ofac \cdot hifac \cdot MACC \cdot n_{prof}}{2}, \tag{3.7}$$

where $MACC$ is the number of points per quarter frequency (see Press et al. 1992), and is set to 4; n_{bins} is the number of bins (after re-binning); and $hifac$ and $ofac$ are as described above. Our power array must therefore take up $n_{bins} \times n_{dim} \times 8$ bytes. Typically 25.6 MB is required for 400 profiles at 400 bins each, although this can increase up to around 4 GB for 4096 profiles at 4096 bins and $hifac = 8$. For this reason, the memory for this array is allocated at the start of *POWERPLOTTER* (an extension to *LOMBPERIOD*).

A further $n_{dim} \times n_{bins} \times 8$ bytes must be available twice over in the statistical analysis for sorting purposes.

All told, the program will require several hundred megabytes, and possibly

several gigabytes, of memory to run. This is not usually a problem on modern computers, although the swap file size must be sufficiently large.

3.6 PCATEST

3.6.1 Function and Parameters

The *PCATEST* subroutine is the second of the two main analysis procedures encompassed by this software. Its purpose is to perform a Principal Component Analysis test on the cross-correlated database profiles.

Due to its purely mathematical nature, the only options defined for this subroutine are the names of the output files it produces, and whether or not to try to reproduce the original data from the principal components as a check that the subroutine has performed as expected.

In this routine, we use a method similar to that set out in the PhD thesis of Michael Blaskiewicz (1991).

3.6.2 Theory

Principal Component Analysis, commonly used in image compression, relies on the basis that a residual pulse profile, $\delta\mathbf{v}_j$, can be thought of as a real vector quantity of n_{bins} dimensions. Thus, each vector can be thought of as comprising of n_{bins} different, orthogonal vectors, $\mathbf{E}$, of n_{bins} dimensions, such that:

$$\delta\mathbf{v}_j = \sum_{j=1}^{n_{bins}} \mathbf{E}_j \left(\mathbf{E}_j \cdot \delta\mathbf{v}\right). \tag{3.8}$$

The choice of vectors E is made such that, for a particular vector, k, $\mathbf{E}_k \cdot \mathbf{E}_k = 1$ and σ_k^2 is maximised, where:

$$\sigma_k^2 = \sum_{j=1}^{n_{prof}} w_j \left(\mathbf{E}_k \cdot \delta\mathbf{v}_j\right)^2, \tag{3.9}$$

for profile j. The solutions to this are the eigenvectors of the covariance matrix of the data, i.e.:

$$\sum_{j=1}^{n_{bins}} C_{ij}E_{jk} = \sigma_k^2 E_{ik}, \tag{3.10}$$

where C_{ij} is the covariance between bins i and j, given by:

$$\mathbf{C}_{ij} = \frac{\sum_{k=1}^{n_{prof}} w_j * \delta v_{ki} * \delta v_{kj}}{n_{prof} - 1}, \tag{3.11}$$

Thus, the eigenvector matrix, E, is the component matrix. By sorting these components in decreasing order, according to their eigenvalue, we can identify the *principal* components, i.e. those which contribute most to the residual profiles, as being the eigenvectors with the lowest index (corresponding to the highest eigenvalue).

A new dataset, $\mathbf{rv}$, can then be obtained by performing a vector multiplication of the original residual profiles with the sorted eigenvector matrix, $\mathbf{E}^s$:

$$rv_j(k) = \sum_{i=1}^{n_{bins}} \delta v_{ik} E^s_{ij}. \tag{3.12}$$

This matrix will be the residual profile matrix in terms of the principal components, e.g. $rv_j(1)$ will be the amplitude of the first (principal) component in the jth profile.

3.6.3 Method

To begin with, *PCATEST* reads in the profiles, $\mathbf{v}$, created using *DORESID*, into an array of size n_{bins} by n_{prof}. It then reads in statistical weighting data for the profiles, $\mathbf{w}$. In our analysis, we use uniform weighting, but a weighting based on, for example, signal-to-noise ratio could theoretically be used instead. For each bin, a mean value ($\bar{\mathbf{v}}$) is calculated and subtracted from the data, leaving a data array of 'residual' profiles, $\delta\mathbf{v}$, with a mean of zero. Thus for each profile, j:

$$\delta\mathbf{v}_j = \mathbf{v}_j - \bar{\mathbf{v}}. \tag{3.13}$$

PCATEST then calculates the covariance between each pair of bins and forms a matrix, **C**, as satisfied by equation 3.11. The eigenvectors of this matrix, **E**, and their corresponding eigenvalues, henceforth denoted **e**, are then found. To do this, we use the *Numerical Subroutines* subroutine *JACOBI* (Press et al. 1992). *JACOBI* also has the added advantage of returning the eigenvectors as unit-length eigenvectors.

These eigenvectors are then sorted in descending order, according to the magnitude of their corresponding eigenvalue, to form a new eigenvector matrix, $\mathbf{E}^s$, using a modified version of the *Numerical Recipes* subroutine *SORT2*. This sorted eigenvector matrix contains the principal components, in descending order of significance. *PCATEST* then performs the transformation described in equation 3.12 to find the significance levels of the principal components.

The conversion from having data in terms of principal components to the original dataset is easy, and one that is optionally done here as a method of checking that the subroutine has worked correctly. The conversion is simply given by:

$$v_{ij} = \sum_{k=1}^{n_{bins}} E^s_{ik} rv_{kj}. \tag{3.14}$$

The new dataset is then written to file.

PCATEST then calls *FASPER* (as used in *LOMBPERIOD* above) to perform a spectral analysis on the amplitude of the principal component over all profiles (rv_{1j}). *FASPER* yields an array of powers for a range of frequencies; the highest power corresponding to the most significant periodicity. This allows us to find the regular changes in pulse shape associated with precession.

3.6.4 Restrictions of *PCATEST*

A major restriction of *PCATEST* is the number of profiles that can be analysed. This must not exceed the number of bins in the profile. A further complication is

that, strictly speaking, a number of bins should be cut from the profile in order to find an independent estimate of the noise level of the profiles in order to find the significance of the components, as described below.

If a number of profiles greater than the number of bins used in the analysis is used, it will require a greater number of eigenvectors to represent them. It therefore cannot be guaranteed that all principal components will be represented. By passing an increasing number of profiles through *PCATEST*, then reconstructing them using the eigenvectors, it can be seen that the profiles represent the data less and less accurately as we increase the number of profiles beyond the number of bins.

On the other hand, if the number of profiles used is *less* than the number of *used* bins, then principal component analysis will still be able to reproduce the dataset with n_{bins} non-zero, orthogonal components.

Despite this substantial drawback, principal component analysis has one unique advantage over the direct Lomb-Scargle periodogram used in *LOMBPERIOD*: it also gives the user information, not only on the strength and period of the variation, but on exactly how the profiles vary over time, allowing detected periodicities due to factors other than precession to be weeded out.

3.6.5 Finding the Significance Levels of Components

The significance level of the components is found by comparing the first two principal components with a Gaussian noise model of the same width.

To do this, we represent the two most principal components, denoted rv_1 and rv_2, as a two-dimensional plot. We then calculate the mean and standard deviation for both rv_1 and rv_2. For pulsars that are not precessing, we expect a plot of rv_1/rv_2 to be purely noise, hence distributed as a Gaussian. We then use the *Numerical Recipes* (Press et al. 1992) subroutine *ks2d1s* to perform a

Kolmogorov-Smirnov test to compare our rv_1/rv_2 plot with a Gaussian model of the same centre and standard deviation. *ks2d1s* returns an estimate of the significance of a match between our dataset and the noise model, which can be interpreted as a probability that shape changes are not occurring in the pulsar.

3.6.6 Additional Tests

3.6.6.1 The Output of *PCATEST*

Of course, identifying change in principal components is only the first stage. Finding one or more significant components only means that we know the pulse profile is changing. This could be due to a variety of factors, such as those explained in Chapter 2. To identify precessing pulsars from pulsars exhibiting profile shape changes for other reasons, we need to know *how* the profile is changing. There are several further tests we can subject the data to in order to do this.

3.6.6.2 rv_1 vs. Time

One useful plot we can make is of rv_1, the contribution of the most principal component to the data, as a function of time. Using this, we can see the primary variations in the pulse profile one would expect from interference such as changes in instrumental errors, long-term moding, etc., and separate them from those we would expect to find from precession.

For a precessing pulsar we would expect to find a sinusoidal, or at the very least pseudo-sinusoidal, variation in the rv_1/time plot, although this may be complicated by other, less significant principal components, or by systemic changes in our receiver setup. Changes in instrumental errors could occur on long or short timescales, hence could manifest themselves as either white noise (which could form co-incidentally to appear to be periodic for large enough samples), or as step functions or similar patterns, respectively.

3.6.6.3 rv_1 vs. rv_2

More information can be gleaned from the $rv_1 - rv_2$ plot — i.e. plotting the contributions of the first two significant components against each other. By doing this, we can tell how the profile is changing between its extrema. For a moding pulsar, we should expect to see two or more large 'islands' in this plot, corresponding to the different modes. For a precessing pulsar, these islands would be connected be a weak bridge as the profile moves (pseudo-)sinusoidally between two extrema. For noise and most instrumental effects (including insufficient integration time for noisy pulsars, or pulsars moding on short timescales), one would expect to find a noisy, Gaussian-like $rv_1 - rv_2$ plot.

This plot can be used in conjunction with the rv_1 – time plot in order to identify true variations from statistical noise by matching visual variations in periodicity observed in the rv_1 – time plot with islands observed in the $rv_1 - rv_2$ plot. For complex changes in pulse profile, an rv_1 – rv_2 – rv_3 plot, in three dimensions, can also be useful.

3.6.6.4 Lomb-Scargle Periodogram of rv_1

Naturally, for precessing pulsars, one of the key features is that the pulsars are periodic in the nature of their profile changes. By constructing a Lomb-Scargle periodogram of rv_1, we can identify periodicities in the principal component. If we suspect that a pulsar is varying periodically, we can use this to identify at what rate the variation is taking place.

This stage is performed automatically by *PCATEST*. We again use the *Numerical Recipes* subroutine *FASPER* (Press et al. 1992).

For this plot, as for the above plots, it may also be instructive to plot successive components, e.g. a periodogram of rv_2 and rv_3, etc., to identify secondary changes in pulsar profile, which could be due to a combination of factors, such as precession

on multiple periods, or moding superimposed on precessional change, or similar factors.

3.6.7 Note on Analysis

We expect that pulsars that exhibit precession should show concurrent periodicities using both *LOMBPERIOD* and *PCATEST*. We also expect them to show *periodic* (or quasi-periodic) changes of one or more principal components over time. In addition to this, we also expect the timing residuals of the pulsars to show (pseudo-)sinusoidal variations, which we can again test with *FASPER*. Therefore, in order to be certain that precession exists we must find changes in all of the above.

Chapter 4

Application and Results

4.1 The Data

4.1.1 Jodrell Bank Pulsar Database

Jodrell Bank's pulsar database contains timing and profile data for all the pulsars observed at Jodrell Bank using the Mk I Lovell, Mk II and 42-foot telescopes as far back as 1978. This unique dataset provides the basis for a major study of precessing pulsars in the Northern (and a significant part of the Southern) Sky.

The database covers several hundred pulsars down to a declination of about -30, thus covering three-quarters of the sky. The majority of these pulsars are concentrated in the Galactic Plane and near the Galactic Centre. Although this is a true concentration, due to the shape of the galaxy and our location in it, it is enhanced by the fact that search surveys, such as the Parkers survey, concentrate in this area. This is a potentially important selection effect.

The data is stored in an internal format, which can be converted to the EPN format (Lorimer et al. 1998) used in the program using the program PSRPROF. This allows a concatenated EPN file containing all the information on profile changes to be created.

4.1.2 Our Analysis

Our analysis covered 644 pulsars from the database, each with several years of data from the Mk I Lovell and Mk II telescopes at Jodrell Bank (the vast majority of these are from the Lovell telescope, with the Mark II telescope being used to 'fill-in' during the upgrade of the Lovell telescope). A total of 15 of these pulsars also had data taken on a near-daily basis using the 42-foot telescope, also at Jodrell Bank.

Since periodicity searches require a statistically significant number of profiles in order to produce convincing results, a criterium was put in place that a full analysis was only performed on pulsars with (arbitrarily) 15 or more "suitable" observations. In this context, suitable means that the profiles are in the correct frequency range and of sufficient signal-to-noise. The frequency criterium was necessary as pulse profiles are known to change dramatically with frequency. The majority of the observations available were taken in the L-band; thus, a range of 1400 ± 100 MHz was deemed acceptable. The exception to this was the 42-foot data, for which a range of 600 ± 50 MHz was used. The signal-to-noise criterium was put in place to avoid including non-detections and observations contaminated by RFI. Here, a signal-to-noise ratio (peak to r.m.s.) of 12 or more (again chosen somewhat arbitrarily, see below) was required to 'pass' a profile.

A total of 281 pulsars passed these selection criteria and ran successfully through the program for the Lovell/Mk II data, as well as nine pulsars for the 42-foot data. There was insufficient memory to cover the Crab Pulsar (B0531+21) on the Lovell/Mk II data, and B1929+10, B0950+08, B1133+16, B1933+16, B1642−03 and B0329+54 on the 42-foot data. For that reason, the data for these pulsars were split into 1000-day sections and each section analysed separately.

A brief analysis was also done of the timing residuals for the most significant pulsars. While all the available data was used in our profile shape analysis, the

timing residual data extends over a greater period of time, and does not require such a high signal-to-noise to fit a timing point. We have therefore used this data to better corroborate (or refute) any significant frequencies we have found.

4.1.3 Excluded Data

During initial trials of the program, we found a number of periodicities present around 4000 days in a significant proportion of the pulsars. Further inspection of the data found that they were caused by changes in the filterbanks used. Due to the dispersion of the signal by the interstellar medium (see Chapter 1), the increased bandwidth caused an extra 'smearing' of the signal in the time-domain, resulting in a wider (hence differently shaped) profile.

From the observation log books at Jodrell Bank, we identified changes from a 32×1 MHz filterbank to a 40×1 MHz filterbank and back between around 5th August 1988 and on 18th August 1989. A similar change was noted to a 32×3 MHz filterbank between roughly 4 November 1997 and 21st August 1999. Several other changes were noted, in particular a major hardware upgrade in December 1988 – January 1989. A multi-beam receiver, which uses X and Y linear polarisation, instead of L and R circular polarisation, has also been used on the telescope from time to time. Additionally, prior to the 1997 changeover, the filterbank used a four-channel L, R, Q and U polarisation input, whereas afterwards a L, L, R, R polarisation input has been used. In this study, we only deal with intensity measurements, so polarisation should not affect our data unless the gains of the polarised receivers are incorrect at the time of observation. However, as can be seen in individual cases in Chapter 5, the differences between the pre-1997 and current filterbanks are sufficient to make a substantial difference to some pulsars, which is reflected in our data.

The solution to this problem was to exclude the data during the periods in

which the 32×1 MHz filterbank setup was not used, this data consequently ranges from approximately MJD 50760 to 51415, and from MJD 47380 to 47760.

4.2 Lomb-Scargle Periodogram Results

4.2.1 Effectiveness from Monte-Carlo Simulations

Monte-Carlo simulations were performed using the fake profile generator (*MAKE-MODEL*, see Chapter 3) to assess the effectiveness and limitations of the analysis used. Our tests used models optimised for maximum detectability in order to set lower limits on what we can expect to detect.

For these simulations, we used a model of the emission cone of an B1828−11 - type pulsar. For this model, we created 500 profiles of 512 bins with varying signal to noise. We modelled the emission cone as a nested cone structure, comprising of a hollow cone with a central component. This is unlike the single component of B1828−11, but it is easier to detect changes in this system, as normalisation of the profiles does not result in losing changes in flux density. The beam was characterised by a Gaussian central component with a full-width half-maximum (FWHM) of 3°, and a second, hollow component with a cone radius of 9°.9 (typical for a pulsar with the period of B1828−11), a 3° FWHM and an amplitude 20% of the central component. A line-of-sight cut was taken 1° from the centre of this beam. The variation in this can be seen in Figure 4.1.

Precession was simulated by inserting a sinusoidal variation into the offset of the line-of-sight cut from the centre of the beam. Tests were conducted with differing amounts of white noise added to the profiles, to simulate differing signal-to-noise (S/N) ratios. These are presented in Figure 4.2. Tests were also conducted for different amplitudes of sinusoidal variation, representing different amounts of precession. These are presented in Figure 4.3. The precession period used in

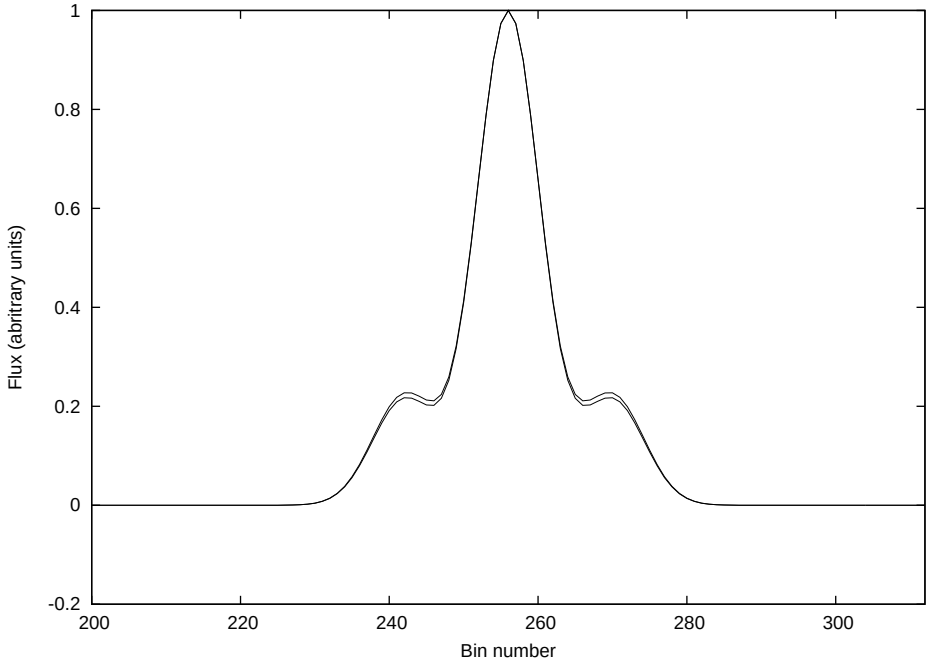

Figure 4.1: The variation of profiles in our Monte-Carlo simulation can be seen in the above plot. This shows two profiles, representing a change in our line of sight of 0°.5 from a beam characteristic of an 1828-11 -type pulsar.

these tests was 250 days, with a varying sampling time between 9.5 and 10.5 days. 'Clumping' of data was avoided to maximise detection to allow lower limits to be set, and S/N was taken to be constant; which is true to first order for an unchanging receiver setup, providing the pulsar maintains constant flux density and neglecting scintillation.

Detection was measured using the 'probabilities' given by the *FASPER* subroutine (Press et al. 1992). This is described as the approximate probability that a detection is due to random variations and is not inherently real, also referred to as a 'null probability'. For convenience, a scale of 'detectability' was used, given by:

$$Detectability = -\log(NullProbability). \tag{4.1}$$

Limits in computing accuracy mean that low probabilities are not always calculable. In these cases, the detectability has been set to 16.7, which is above this

limit.

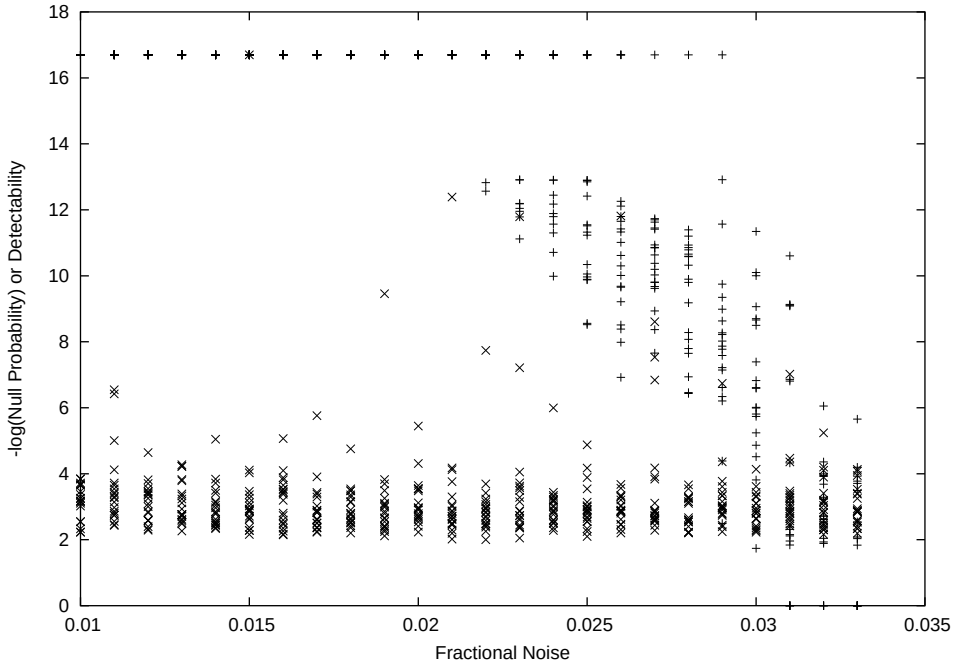

Figure 4.2: This figure shows how the effectiveness of Lomb-Scargle varies as the signal-to-noise ratio is changed, as obtained from Monte-Carlo simulations. The 'plus' signs represent detections and their corresponding 'probabilities' as inferred from the power obtained using *LOMBPERIOD* (see Chapter 3); the crosses represent the highest 'probability' value of false detections (over 5% different from true period). For an B1828–11 -type pulsar with 500 suitable profiles, we can see the detections are comparable to noise below about a fractional noise level of 0.03-0.035, corresponding to a S/N level of 29-33. Refer to the text for details of the model used and for a full description of the 'probabilities' found.

As can be seen from Figure 4.2, even under these near-ideal conditions, Lomb-Scargle requires a S/N ratio of at least ˜30 to detect a 0°.5 precession of our model pulsar. There are a number of situations, however, where a lower S/N ratio should still produce good periodicities. Such circumstances could include more complex emission cones, or cones that show patchy emission, or pulsars whose flux density (and hence S/N) varies with precession angle. There appears to be little harm in adding low S/N profiles to otherwise high S/N data; thus, to account for this and to allow for more complex profiles that may have patchy emission or other more readily changeable structures, while ensuring that RFI (radio frequency

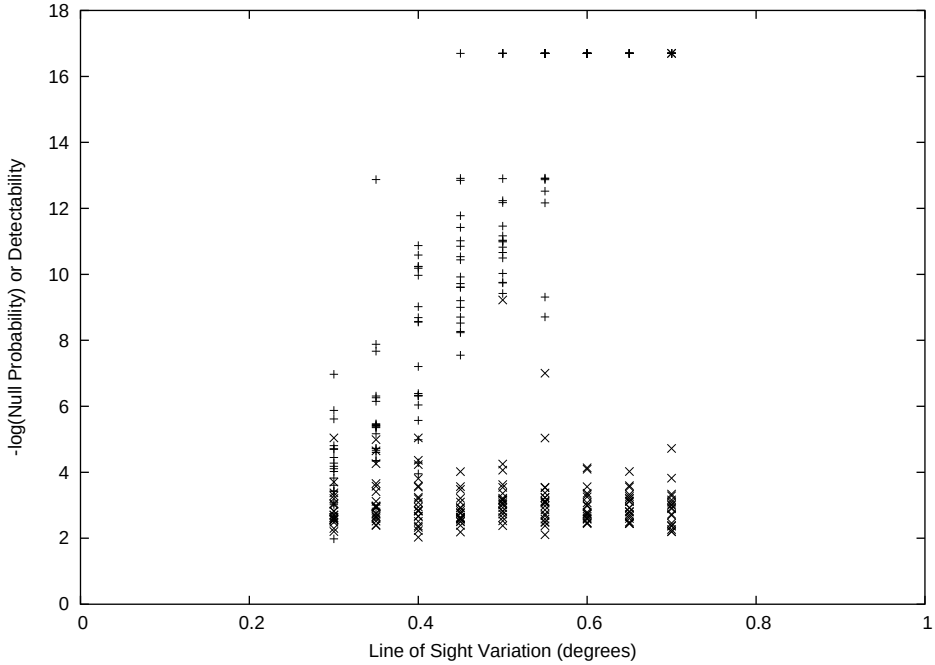

Figure 4.3: This figure shows how the effectiveness of Lomb-Scargle varies as the amount of precession is changed. The symbols are as in the previous figure. This simulation assumes a varying cut through a hollow emission cone as characterised by an 1828-11 -type pulsar, as described in the text. We can see that detection 'probabilities' become comparable with false detection 'probabilities' between 0.3-0.4 degrees of precession.

interference) and other noise sources were kept to a minimum, a S/N limit of 12 was set for our results using the database.

We can also see from this Figure that, regardless of the S/N, the false detection level remains roughly constant. The mean level of false detections is at a probability of $10^{-3.2}$, with a 95% confidence level at $10^{-4.5}$. While this may be simplified, it gives us a rough cutoff for estimating significant results at a probability level of 10^{-4} to 10^{-5}. It is worth noting that most of the false detections that are found at high powers are attributable to harmonics or sub-harmonics of the precession period, with most of these being at twice the input precession period.

For a pulsar with a typical flux (such as 1828-11: 1.4 mJy at 1400 MHz), we

can expect an average S/N ratio of around 50. In Figure 4.3 we have plotted the detection probabilities for the test scenario for varying amplitudes of precession. We can see that, even for favourable conditions, clear evidence of precession only presents itself for pulsars with greater than 0°.6 precessional amplitude, with the detection limit being around 0°.3.

Again, it must be stressed that this is a simplified model. For pulsars with higher signal-to-noise, it should be possible to detect lower amounts of precession, and *vice versa*. Figure 4.2 shows that detectability is roughly a linear function of the fractional noise component. It will also depend on a number of other factors, such as the number of profiles available, the 'clumping' of the data, the number of precessional cycles observed, along with many other factors.

These tests also gave an indication as to the accuracy of the periodicities found. The accuracy was found to vary as a weak, approximately linear function of fractional noise, having an uncertainty of around 2.5% at a S/N ratio of 50 and 2% at a S/N ratio of 100 in the above tests. Independent tests also found it to be a function of the number of observed profiles, varying as roughly $(\textit{number of profiles})^{-1/2}$. It is useful also to note that the periods of the false detections are usually close to the sample rate of the data.

4.2.2 Results from the Database

4.2.2.1 Significant Pulsars

Of the 281 pulsars examined from the Lovell/Mk II database, 37 show periodicity detections more significant than our estimated 95% confidence level. These are presented in Table 4.1. The rough uncertainties in the periods given in this table, and in the rest of the Lomb-Scargle analysis, are given by:

$$\delta p = \frac{1}{4}\frac{p}{n_p} \tag{4.2}$$

where p is the period detected, n_p is the number of these periods covered by the data.

Pulsar Name	Detected Periods (days)	(days)	(days)	(days)	Detectability				N°of Periods Covered by Data			
J1713+0747	4705.3	4705.3	4705.3	1764.5	16.70	16.70	16.70	13.45	0.75	0.75	0.75	2.00
B1828–11	246.8	246.8	498.4	488.8	16.70	16.70	16.70	13.00	25.75	25.75	12.75	13.00
B1737–30	7214.3	7214.3	1154.3	189.8	16.70	16.70	5.90	3.96	1.00	1.00	6.25	38.00
B1830–08	5696.6	5696.6	7120.8	7120.8	16.70	13.32	10.24	8.72	1.25	1.25	1.00	1.00
B1821–19	6317.1	5264.3	1974.1	2105.7	16.70	12.16	6.19	3.60	1.25	1.50	4.00	3.75
B1933+16	16648.3	16648.3	5549.4	11098.9	12.96	10.58	10.18	6.83	0.50	0.50	1.50	0.75
B0144+59	310.2	310.2	69.5	1816.7	11.13	9.50	2.91	2.89	20.50	20.50	91.50	3.50
B1930+22	5312.2	5312.2	32.2	215.9	9.93	6.31	3.54	3.10	1.25	1.25	206.00	30.75
B1913+10	5379.9	5379.9	43.6	41.0	8.62	7.80	2.75	2.38	1.50	1.50	185.00	197.00
B1859+03	5069.8	6337.2	86.5	32.9	8.43	7.34	3.01	2.91	1.25	1.00	73.25	192.50
B1834–10	6544.1	6544.1	8725.4	2013.6	8.42	6.61	5.49	4.43	1.00	1.00	0.75	3.25
J1022+1001	4869.6	3652.2	202.9	21.5	7.59	5.03	2.06	2.02	0.75	1.00	18.00	170.00
B1742–30	6354.6	12709.1	651.8	462.2	7.09	4.05	3.61	3.29	1.00	0.50	9.75	13.75
J0631+1036	454.3	563.3	313.0	880.2	6.98	6.67	6.35	6.16	7.75	6.25	11.25	4.00
B0834+06	5048.1	6057.7	59.4	6057.7	6.96	4.21	3.25	2.81	1.50	1.25	127.50	1.25

Continued on next page

Table 4.1 — continued from previous page

Pulsar Name	Detected Periods (days)	(days)	(days)	(days)	Detectability				N°of Periods Covered by Data			
B1838–04	4801.6	5762.0	38.2	51.4	6.58	3.72	2.60	2.34	1.50	1.25	188.75	140.00
B0919+06	15128.6	133.3	2017.1	55.7	6.40	2.65	2.58	1.94	0.50	56.75	3.75	135.75
B0525+21	17004.7	11336.5	51.9	3400.9	6.37	4.29	2.63	2.59	0.50	0.75	163.75	2.50
B1826–17	6307.9	6307.9	1940.9	6307.9	6.36	5.25	3.74	3.27	1.00	1.00	3.25	1.00
B1822–09	6686.5	16716.3	434.2	65.6	6.10	5.49	2.55	2.51	1.25	0.50	19.25	127.50
J2043+2740	6518.1	1086.4	2172.7	931.2	5.83	4.68	4.36	3.12	0.50	3.00	1.50	3.50
B1620–26	5593.6	154.3	5593.6	65.8	5.69	4.49	4.03	2.84	1.00	36.25	1.00	85.00
B1756–22	5077.4	5077.4	68.4	72.7	5.61	4.09	2.02	1.98	1.25	1.25	92.75	87.25
B1931+24	920.3	285.6	37.3	36.2	5.40	2.98	2.86	2.36	2.25	7.25	55.50	57.25
B1929+10	8451.3	11268.4	184.7	62.4	5.39	4.99	2.17	2.08	1.00	0.75	45.75	135.50
J1835–1031	1935.5	967.7	967.7	38.7	5.26	4.63	3.05	1.86	1.00	2.00	2.00	50.00
B0621–04	11185.4	3195.8	1597.9	272.8	5.20	4.96	2.76	2.74	0.50	1.75	3.50	20.50
B0740–28	59.9	133.0	60.2	133.5	5.13	4.86	4.54	4.46	143.75	64.75	143.00	64.50
B1133+16	56.5	3776.2	68.7	128.0	5.08	4.87	4.78	4.36	133.75	2.00	110.00	59.00

Continued on next page

Table 4.1 — continued from previous page

Pulsar Name	Detected Periods (days)	(days)	(days)	(days)	Detectability				N°of Periods Covered by Data			
B0818–13	15128.7	15128.7	360.2	1592.5	5.01	4.71	3.13	2.49	0.50	0.50	21.00	4.75
B2255+58	8480.7	3634.6	1817.3	669.5	4.95	3.67	2.53	2.26	0.75	1.75	3.50	9.50
B0329+54	54.3	127.9	123.1	325.3	4.90	4.45	4.36	3.70	104.75	44.50	46.25	17.50
B2053+21	618.6	8454.1	85.7	258.8	4.88	4.65	4.53	4.49	10.25	0.75	74.00	24.50
B1732–07	122.2	82.2	223.6	54.8	4.66	4.44	4.11	4.09	45.75	68.00	25.00	102.00
B2020+28	10068.2	10068.2	10068.2	1006.8	4.65	4.38	4.10	3.47	0.75	0.75	0.75	7.50
B2045–16	3774.3	228.7	44.0	67.5	4.55	2.74	2.64	2.58	2.00	33.00	171.75	111.75
B2035+36	3102.4	10858.3	1085.8	3102.4	4.51	3.66	3.22	3.20	1.75	0.50	5.00	1.75

Table 4.1: Periodicities derived from a Lomb-Scargle periodogram analysis of the Jodrell Bank pulsar database, along with the strength of the periodicity, as given by their 'detectability' (described in the text), and the number of periods covered by the data.

While individual cases will be dealt with in the next chapter, it is worth emphasising here that, due to the sensitivity and timescale of the measurements we are making, it is certain that not all of the above periodicities are attributable to precession: many will be caused by instrumental changes, such as the filterbank changes described above, or by processing artifacts to do with the timespan of the available data, while others will be caused be real effects in the pulsar, such as moding.

4.2.2.2 Data from the 42-foot Telescope

Significant results were also found from data taken using the 42-foot telescope. The changes in configuration over the last 20 years have been minor, so this should represent an accurate source of data for changes in pulse profile shape.

The data for several of these pulsars is too large to be analysed in one run, so the data for each pulsar was split into 1000-day segments and each segment analysed separately. The results are shown in Table 4.2.

Start MJD '000s	Pulsar Name	N° profiles used	Detected Periods (days)	(days)	(days)	(days)	Detectability				N°of Periods Covered by Data			
48	B0329+54	774	47.5	44.3	45.3	64.6	12.54	10.09	8.36	6.97	20.73	22.23	21.74	15.24
49	B0329+54	899	80.0	125.0	88.9	97.6	15.00	12.62	8.93	8.86	12.50	8.00	11.25	10.25
50	B0329+54	643	276.0	112.4	178.6	758.9	15.00	10.39	9.96	8.21	2.75	6.75	4.25	1.00
51	B0329+54	540	291.7	583.4	89.8	86.4	15.00	8.36	6.12	5.64	2.00	1.00	6.50	6.75
52	B0329+54	820	74.1	363.7	571.6	190.5	15.00	15.00	12.02	8.74	13.50	2.75	1.75	5.25
53	B0329+54	477	199.5	498.6	51.1	199.5	11.45	11.36	11.35	11.05	2.50	1.00	9.76	2.50
47	B0950+08	83	83.3	83.3	83.3	83.3	5.24	4.97	4.89	4.80	10.52	10.52	10.52	10.52
48	B0950+08	506	652.8	652.8	652.8	186.5	7.76	6.05	5.92	5.07	0.11	0.11	0.11	0.38
49	B0950+08	618	3.3	665.5	8.1	3.7	2.35	2.31	2.22	2.22	230.58	1.14	93.94	205.65
50	B0950+08	404	4.6	736.0	41.5	2.4	3.10	2.65	2.31	2.29	57.45	0.36	6.37	110.11
51	B0950+08	389	388.9	466.7	5.5	1.7	15.00	2.84	2.26	2.26	0.48	0.40	34.09	110.28
52	B0950+08	517	2.9	6.9	3.4	88.6	3.35	2.81	2.62	2.52	337.64	141.91	287.99	11.05
53	B0950+08	304	4.4	21.1	4.2	9.0	2.45	2.08	1.89	1.85	226.88	47.31	237.68	110.92

Continued on next page

Table 4.2 — continued from previous page

Start MJD '000s	Pulsar Name	N^o profiles used	Detected Periods (days)				Detectability				N^{o}of Periods Covered by Data			
47	B1133+16	61	3.8	5.3	4.2	3.9	2.14	1.74	1.70	1.68	153.53	110.08	138.91	149.59
48	B1133+16	578	356.1	979.2	979.2	178.0	15.00	4.70	3.91	2.57	2.80	1.02	1.02	5.60
49	B1133+16	600	571.0	499.6	363.4	41.2	15.00	7.73	3.38	3.09	0.87	0.99	1.36	12.03
50	B1133+16	406	726.0	2.3	2.0	2.0	9.56	2.39	2.35	2.31	0.26	80.65	92.75	92.75
51	B1133+16	435	97.2	129.6	145.9	10.2	15.00	5.71	3.75	2.98	10.07	7.56	6.71	96.00
52	B1133+16	525	68.4	77.8	59.2	86.3	9.72	7.36	4.57	3.88	14.61	12.84	16.88	11.58
53	B1133+16	241	46.5	381.4	2.6	4.4	15.00	4.52	2.55	2.52	15.61	1.90	279.24	165.00
47	B1642–03	98	7.2	2.4	19.2	30.0	2.20	1.85	1.64	1.58	137.82	413.45	51.68	33.08
48	B1642–03	722	2.1	1.9	38.8	2.8	2.68	2.46	2.12	1.97	227.00	250.89	12.29	170.25
49	B1642–03	814	1.6	2.6	10.9	3.2	2.62	2.53	2.31	2.22	371.49	228.61	54.53	185.74
50	B1642–03	586	2.0	1.6	2.7	77.8	12.97	4.17	3.81	2.73	93.74	117.18	69.44	2.41
51	B1642–03	517	2.0	4.9	1.3	26.2	7.65	2.46	2.45	2.43	489.56	199.82	753.17	37.37
52	B1642–03	698	4.4	1.7	2.3	14.0	3.34	2.68	2.63	1.98	227.33	588.39	434.90	71.45
53	B1642–03	413	481.7	1.3	481.7	4.5	2.15	2.11	2.11	2.04	1.58	583.79	1.58	168.65

Continued on next page

Table 4.2 — continued from previous page

Start MJD '000s	Pulsar Name	N° profiles used	Detected Periods (days)				Detectability				N°of Periods Covered by Data			
47	B1929+10	32	67.8	67.8	67.8	67.8	3.83	3.77	3.61	3.57	14.75	14.75	14.75	14.75
48	B1929+10	407	978.9	978.9	978.9	978.9	15.00	15.00	15.00	15.00	0.49	0.49	0.49	0.49
49	B1929+10	218	91.7	8.9	6.8	5.6	3.02	2.35	2.00	1.84	0.74	7.62	9.97	12.11
50	B1929+10	129	83.7	21.2	6.2	7.3	2.26	2.25	2.07	2.01	11.70	46.18	157.89	134.10
51	B1929+10	181	8.7	4.5	3.9	5.2	2.90	1.52	1.52	1.48	113.37	219.18	252.90	189.67
52	B1929+10	197	69.4	5.5	304.4	6.4	2.90	2.47	2.29	2.03	10.85	136.90	2.47	117.65
53	B1929+10	119	7.4	8.5	4.4	10.4	2.05	1.90	1.82	1.79	78.43	68.28	131.91	55.81
48	B1933+16	623	4.9	1.8	1.6	1.4	2.65	1.88	1.84	1.78	98.10	267.04	300.42	343.34
49	B1933+16	828	666.8	2.0	2.0	2.0	15.00	15.00	15.00	12.43	1.22	406.74	406.74	406.74
50	B1933+16	592	2.0	216.8	4.6	1.7	3.89	3.32	3.06	2.63	500.13	4.61	217.45	588.39
51	B1933+16	525	2.0	2.0	2.0	2.2	15.00	10.74	3.40	2.82	379.46	379.46	379.46	344.96
52	B1933+16	750	2.0	2.0	2.0	2.0	8.47	5.73	5.45	4.23	291.70	291.70	291.70	291.70
53	B1933+16	436	2.0	2.0	2.0	2.0	10.01	9.32	8.22	7.86	500.13	500.13	500.13	500.13

Continued on next page

Table 4.2 — continued from previous page

Start MJD '000s	Pulsar Name	N^o profiles used	Detected Periods (days)				Detectability				N^{o}of Periods Covered by Data			
	B0740–28	410	162.5	156.5	167.6	174.4	15.00	15.00	15.00	12.80	32.74	34.00	31.75	30.51
	B0355+54	63	149.5	308.1	109.9	338.9	3.88	3.81	3.66	3.61	34.00	16.50	46.25	15.00
	B1508+55	29	151.3	165.0	680.7	259.3	4.06	4.03	3.87	3.84	26.99	24.75	6.00	15.75

Table 4.2: Periodicities derived from a Lomb-Scargle periodogram analysis using data from the 42-foot telescope, as in Table 4.1. For all except the last three pulsars (which were analysed as described previously), the data was split into 1000-day chunks, with the start date (MJD/1000) shown in the left-most column. The number of profiles used is also shown — a small dataset reduces the chances of a periodicity being found.

4.2.2.3 Statistical Properties of the Significant Pulsars

Information about the observed pulsars was taken from the ATNF pulsar catalogue (Manchester et al. 2005)[1].

At first glance, there appears to be very little separating the aforementioned pulsars from the general population, and to a large extent, this is true. The only disparity between the 'periodic' and 'non-periodic' sets are in the flux received, the inferred pulsar luminosity, the estimated rate of energy loss ($\dot{E}$), the rate of change of period ($\dot{P}$) and the inferred age (t) of the pulsars. Naturally, the first three values are directly related, and it is expected that the fourth and fifth should be also.

As a comparison, the median values of pulsar flux at 1400 MHz are $10^{0.62\pm0.55}$ mJy and $10^{0.32\pm0.47}$ mJy for the 'periodic' and 'non-periodic' datasets, respectively, and similarly $10^{1.64\pm0.66}$ mJy and $10^{1.30\pm0.52}$ mJy at 400 MHz; the median inferred luminosities at 1400 MHz are $10^{1.62\pm0.80}$ mJy kpc^2 and $10^{1.37\pm0.74}$ mJy kpc^2; the median $\dot{E}$ are $10^{33.6\pm1.2}$ ergs/s and $10^{32.6\pm1.3}$ ergs/s; the median $\dot{P}$ are $10^{-14.2\pm1.6}$ and $10^{-14.6\pm1.3}$; and the median ages are $10^{6.1\pm1.2}$ yr and $10^{6.6\pm1.1}$ yr (all values given are median values with standard deviation).

From the above data, we conclude that the pulsars identified in the 'periodic' dataset are, by and large, representative of the dataset as a whole. There is a slight bias towards younger, brighter pulsars, but not enough to warrant concern. A full statistical analysis would be required to determine whether this bias is real, or a random bias in a small dataset. Since we do not necessarily believe many of the 'periodic' pulsars are precessing, this process is covered later in more detail.

We must therefore assess whether these periodicities are due to precession or not. As shown in the Monte-Carlo tests, most of the false detections happen at a period close to the sampling frequency, as can be seen in both tables 4.1 and

[1]Web Address: http://www.atnf.csiro.au/research/pulsar/psrcat

4.2, there are a number of very short periodicities, particularly in the latter case. There are also many longer periods, which could be part of a general trend, which is more linear than periodic in nature. In these cases, we must be very careful when assessing whether this is periodicity or not. The cases above are described individually in Chapter 5 and in the Appendix.

4.3 Principal Component Analysis Results

4.3.1 Effectiveness from Monte-Carlo Simulations

4.3.1.1 Simulation Data

Using the same Monte-Carlo simulations done for the Lomb-Scargle periodogram search, we have tested the efficiency with which our Principal Component Analysis software picks up variations in pulse profile. The results for this analysis are presented in Figures 4.4 through 4.9.

Figures 4.4 and 4.5 show how the strongest periodicity changes with changing signal to noise and precession amplitude for the system used in the Lomb-Scargle analysis. A fairly sharp cutoff can be seen in both cases. It could be that, at this point, the principal component is no longer the precessional variation, but a noise term instead, with the precessional variation being moved to a 'less principal' position, or being split among the noise terms.

Figures 4.6 and 4.7 show the corresponding detection levels, as given by the null probability. A clear cutoff can also be seen in these plots between the correctly found periods and the false detections, corresponding to a probability of around 10^{-3} to 10^{-4}. This gives a limit on how much we should believe any periodicities we obtain from Principal Component Analysis from the database.

Figures 4.8 and 4.9 show the probability of the departure of the rv_1/rv_2 plot

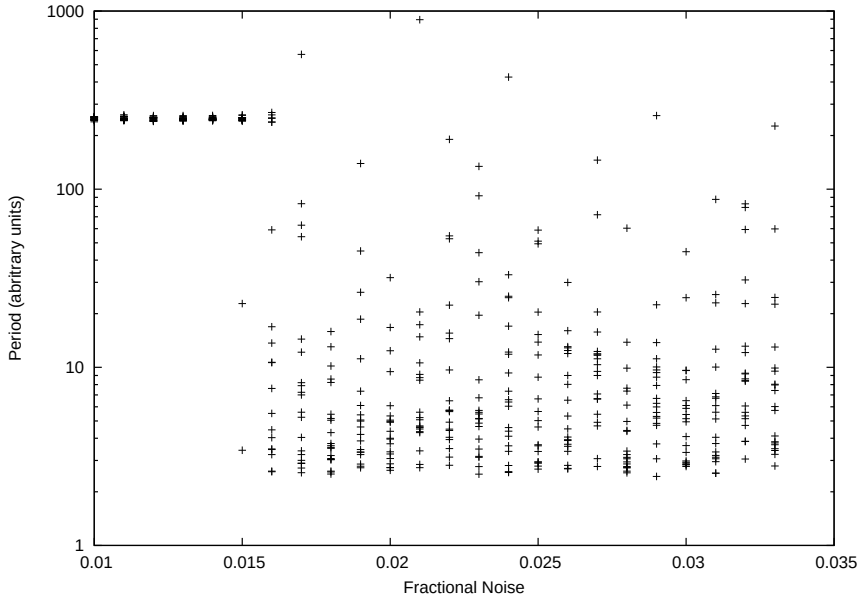

Figure 4.4: Detected periods as a function of fractional noise level for an input period of 250 units and a sample time of 5 units. Periodicities are correct up to around a fractional noise level of 0.015, corresponding to a S/N ratio of 67. An increasing spread of periods can be seen up to this point, with periods generally clustering towards the sample time beyond it.

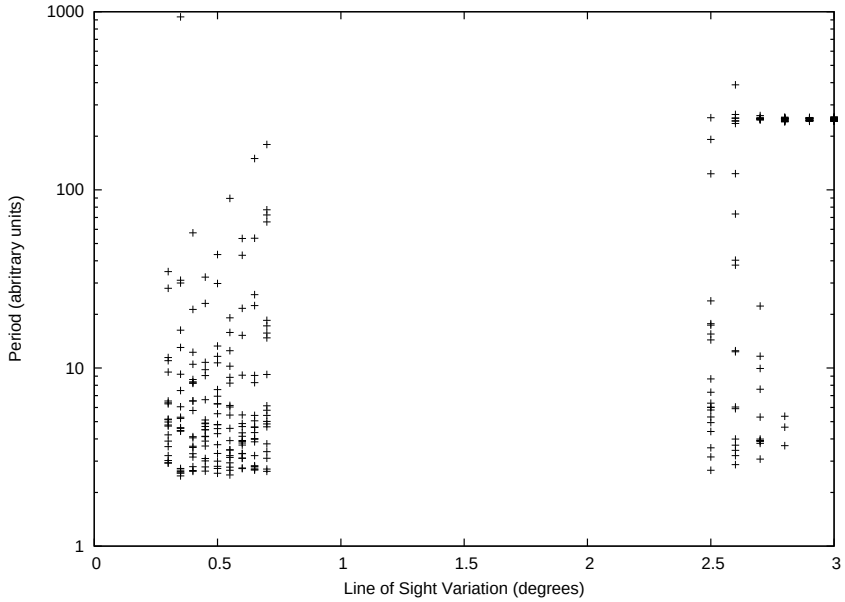

Figure 4.5: Detected periods as a function of precessional amplitude in degrees. Low amplitudes result in clustering around the sample time, as seen in Figure 4.4. Only for amplitudes greater than around 2°.6 is the true period picked up.

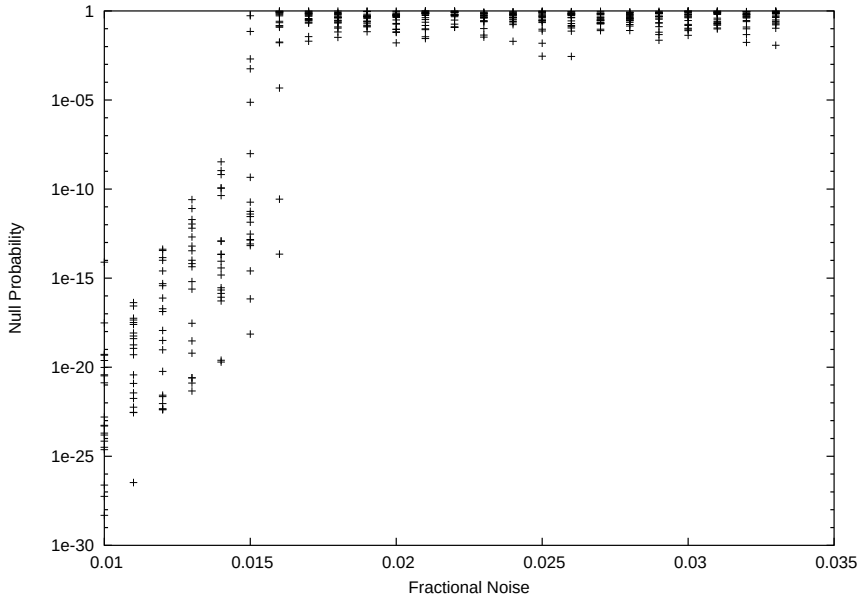

Figure 4.6: Periodicity strength, given as a function of null probability, or 'detectability' (see text). This figure accompanies Figure 4.4. The corresponding 'probability' cutoff for background noise is approximately 10^{-3} to 10^{-4}.

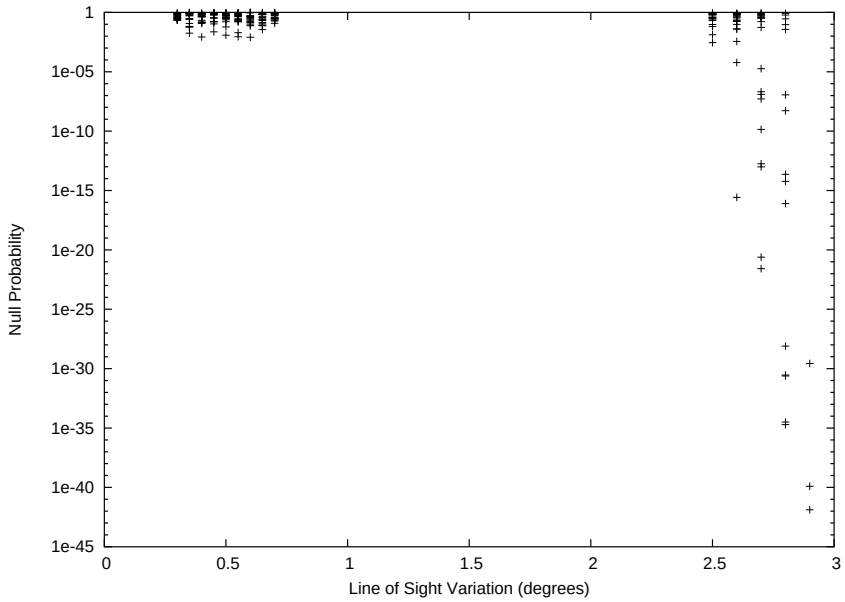

Figure 4.7: As Figure 4.6. This figure corresponds to Figure 4.5. The cutoff can again be seen at approximately 10^{-3} to 10^{-4}.

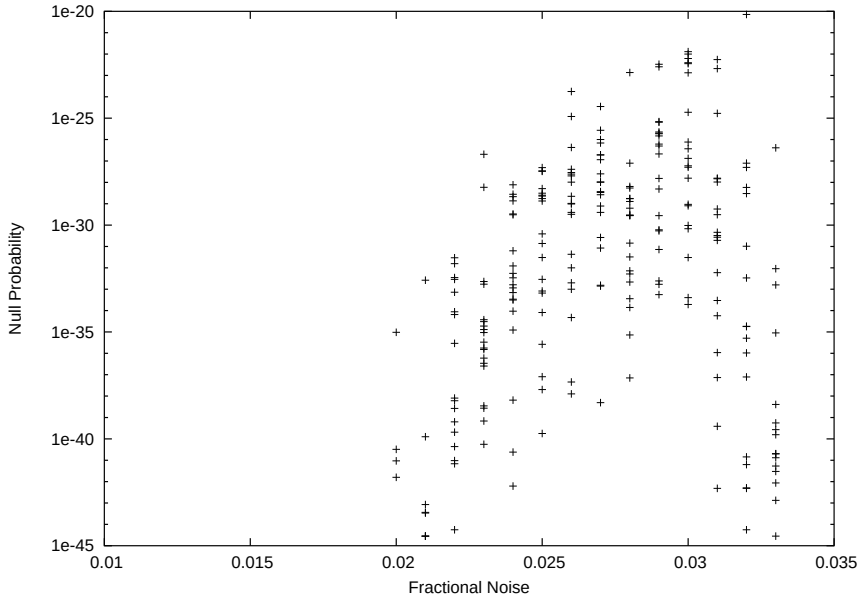

Figure 4.8: Null probabilities from a Kolmogorov-Smirnov test of the first two principal components as a function of fractional noise. An effective zero null probability can be seen for fractional noise levels of less than approximately 0.02. This gradually increases, then, remarkably, decreases again. The cause for this decrease is unknown.

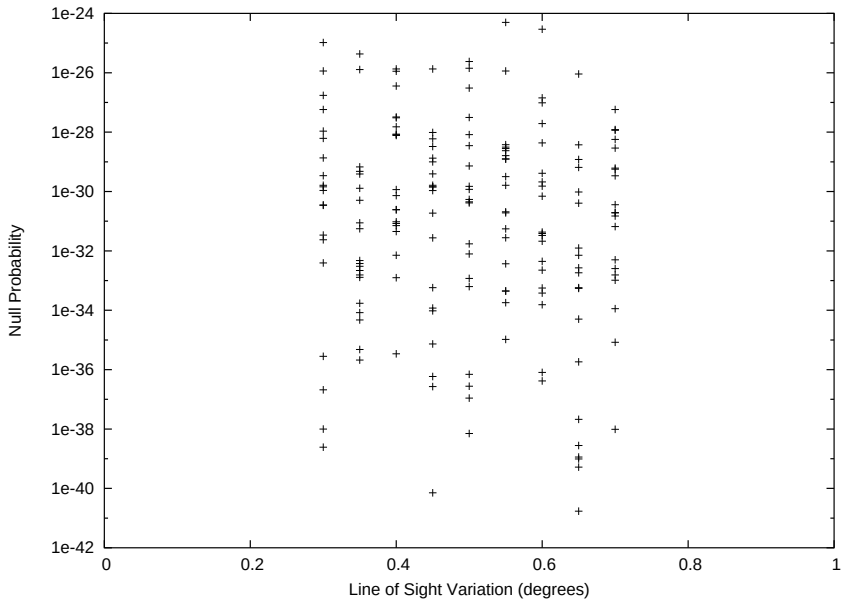

Figure 4.9: Null probabilities from a Kolmogorov-Smirnov test of the first two principal components as a function of precessional amplitude. Low amplitudes result in relatively high null probabilities, as can be seen between amplitudes of $0°.3$ to $0°.7$. Further tests were done (see figs. 4.5 and 4.7) at higher amplitudes, but these result in zero null probabilities, so are not plotted.

(as described in Chapter 3, a plot of the contributions of the first two principal components for each profile against each other) from a two-dimensional Gaussian fit. Generally, the probability shows a decrease as the precession becomes stronger, either through reduced noise or increased amplitude. However, there is a perplexing drop at low S/N as the probability tends once more to zero. It is not known why this is present.

The rv_1/rv_2 probability is only useful to tell us that profile changes are taking place, but not whether they are periodic or not. Thus, it gives us an more of an insight into the existence of long-period moding, which in itself is useful, rather than precession.

4.3.1.2 A Comparison with the Lomb-Scargle Periodogram Method

Of interest to further searches is the relative sensitivity of the two methods. It is interesting to note that, in this particular case (although this cannot necessarily be said in general), the Lomb-Scargle periodogram correctly identifies periods to roughly twice the fractional noise level of the Principal Component Analysis, or alternatively about $\frac{1}{6}$–$\frac{1}{9}$ times the amplitude of precession, making the Lomb-Scargle method clearly advantageous.

This is interesting, as the Principal Component Analysis is the tool most widely used to search for profile changes in the pulsar community, and let to the conclusive evidence that B1828–11 was precessing (Stairs et al. 2000). However, it seems, at least in this implementation, that the Lomb-Scargle method will be able to test better for precession.

Pulsar Name	N°of profiles used	Detected period (days)	Null Probability	log(Null Probability) ['Detectability']
J1713+0747	171	4458	1.35×10^{-16}	15.87
B1828–11	531	249.3	3.31×10^{-15}	14.48
B0144+59	209	310.6	8.27×10^{-9}	8.08
B1830–08	264	5342	1.36×10^{-8}	7.87
B0355+54	407	2459	4.44×10^{-6}	5.35
J0631+1036	202	877.1	1.43×10^{-5}	4.85
B1826–17	158	5778	1.53×10^{-5}	4.82
B1805–20	115	106973	1.53×10^{-5}	4.81
B2035+36	56	3191	3.07×10^{-5}	4.51
J1835–1031	53	2077	8.26×10^{-5}	4.08
B1834–04	131	106892	1.24×10^{-4}	3.91
B1913+10	265	5349	2.60×10^{-4}	3.58
J1022+1001	181	4113	2.64×10^{-4}	3.58
J2043+2740	63	1103	3.15×10^{-4}	3.50

Table 4.3: Periodicities derived from a Principal Component Analysis of the Jodrell Bank pulsar database, along with the strength of the periodicity detected by a Lomb-Scargle periodogram analysis of the most principal component, as given by their null probability (see text).

4.3.2 Results from the Database

4.3.2.1 Significant Pulsars

Of the 281 pulsars examined from the Lovell/Mk II database, 14 show periodicity detections more significant than our estimated cut-off level. These are presented in Table 4.3.

For the Principal Component Analysis (PCA), a period limit was not set. This produces some artifacts, such as those seen in B1805−20 and B1834−04 — clearly these periodicities are not detectable in a 4000-day observation set. We must also view the other longer periodicities, such as those of J1713+0747, B1830−08, J1022+1001 and B1913+10 with suspicion (see next Chapter). Again, we must be careful of instrumental changes and other factor which can pose as precession.

4.3.2.2 Data from the 42-foot Telescope

The 42-foot telescope data was analysed using the Principal Component Analysis routines in the same way, and using the same segmentation as in the Lomb-Scargle analysis. The results are presented in Table 4.4.

There are three pulsars here which make it above the detection threshold, namely B1929+10, B0740−28 and B0950+08. In the case of B1929+10, the periodicity observed is very close to the sampling time, so we should be wary of this. Pulsar B0740−28's periodicity does not give any cause for concern, nor does B0950+08's, although it is close to the detection limit. All three cases will be discussed in more detail in the next Chapter.

4.3.2.3 General Profile Changes

Another question we can ask is whether the pulsar profiles are changing *in general*, rather than periodically. This should find pulsars which exhibit moding on long timescales, and precessional effects that might not exhibit periodic behaviour, such as the 3–7 year periodicities observed in B1642−03 (see Shabanova & Urama (2000) and Shabanova et al. (2001)). What it will not pick up is pulsars which mode on timescales shorter than the length of the observation used to create the profile.

We can obtain these by plotting the two most significant eigenvectors (or 'principal components') from the PCA against each other, in an 'rv_1/rv_2 plot (or subsequent plots for subsequent eigenvectors), as done in the Monte-Carlo trials. For unchanging profiles, these should represent a Gaussian distribution, but will become increasingly non-Gaussian for profile changes. By measuring this amount of change, and representing it as the probability that this could occur randomly (the 'null probability' or 'detectability' described in the Lomb-Scargle analysis), we can find the probability that the pulse profile is changing.

Start Date (MJD) '000s	Pulsar Name	N°of profiles used	Detected period (days)	log(Null Probability) ['Detectability']
48	B0329+54	774	26.29	0.03
49	B0329+54	899	15.64	0.12
50	B0329+54	643	1.99	0.12
51	B0329+54	540	302.37	3.08
52	B0329+54	820	1464.00	2.12
53	B0329+54	477	244.66	0.02
47	B0950+08	83	576.22	2.15
48	B0950+08	506	612.88	4.53
49	B0950+08	618	1.88	0.09
50	B0950+08	404	808.88	0.11
51	B0950+08	389	609.94	0.01
52	B0950+08	517	190.64	1.48
53	B0950+08	304	350.78	0.00
47	B1133+16	61	4264.10	0.00
48	B1133+16	578	2.38	0.72
49	B1133+16	600	346.05	0.42
50	B1133+16	406	50757.41	0.00
51	B1133+16	435	256.79	0.29
52	B1133+16	525	69.12	0.09
53	B1133+16	241	262.80	0.00
47	B1642–03	98	1464.86	0.00
48	B1642–03	722	1.71	0.14
49	B1642–03	814	100.68	0.02
50	B1642–03	586	41.31	0.31
51	B1642–03	517	2.18	0.00
52	B1642–03	698	18.57	0.01
53	B1642–03	413	215.87	0.00
47	B1929+10	32	5643.82	0.13
48	B1929+10	407	1010.25	37.11
49	B1929+10	218	809.47	0.00
50	B1929+10	129	447.18	0.00
51	B1929+10	181	454.12	0.00
52	B1929+10	197	787.99	1.09
53	B1929+10	119	447.52	0.00
48	B1933+16	623	2.49	0.00
49	B1933+16	828	6.16	0.03
50	B1933+16	592	2.28	0.74
51	B1933+16	525	1.59	0.15
52	B1933+16	750	29.59	0.67
53	B1933+16	436	166.09	0.00
	B0740–28	410	156.88	14.62
	B0355+54	63	52953.73	0.01
	B1508+55	29	3627.57	0.55

Table 4.4: Periodicities derived from a Principal Component Analysis of the Jodrell Bank pulsar database, along with the strength of the periodicity detected by a Lomb-Scargle periodogram analysis of the most principal component, as given by their *estimated* null probability (see text).

Table 4.5: General profile changes as inferred from a Principal Component Analysis of the Jodrell Bank pulsar database, along with the strength of the change as given by the null probability for the first four eigenvectors (see text). The asterisked pulsars show pulsars known to be mode changing.

Pulsar Name	log(Null Probabilities) or 'Detectability'		
	rv_1/rv_2	rv_2/rv_3	rv_3/rv_4
B1933+16	50.00	50.00	50.00
B0329+54*	50.00	50.00	50.00
B1828–11	50.00	50.00	21.09
B0950+08	42.27	50.00	50.00
B0540+23	40.73	29.83	32.97
B0355+54*	37.11	43.95	40.16
J0614+2229	36.84	4.78	11.71

The difficulty in this case is knowing where to put the cut-off point. As can be seen in the Monte-Carlo trials, the levels at which we find the null probability for non-detections can be anything down to 10^{-40}, or even 10^{-45}. In Table 4.5, we present the pulsars showing rv_1/rv_2 probabilities of less than 10^{-35}.

It is fairly obvious that this method works quite well. Pulsars B0329+54 and B0355+54 are known to be mode changing (Rankin 1986) and B1828−11 has also been picked up well. The remainder of these cases will be discussed in the next section.

4.4 Comparing the Two Methods

For all but the strongest few pulsars, the Lomb-Scargle periodogram method and the Principal Component Analysis method do not appear to be complimentary. As has been seen before, there is a wide range where Lomb-Scargle can pick up periodicities where our PCA–Lomb-Scargle analysis cannot.

The success of Principal Component Analysis is our investigation relies on the precessional change being represented in the Principal Component, rather than subsequent components. A more complete analysis could be done of these

subsequent components, and a Lomb-Scargle periodogram performed on these. This is not included here, but may be the subject of a further study.

A case in point here is that of pulsar B1737-30. Lomb-Scargle results gave very strong periodicities at 7214 days (not necessarily attributable to precession), whereas a periodogram of the PCA results give essentially a zero strength periodicity, with a 68% null probability. An asymmetry analysis of the eigenvectors shows a weak asymmetry in rv_1/rv_2, but stronger asymmetries in rv_2/rv_3 and rv_3/rv_4, suggesting a real profile change is actually in the *third* eigenvector. In cases such as these, it may be that changes in the instrumentation are sufficient to produce profile changes leading to the first and second eigenvectors, with the real change in the pulsar profile then only represented by the third.

The fact that precession was correctly detected in B1828–11 using both methods in concurrence with other studies shows that both methods do indeed work, which allows us to put a sensible limit on the number of pulsars exhibiting strong precessional behaviour to perhaps no more than a handful and certainly to say that it is only a minority of pulsars that exhibit strong precessional effects. The accuracy of the results for strong detections (at least in the Monte Carlo simulations) is similar for results where the periodicities were correctly determined, with a standard deviation of 3.8 days for Lomb-Scargle and 4.2 days for PCA/L-S in a 250 day period.

It should be remembered that, in addition to pulse profile changes, pulse timing should also be affected by precession. Thus, we should also expect to see a corresponding change in the pulse timing residuals as well. We must therefore collate the results from the Lomb-Scargle periodogram analysis; the Lomb-Scargle analysis and the asymmetry analysis of the Principal Component Analysis; and the timing residuals for each pulsar. The results of this are presented in the next Chapter.

Chapter 5

Individual Cases

5.1 Overview

In Chapter 4, a statistical overview of the results from our analysis was presented. As stated, all the pulsars found using the periodicity searches described are not necessarily precessing. There are a significant number of other factors, mostly changes in instrumental configuration, which would cause apparent periodicities in the data.

Changes of the filterbanks, which has led to some of the data not being included in the analysis, are described in detail in Chapter 4 and, as noted there, many problems due to changes in filterbanks still remain. A multibeam receiver was also used on the telescope to collect some of the profiles used here. The receiver used is not expected to make a significant difference to the resulting profile. However, this does depend on both left and right polarisations being used to form total intensity with appropriate gain factors. If they are not, this could make a significant enough difference in highly polarised pulsars to affect our results, as the multibeam system is recording linear polarisation in contrast to the circular polarisation used otherwise.

In order to find out which, if any, of the pulsars in our lists are precessing, we

need to examine them on an individual basis, and collate the data from all our sources — our Lomb-Scargle (L-S) periodogram results, our L-S analysis of our Principal Component Analysis (PCA) results, our asymmetry tests on our PCA results, and the timing residuals from the Jodrell Bank pulsar database.

In the following sections, we present the case for each pulsar in turn, beginning with the prototype precessing pulsar, B1828–11, and examine the evidence for each one.

5.2 B1828–11 — The Prototype

5.2.1 Literature

Since the discovery of profile shape changes and timing residuals consistent precession in B1828–11 by Stairs et al. (2000), there have been several follow-up studies. Link & Epstein (2001) confirm Stairs *et al.*'s periodicities in the timing residuals of 250, 500 and 1000 days and go on to imply a 3° amplitude, or 'wobble angle' "if the star's dipole moment is nearly orthogonal to its symmetry axis", and suggest that the beam has an 'hourglass' shape. This is significantly larger than the 0°.3 estimated by Stairs et al. (2000).

Jones & Andersson (2001) find that the wobble angle should be 2° for a near-orthogonal beam ($\chi > 89°$). Rezania (2003a) gives another model which finds that for a 3° wobble angle, the second (500 day) and fourth (250 day) harmonics are dominant. In Rezania (2003b), he goes on to suggest a dumbbell-shaped beam, which is closer to the standard cone model.

Cutler et al. (2003) find that the precessional period is shorter than expected, and go on to suggest that the crust is under considerable magnetic stress to produce this precession. Wasserman (2003) follows this by stating that, in this scenario, precession should not be damped considerably.

However, consensus on the free precession model for B1828–11 and other pulsars is not entirely agreed upon. Qiao et al. (2003) suggest that an accretion disc with its axis misaligned to the pulsar's rotation axis could also produce profile changes due to gyroscopic precession. What is agreed on, though, is that 250 and 500 day periodicities are visible in the profile changes and 250, 500 and 1000 day periods are visible in the timing residuals.

5.2.2 Lomb-Scargle Results

Figure 5.1 shows the L-S periodogram results for B1828–11, showing the strength of periodicities as a function of phase and frequency over the full profile. Stairs et al. (2000) modelled the varying beam shape of B1828–11 to be a weighted sum of two Gaussian profiles of different widths. We therefore expect that both sides of the profile should be showing these periodic changes, which is born out by the high periodicities we see in these regions.

We observe the 250 and 500 day (0.004, 0.002 d^{-1}) periods found by Stairs et al. (2000), and measure them at 247 and 493 days. From our Monte-Carlo simulations we estimate errors on these values of $\pm$ 4 and $\pm$ 8 days, respectively. We also find periodicities at 119$\pm$2 and 157$\pm$3 days, which presumably correspond to the eighth and sixth harmonics.

We also find two other noteworthy periodicities. A weak periodicity exists at 1210 $\pm$ 15 days, which, due to its spread in the frequency domain (i.e. noisy structure) evident from the figure, is likely instrumental. More interesting, however, is a stronger periodicity at 227$\pm$4 days, which is the strongest frequency visible in a number of seemingly resonant frequencies, each separated by roughly a factor of $\frac{23}{25}$ in the frequency domain. This may imply some sort of inherent interference or secondary periodicity causing a beating effect, some unknown instrumental effect. More likely, however, is that it is a byproduct of the sampling

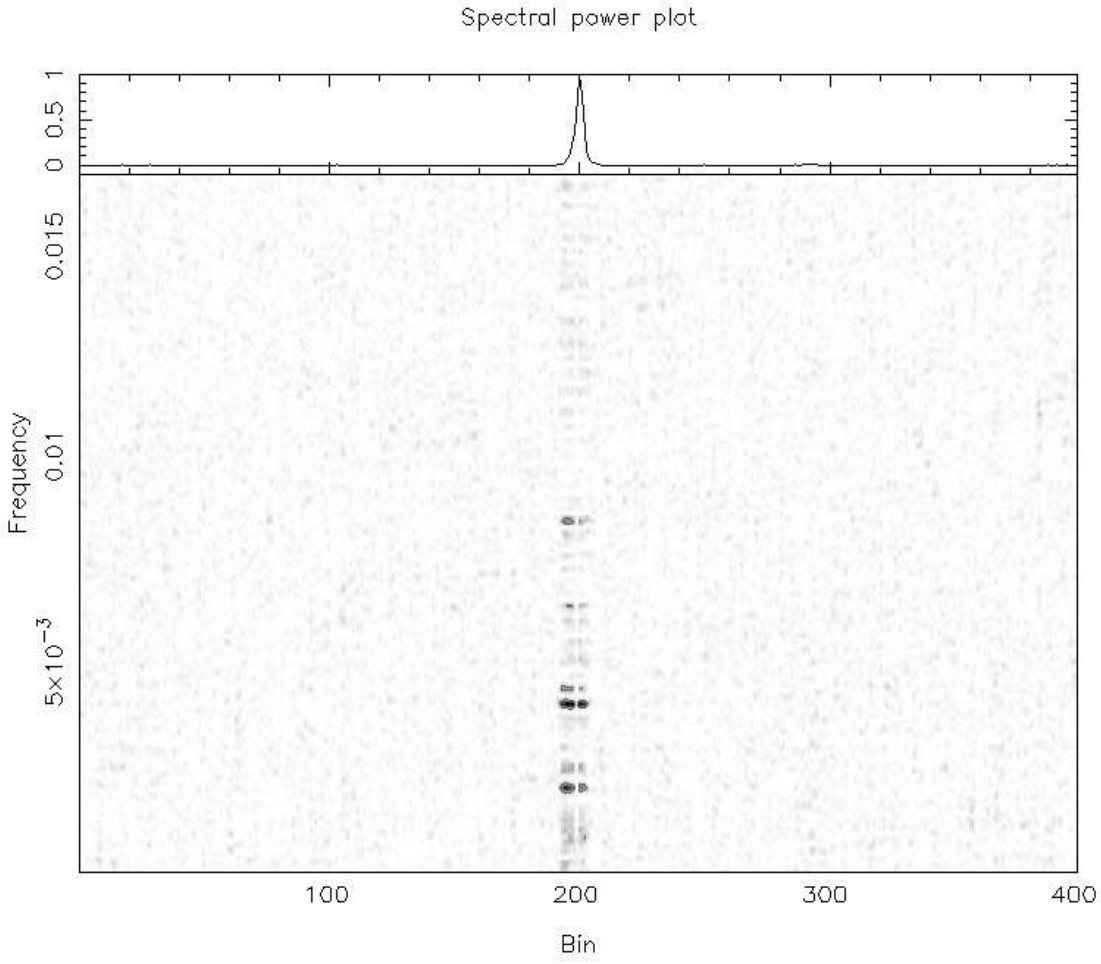

Figure 5.1: Signal strength for B1828–11 from Lomb-Scargle periodogram analysis. The greyscale represents periodicity strength from noise (white) to strong periodicity (black). Contours are plotted at null probability levels of $\frac{5.73\times10^{-7}}{n}$ for contour number n (c.f. background noise has a mean of 3×10^{-4}). The x-axis shows pulse phase and the y-axis shows frequency in units of $\frac{1}{days}$. Clear periodicities can be seen at the expected 250 and 500 day periods. Also visible are harmonics around 167 and 125 day periods, as well as substantial evidence for periodicities at non-harmonic periods.

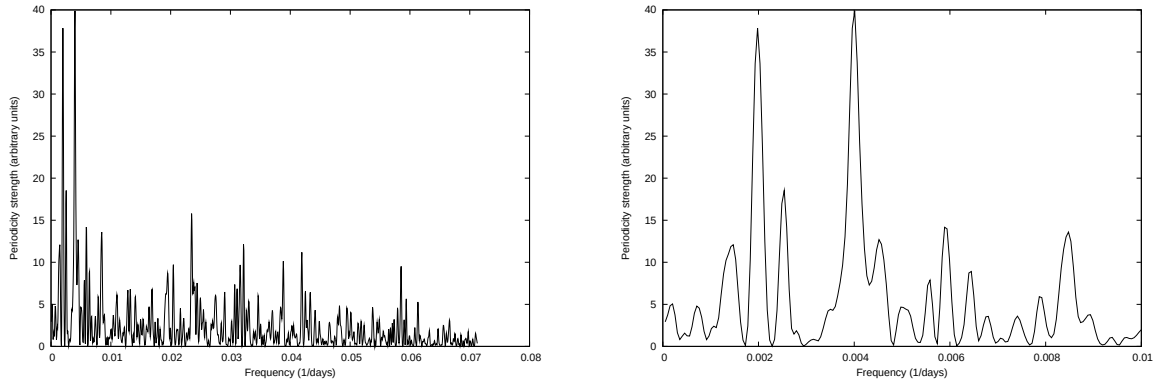

Figure 5.2: Signal strength against frequency for B1828–11 from a Lomb-Scargle periodogram analysis of the Principal Component Analysis. The right-hand plot shows a zoomed-in version from frequencies of 0–0.01 days^{-1}. Peaks can clearly be seen at frequencies of 0.002 and 0.004 days^{-1} (500 and 250 days), along with other, weaker frequencies described in the text.

of the observation times, combined with a high value of *ofac*, the oversampling factor in the Lomb-Scargle analysis.

To test the last hypothesis, we performed a Monte-Carlo test similar to those used in the previous chapter, but using the observation times for B1828–11. The results show periodicities clumping around 3–8 days — near the sampling time, as expected — at null 'probability' levels for around 10^{-3}, which is towards the top end of those expected for background noise. Thus, assuming the 227-day periodicity (and other associated periodicities) are not real, they must either be due to processing artifacts, interference from instrumental effects (such as filterbank changes, as seen later in other pulsars), or some other local phenomenon.

5.2.3 Principal Component Analysis Results

Figure 5.2 shows the periodicities obtained using a Lomb-Scargle Periodogram analysis of the first eigenvector from the Principal Component Analysis (PCA). Clear periodicities can be seen around 250±7 and 505±15 days. This is concurrent with the above Lomb-Scargle results and the works listed previously. Other

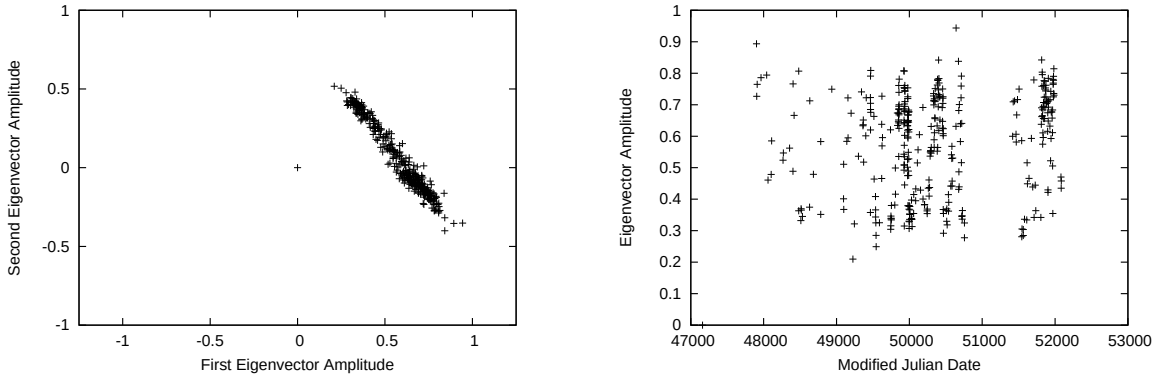

Figure 5.3: The variation of the principal components (eigenvectors) from Principal Component Analysis for B1828–11. The left-hand panel shows a plot of the first and second most significant eigenvectors against each other (the dimensions are set as a comparison to other pulsars shown later). For a static system, this should represent a two-dimensional Gaussian. For a system precessing between two states, a linear feature should be seen, which is clearly evident here. Outlying points (here, and on similar plots later) are usually due to RFI in the profiles. The right-hand panel shows the evolution of the first eigenvector over time, comparative to the 'shape parameter' used by Stairs et al. (2000). A definite variation can be seen on scales of around 250 days.

periodicities can also be seen at around 667 days, 400 days and 220 days. The 157 day periodicity is picked up well, although at around 169±2 days, which is closer to what would be expected. A periodicity at 118±2 days is also found, consistent with the 119 day periodicity found from the phased-binned Lomb-Scargle analysis above.

Figure 5.3 shows the variation the first two eigenvectors. A clear linear variation is visible when the two most significant eigenvectors are plotted against each other, which is very distinctly different from the Gaussian one would expect if there were no variation at all. This plot gives no evidence of precession, just that consistent shape changes are taking place. The temporal evolution of the principal eigenvector shows a clear variation unattributable to white noise and is suggestive of a periodicity of around 250 days. Our data also reproduces the broadening and narrowing of the pulse profile (Figure 5.4, as seen in Stairs et al.

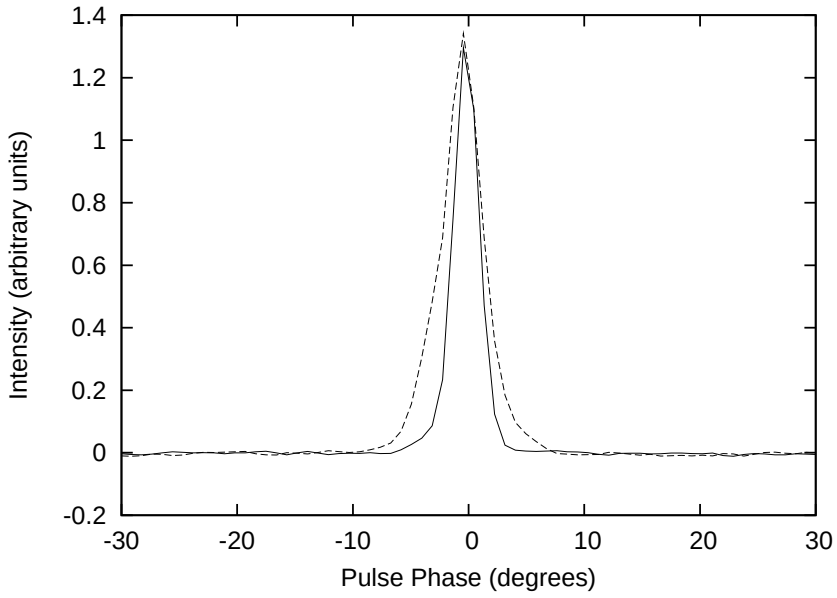

Figure 5.4: Possible profile changes from Principal Component Analysis of B1828–11, showing profile extrema reconstructed from a mean profile and the two principal eigenvectors. This plot shows the average profile, plus the first two components at an amplitude of 0.4 and 0.3, respectively, for the solid profile, and at 0.7 and -0.25 for the dashed profile (c.f. Figure 5.3).

(2000).

5.2.4 Timing Residuals

Figure 5.5 shows the timing residuals from the Jodrell Bank database. These were obtained from observations using the program *PSRTIME*. Much of the work done on this pulsar has concentrated on the timing residuals, as these are easier to obtain (and much more accurate) that shape change variations.

The residuals show a very distinct 500-day periodicity with other periods superimposed on it. An analysis of these residuals is not done here, as they are well-described elsewhere (e.g. Stairs et al. 2000).

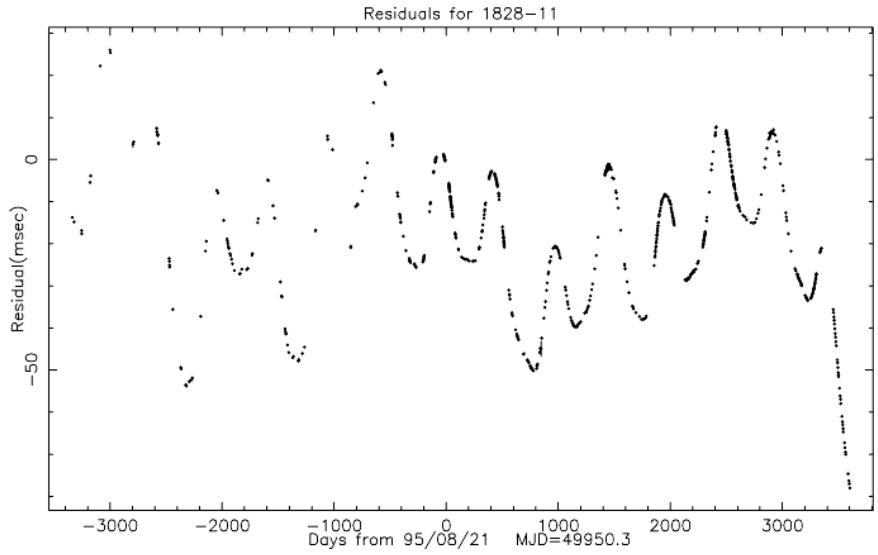

Figure 5.5: The timing residuals observed at Jodrell Bank for B1828–11 over the last 20 years. The 500-day periodicity can be seen here very clearly.

5.2.5 Conclusions

Overall, the periodicities from L-S analysis of our PCA results appear to be concordant with the phase-binned L-S results above. The only minor discrepancy is that the periods determined by the two methods are slightly different, although they are consistently short for the L-S and consistently long for the PCA/L-S and within each others' errors. Phase-binned L-S implies a fundamental periodicity of 986±11 days and PCA/L-S implies a period of 1011±20 days.

The results from investigation of the eigenvector analysis shows a clear variation between two profile extrema. This has previously been characterised as movement between two Gaussians of differing widths, which seems likely to correspond to a varying cut through a standard hollow cone model. The timing residuals also provide a clear periodicity at around 500 days.

This pulsar shows clear signs of precession-like behaviour in all the components of our analysis — phase-binned L-S results, L-S analysis of PCA data, consistent eigenvector variations in PCA data and periodic variations in timing, all occurring on harmonics of the 1000-day timescale. We have not observed

shape changes corresponding to the base frequency of this 1000-day period, but have good evidence of having observed the second, fourth and sixth harmonics, and may also have observed an eighth or ninth harmonic. We believe the 227-day periodicity and its associated harmonics are not real.

5.3 B1642–03 — A Previous Timing Candidate

5.3.1 Literature

The main piece of literature involving B1642–03 as a candidate for precession has been an investigation of timing irregularities performed by Shabanova et al. (2001) and by Shabanova & Urama (2000).

In these works, the case for precession was presented based on pseudo-sinusoidal behaviour. The study found cyclical changes in amplitude ranging in period from three to seven years, clearly evident in the timing residuals. A power spectrum analysis of the timing residuals found periodicities at 5000, 2500 and 1250 days, approximately.

Earlier work was done on shape changes by Blaskiewicz (1991). This also used a Principal Component Analysis and showed a periodic variation in the first eigenvector on a timescale of around three years. However, this work used profiles of only one linear polarisation. Polarisation data for this pulsar (Gould & Lyne (1998), von Hoensbroech & Xilouris (1997)) show that the polarisation is not negligible and varies over the profile. Thus, the profile shape is likely to change depending on the parallactic angle, which in turn is dependant on the time of day of the observation.

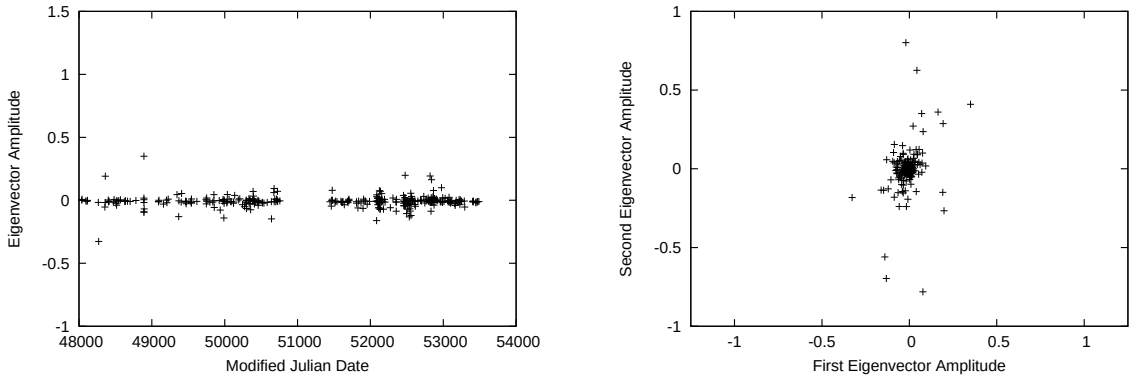

Figure 5.6: The variation of the principal components (eigenvectors) from Principal Component Analysis for B1642–03. For a static system, this should be entirely noise. The left-hand panel shows the evolution of the first eigenvector over time. No clear variation or significant departure from a zero mean can be seen, and it does not confirm the timing plots of Shabanova et al. (2001). The outlying points mostly come from profiles with RFI not successfully removed during automatic profile selection (see Chapter 3). The right-hand panel shows a plot of the two most significant eigenvectors against each other (the dimensions of the plot are identical to those used in B1828–11 and later examples), each point representing a profile. For a static system, this is expected to be a two-dimensional Gaussian. There is a statistically significant departure from this, but the uniformity of the plot suggests this is due to a combination of two different datasets with different signal-to-noise (e.g. Lovell and Mark II data).

5.3.2 Results from the Lovell and Mark-II Telescope Data

The results from the analysis of B1642–03 show no correspondence between either Blaskiewicz's work or the clear periodicities in the timing residuals. In this case Lomb-Scargle analysis would be ineffective (there are no significant periodicities found) as the maxima in the timing residuals are separated by varying amounts (presumably due to the addition of several harmonics). For such a system, we would still expect to find periodicities in the principal components, or even a non-Gaussian variation in them. Figure 5.6 shows that this is not the case. From this it is assumed that either precession is not taking place in B1642–03, is taking place in such a way that the pulse profile is not changing considerably, or is below the detection limit of our software (although this is not thought to be the case, given the large amplitude of the timing variations and the high signal-to-noise ratio).

5.3.3 Results from the 42-foot Database

B1642–03 has also been observed with the 42-foot telescope due to its high brightness. This allows us to do a further independent test of our null result. As described previously, the data have been split up into 1000-day segments and each analysed separately. When the amplitudes of the principal components are plotted from these segments (see Figure 5.7) we once again find a very stable pulse profile. The variations described by Blaskiewicz are on the same timescale as the segment length, so longer period variations may not be easily detectable in the 42-foot data.

From our results from both the Lovell/Mark II and 42-foot databases, we conclude that no profile changes are taking place for this pulsar. Hence, if the variations seen by Shabanova *et al.* are due to precession, we expect it to be occurring at a level below our detection threshold, and that it is possible that the

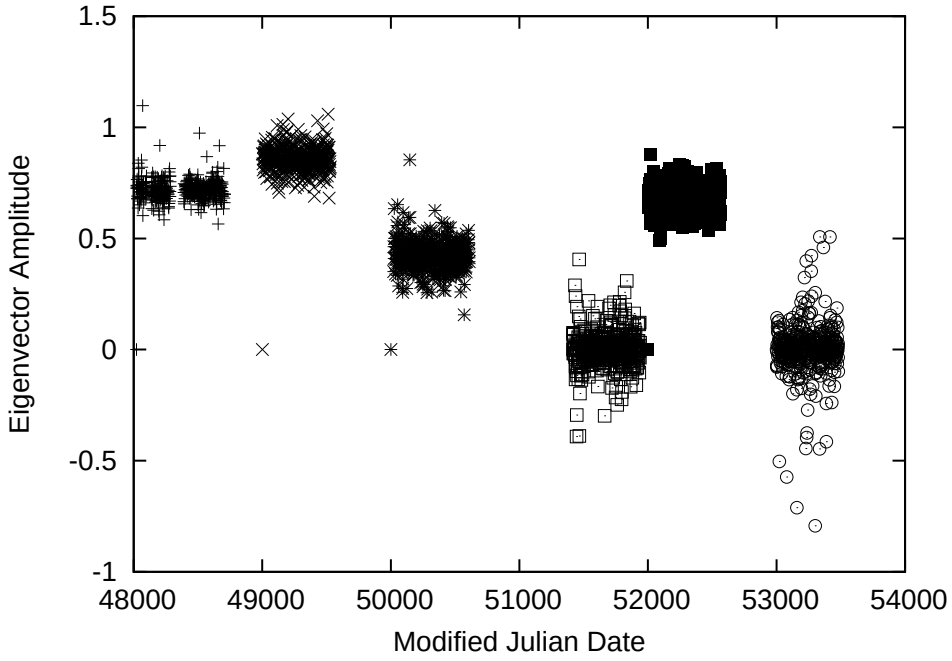

Figure 5.7: This figure shows the variation of the principal components using data from the 42-foot telescope. Since the data have been segmented into 1000-day blocks, the eigenvectors for each segment are different. The discontinuities between the segments reflect the fact that different principal (and other) components have been assigned under the P.C.A. subroutine for each segment. This data only includes the first 512 profiles from each segment due to restrictions in the length of dataset for P.C.A. No significant changes can be seen in any of the data segments which might correspond to a long-period profile variation such as those described in Shabanova et al. (2001).

shape changes provided by Michael Blaskiewicz are due to the single polarisation data used in that study.

5.4 J1022+1001 — A Millisecond Pulsar with Profile Changes

5.4.1 Literature

J1022+1001 is known to exhibit profile shape changes, as described in Kramer et al. (1999). It is also a 'millisecond' pulsar, with a period of 16.5 ms, orbiting

an 0.87 solar mass companion (Camilo et al. 1996). This makes acquiring sufficiently high temporal resolution data to detect profile changes difficult. The pulsar is also very close to the ecliptic, with an ecliptic latitude of only −0°3'50", meaning that it is liable to be affected significantly by the interplanetary medium, which could produce profile changes on an annual basis, or potentially at other periodicities, although Kramer *et al.* suggest that this is not the case here. The timescales of changes given in the above reference are only on the order of hours, which would appear as noise in our data — a periodicity search was conducted, ranging in period from several hours to several months without success.

Ramachandran & Kramer (2003) also showed profile changes in this pulsar, which are strongly dependant on frequency and time. J1022+1001 is strongly polarised (Stairs et al. 1999), with the right-hand component being almost completely linearly polarised, and the left-hand component less so. The pulsar also exhibits a considerable amount of circular polarisation. Kramer *et al.* found that the profile changes were occurring in the left-hand, less-polarised component, suggesting that this was not an instrumental effect due to poorly combined polarisations; however, their study used a narrow bandwidth. Hotan et al. (2004), using a wide bandwidth (60 MHz) failed to show significant profile changes at all beyond their instrumental errors of a few percent. As noted in Chapter 4, our data were taken using a 32 MHz bandwidth before 1995, and a 64 MHz bandwidth post-1997 (the intermediate data being excluded). The changes in profile over time noted by Kramer *et al.* therefore seem to be due to a frequency-dependance of the pulse profile and a modulation of the pulses by the changing scintillation caused by the ISM.

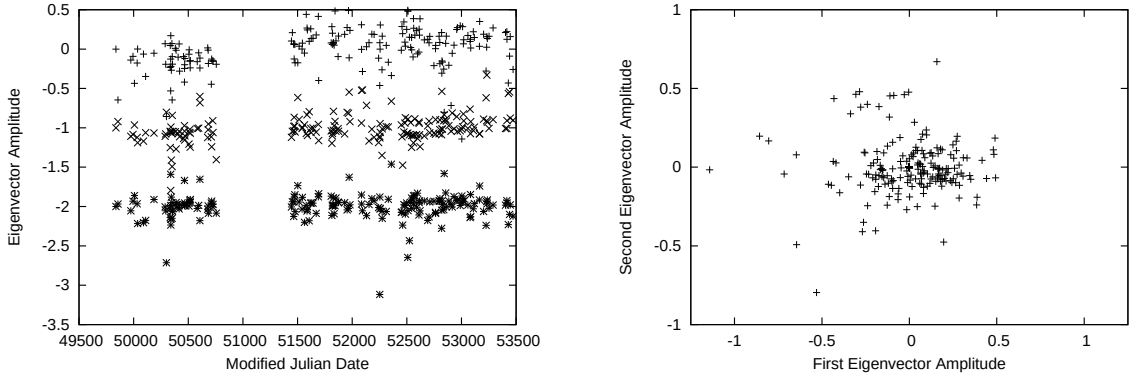

Figure 5.8: The variation of the second and third principal components (eigenvectors) from Principal Component Analysis (the first characterising an instrumental variation caused by the change in filterbanks) for J1022+1001. The left-hand panel shows the evolution of the first (solid) and second (dashed, offset by -1) and third (dotted, offset by -2) eigenvectors over time. The first eigenvector appears to represent a difference in the dispersion of the profile, caused by the two different filterbanks in use over the dataset (note the left-hand side is lower than the right). The second term appears to represent the brightness of the bridge between the two components and the third the ratio of the amplitudes of the two components — the parameter used by Kramer et al. (1999). The right-hand panel shows a plot of the second and third most significant eigenvectors against each other (the dimensions of the plot are identical to those used in other examples), each point representing a profile. This appears to maintain a high degree of Gaussianity, suggesting that the profile changes appear to be random in nature, rather than a systematic change between two or more states.

5.4.2 Results

Figure 5.8 shows the results of our Principal Component Analysis on the data for J1022+1001. There is a very characteristic change visible between the earlier (before MJD 51000) and later data. We suggest that this is an artificial change, produced by the change in bandwidth of the filterbank. The Lomb-Scargle analysis also picks up this change and interprets it as a periodicity at a period of 3600–4900 days. The pulsar is of low DM (10.25 cm^{-3} pc), it is of very short period, meaning the smearing caused by dispersion of the pulse is longer as a fraction of the pulse period. No other significant periodicities were detected.

Significant changes do appear to be taking place in J1022+1001, with the profile changing by up to 20%, based on the eigenvector amplitudes — significantly larger than the 8.3% expected from our signal-to-noise limit. These changes do not appear to be periodic or consistent, but instead appear to be random, both in the nature of the change and the timescale it occurs on. We suggest that this variation is due to problems caused by a small number of samples across the pulse period ($\sim$ 17), caused by its rapid rotation and our sampling time, rather than the effects observed in previous literature or precessional behaviour.

5.5 J1713+0747 — A Binary Undergoing Possible Shape Changes

Pulsar fJ1713+0747 is a binary pulsar in orbit with a companion of around 0.3 solar masses with a period of 68 days (Splaver et al. 2005). It can be timed to very high precision, with timing residuals of around 200 ns. A clear difference can be seen in our PCA results (Figure 5.9) between data before and after MJD 51000. This is likely due to changes in the bandwidth of the filterbank, the effects of which can be seen in a number of other pulsars, such as J1022+1001. However,

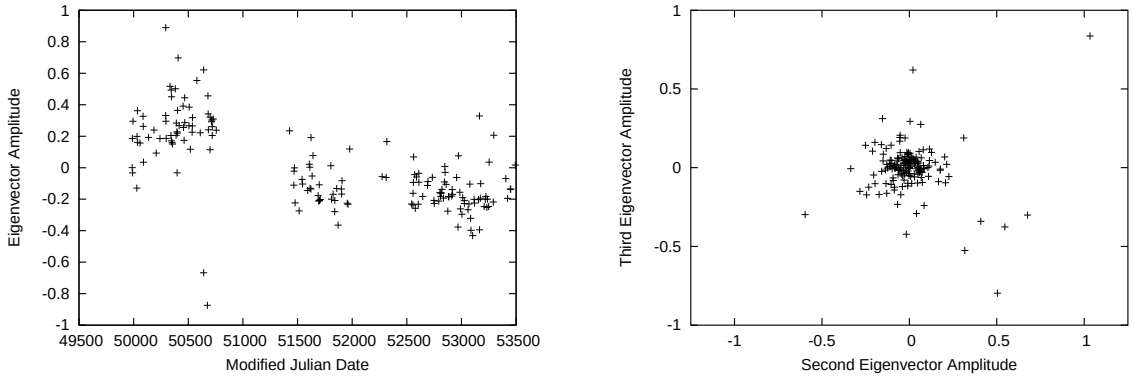

Figure 5.9: The variation of the principal components (eigenvectors) from Principal Component Analysis for J1713+0747. The panels are as described in Figure 5.6. In the left panel, changing the filterbank has resulted in a clear difference that can be seen between the two observed periods. However, structure can be seen in the data, particularly in the left-hand side, which we suggest is due to the small number of bins across the profile. In the right panel, the eigenvector plot largely represents a Gaussian, suggesting random variations, rather than variations between extrema. The group of outliers is likely due to bad observations.

trends can be seen, increasing in the left-hand region and possibly reaching a minimum in the right-hand region.

If precession is occurring, it theoretically could be either free or geodetic precession. However, the timescales on which geodetic precession would occur are too long. The rate of geodetic precession (in radians per second) is given by the following equation (Barker & O'Connell (1975), Boerner et al. (1975)):

$$\Omega_p = \frac{(2\pi)^{\frac{5}{3}} T_{\odot}^{\frac{2}{3}} m_c(4m_p + 3m_c)}{P_b^{\frac{5}{3}}(m_p + m_c)^{\frac{4}{3}}(1 - e^2)}, \tag{5.1}$$

where $T_{\odot}$ is a constant, given by the constant:

$$T_{\odot} = \frac{GM_{\odot}}{c^3}, \tag{5.2}$$

where G is Newton's constant of gravitation, $M_{\odot}$ is a solar mass, c is the speed of light; m_c and m_p are the masses of the companion and primary stars, respectively, in solar masses; P_b is the period of the binary and e is the eccentricity of the orbit. Inserting values for J1713+0747, we arrive at a value of around $0°.05$ degrees per

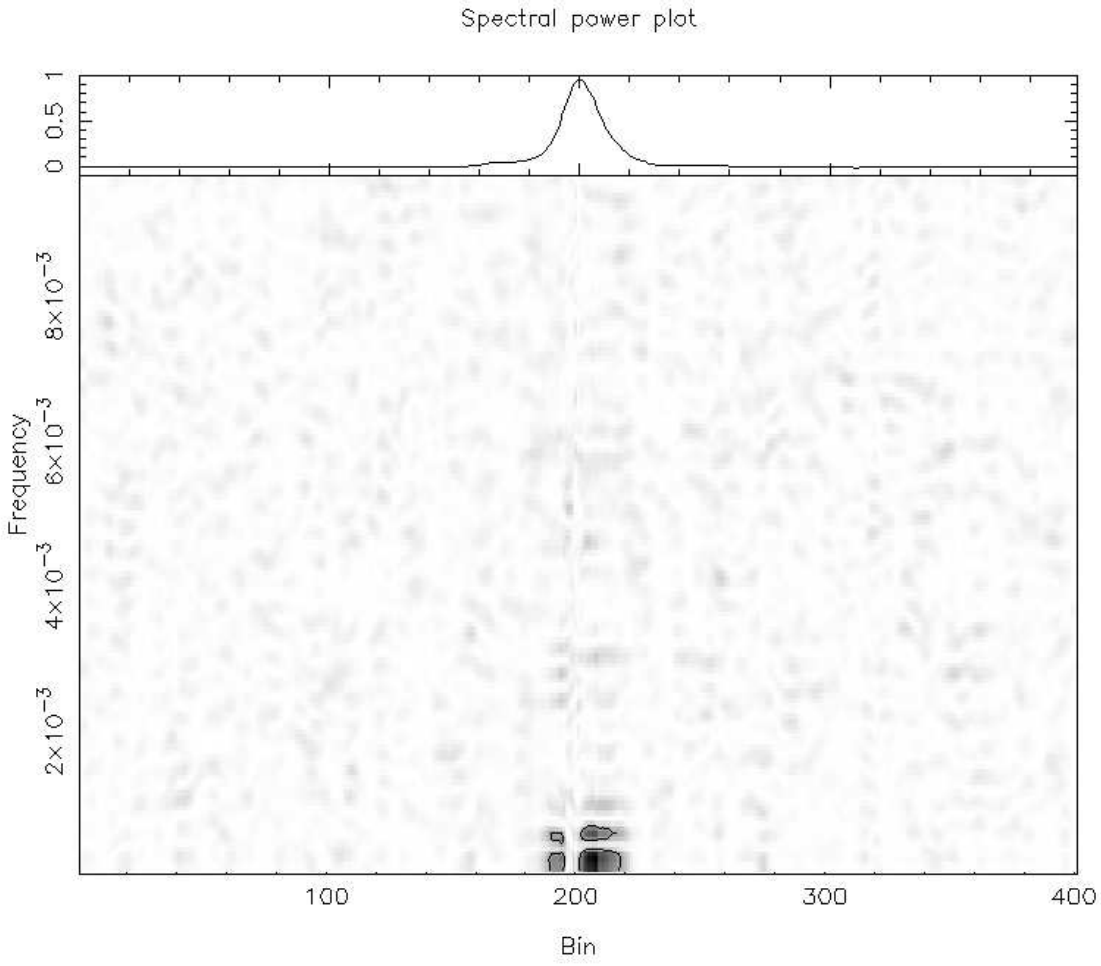

Figure 5.10: Signal strength for J1713+0747 from Lomb-Scargle periodogram analysis. See Figure 5.1 for a full explanation. Periodicities are seen at 1760 days and 2020 days for the left- and right-hand sides of the emission peak, respectively, and at 4700 days for both sides. Not visible is a 53-day period at the level of 5×10^{-5}.

year, or 0°.4 over the entire range our data. Our Monte-Carlo data, suggests that we cannot detect changes in this pulsar due to geodetic precession.

Our Lomb-Scargle results (Figure 5.10) also support a periodicity in our data, but this is most likely due to the change in filterbank systems causing a slight change in the pulse width, which corresponds to the change in pulse width seen in the first eigenvector from our PCA results.

There appears to be no literature involving the case for precession in this object before. We suggest that the changes we see are due to a combination of the poor phase-binning of data of this pulsar (the pulse profile is about 5 samples wide) due to its rapid rotation and effects caused by changes in the filterbanks used to obtain the pulsar profiles. More self-consistent, high-resolution observations would be required to find whether J1713+0747 is precessing.

5.6 B0740–28

B0740–28 is a fairly short-period pulsar, rotating with a period of 167 ms (Hobbs et al. 2004b), and is relatively bright with a flux density of 15 mJy at 1400 MHz (Hobbs et al. 2004a). Due to its brightness, we have data from both the Lovell and 42-foot telescopes, which we can use as near-independent samples for studying precession. The analysis of this pulsar was complicated by the presence of single-polarisation profiles in the Lovell(/Mark II) data, which had been mislabelled and could not be removed without extensive hand-editing of data.

Our data for B0740–28 shows a single pulse with an unresolved component on the right-hand side. High-resolution profiles for this pulsar show up to six components visible in this main pulse, with a possible seventh, unresolved component also present (Kramer 1994). The pulsar appears highly linearly polarised (von Hoensbroech & Xilouris 1997), with the left-hand (leading) four or five components almost entirely linearly polarised, with polarisation decreasing slightly in

the remaining right-hand (trailing) components.

Figure 5.11 shows the Lomb-Scargle results for both the Lovell and 42-foot data. The Lovell data are by far the more noisy. We expect this is due to the bad data, plus the Lovell/Mark-II data have fewer profiles than the 42-foot data (261 versus 410). The 42-foot data also has a combination of a greater number of profiles, a longer integration for each observation and a much more even sampling.

The key point, however, is that the periodicities found in our 42-foot Lomb-Scargle results appear close to those found in the Lovell data. The 42-foot data give periodicities at 152–174 days, 112–116 days and 327–355 days, in order of decreasing significance; the Lovell data give periodicities ranging from 59.8–62.2 days and 126–134 days, as well as a periodicity at 97 days. A significant amount of 'beating' is occurring, as was seen in B1828–11, which makes it difficult to determine frequencies with any precision. This effect can come about if the period of variation is not constant, for example if a glitch upsets the mechanism (though none have been observed for this particular pulsar, this may be important later); or if the body has a tri-axial asymmetry, which would cause a chaotic motion, leading to a disruption of the periodicities. An interpretation of the above results is that there is a fundamental period of around 360 days, and that we are seeing the third and sixth harmonics in the Lovell data and the first, second and third in the 42-foot data. Given the strength of the periodicity in the 42-foot data, and its albeit fairly weak correspondence with the Lovell data, we suggest that the effect may be real. It should be noted that, due to the infringing polarisation profiles, we should take care what conclusions we reach involving the Lovell data. The Lomb-Scargle results suggest that the main profile changes are occurring in the 'partially-resolved' component (see above).

Unfortunately, the P.C.A. of the Lovell data appear to be more strongly affected by the single-polarisation profiles in the database than the phase-binned

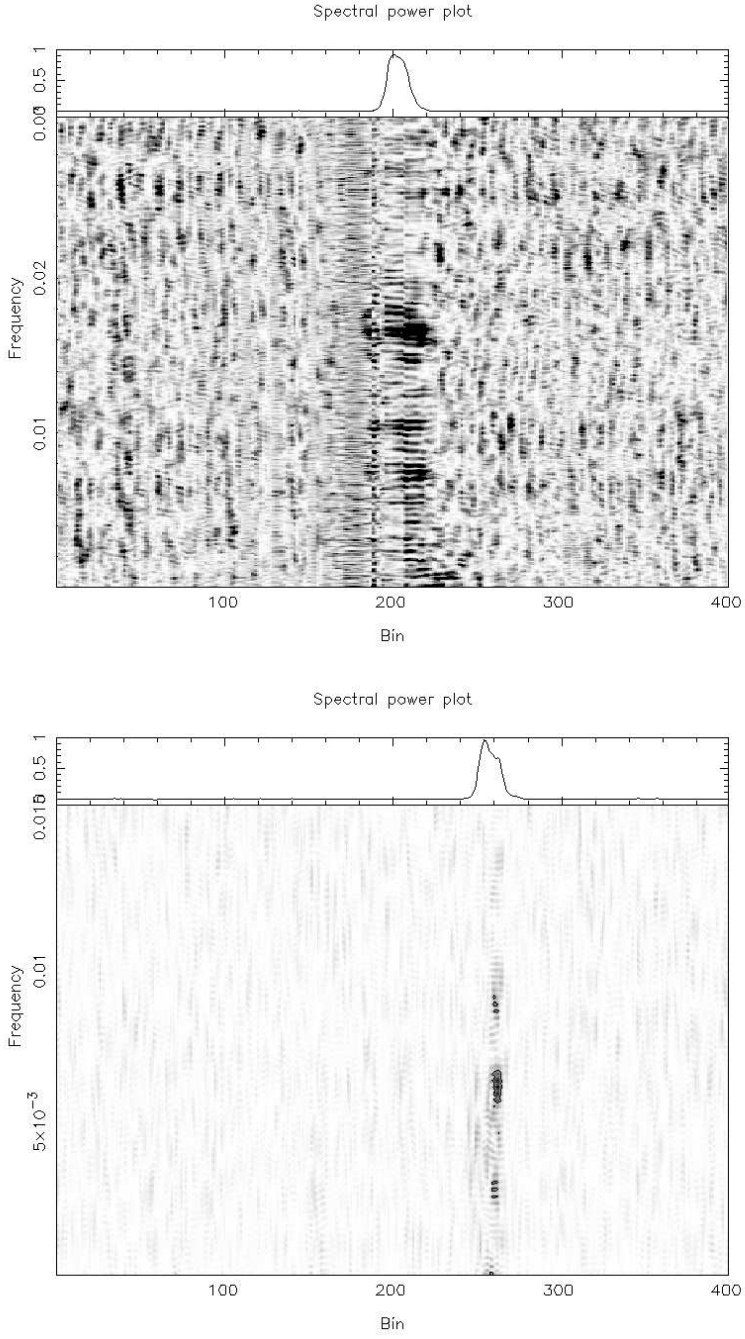

Figure 5.11: The results from phase-binned Lomb-Scargle of B0740–28. For a description of the figures see 5.1. The top plot shows data for the Lovell/Mark II telescopes, based on 261 profiles over 8612 days. The bottom plot shows data for the 42-foot telescope, based on 410 profiles over 5320 days, though mostly in the range MJD 47900–48800. Both show strong periodicities between periods of 110 and 170 days. Additionally, the Lovell data also show a periodicity at 60 days.

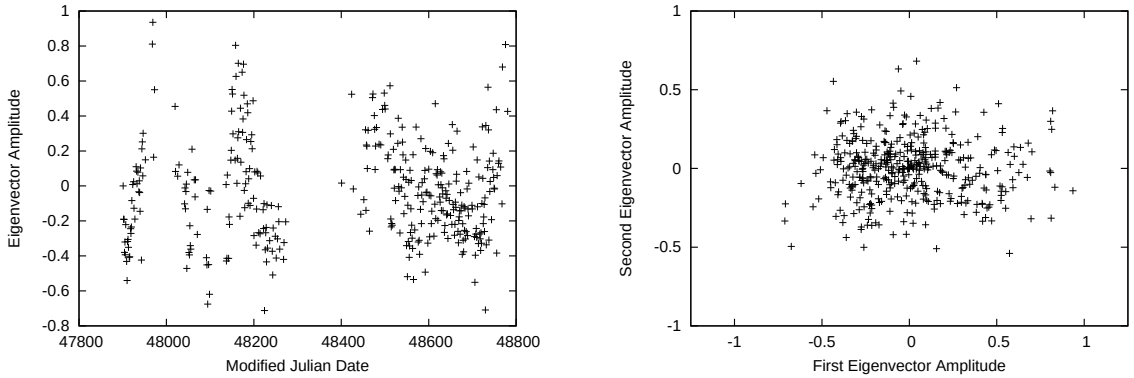

Figure 5.12: The variation of the principal components (eigenvectors) from Principal Component Analysis for B0740–28 using 42-foot data only. The panels are as described in Figure 5.6. The left-hand panel only contains data from our main sampling period (the 44 profiles used from MJD 52400 onwards were not included for clarity). A 160-day period is apparent at the beginning of the data (first peak at around MJD 48000), but is less apparent in the later data. The first/second eigenvector plot shows some non-Gaussianity, but lacks any correlation between the first and second eigenvectors, forming a more linear structure, suggesting the first eigenvector fully explains the stronger variations in the data.

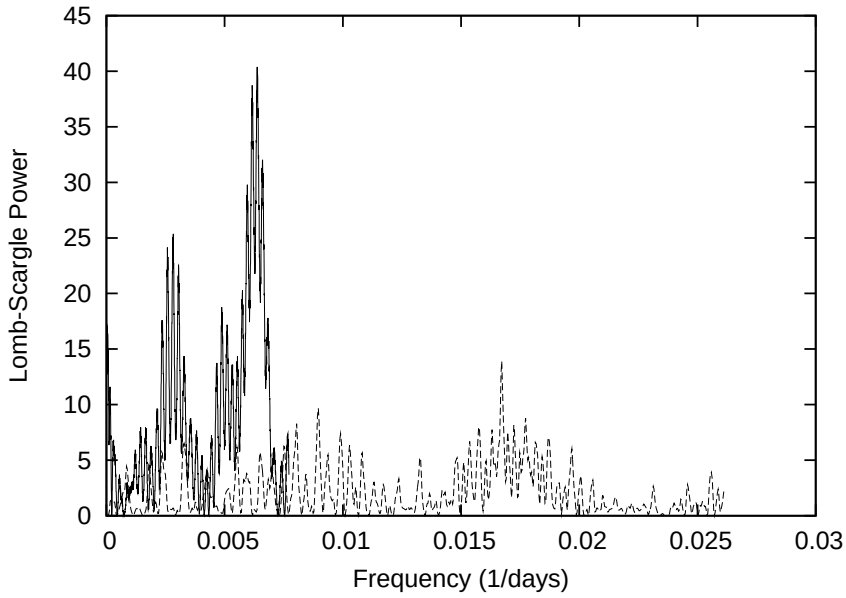

Figure 5.13: Periodicities from a Lomb-Scargle analysis of the Principal Component Analysis of the 42-foot data (solid line) and Lovell/Mark II data (dashed line) for B0740–28. Higher powers represent stronger periodicities. Peaks can be seen around 160 days and 360 days in the 42-foot data, which is only analysed to roughly 150 days. Less obvious peaks can be seen in the Lovell data at 120 and 60 days.

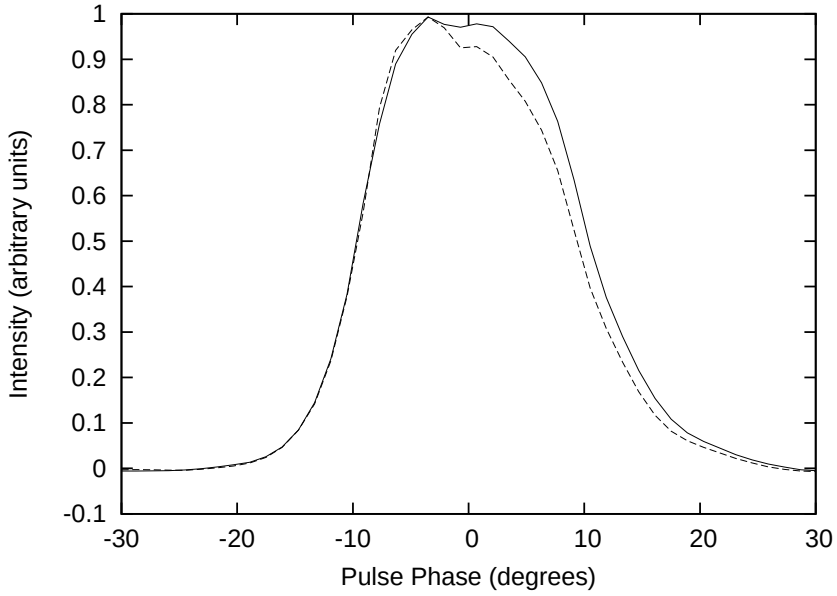

Figure 5.14: Possible profile changes from Principal Component Analysis of B0740–28, showing profile extrema reconstructed from a mean profile and the first eigenvector. This plot shows the average profile, plus the principal component at an amplitude of 0.5 (solid line) and -0.3 (dashed line) (c.f. Figure 5.12). This variation is likely due to contamination by bad data in the form of single-polarisation profiles in the database.

Lomb-Scargle data. Evidence for this comes from the change in amplitude of the right-hand side of the profile with the first eigenvector (see Figure 5.14). Despite this, we can see a strong periodicity in the main section of our 42-foot data (Figure 5.12) on a period of around 160 days. A Lomb-Scargle analysis was performed of this and the contaminated Lovell data, and are presented in Figure 5.13. The 160-day periodicity is picked up well, along with a further periodicity at approximately 360 days, although the maximum of this is very difficult to place. The Lovell data also supports a periodicity at 60 and 120 days, but extreme caution should be exercised here. In both cases, the rv1 - rv2 plot (right hand frame of Figure 5.12) shows a distinct non-Gaussianity in the first eigenvector, suggesting that profile changes are indeed taking place, with the first eigenvector describing the changes completely. This change is found to correspond to a change in amplitude of the right-hand component (see Figure 5.14), in a similar way to that seen in B1828–11.

Investigation of the timing residuals for this pulsar were also looked into, shown in Figure 5.15. Initially a broad change in period can be observed on timescales of thousands of days, with the possibility of a periodic structure around 4000 days. Closer examination reveals other waves superimposed on top of this. Analysis of the Lovell data yields several possible periodicities at 130.1 $\pm$ 1.9 days, 200.2 $\pm$ 6.1 days, 253.2 $\pm$ 9.1 days, 296.5 $\pm$ 7.7 days, and 487 $\pm$ 41 days. The 42-foot data, which has independent sampling, confirms periodicities at 296.5 $\pm$ 7.7 days and 500 $\pm$ 23 days, also giving periodicities at 397 $\pm$ 12 days, and 632 $\pm$ 32 days. Independent studies by Hobbs *et al.* (*private communication*) have shown a periodicity at 379.8 $\pm$ 4.2 days, along with further periodicities at 449 $\pm$ 7 days, 536 $\pm$ 13 days and 1430 $\pm$ 74 days above a null probability level of 10^{-9}. Hobbs *et al.* also found numerous other weaker periodicities, including ones at 128.9 $\pm$ 1.0 days, 248.2 $\pm$ 2.1 days and 258.9 $\pm$ 2.3 days, which match

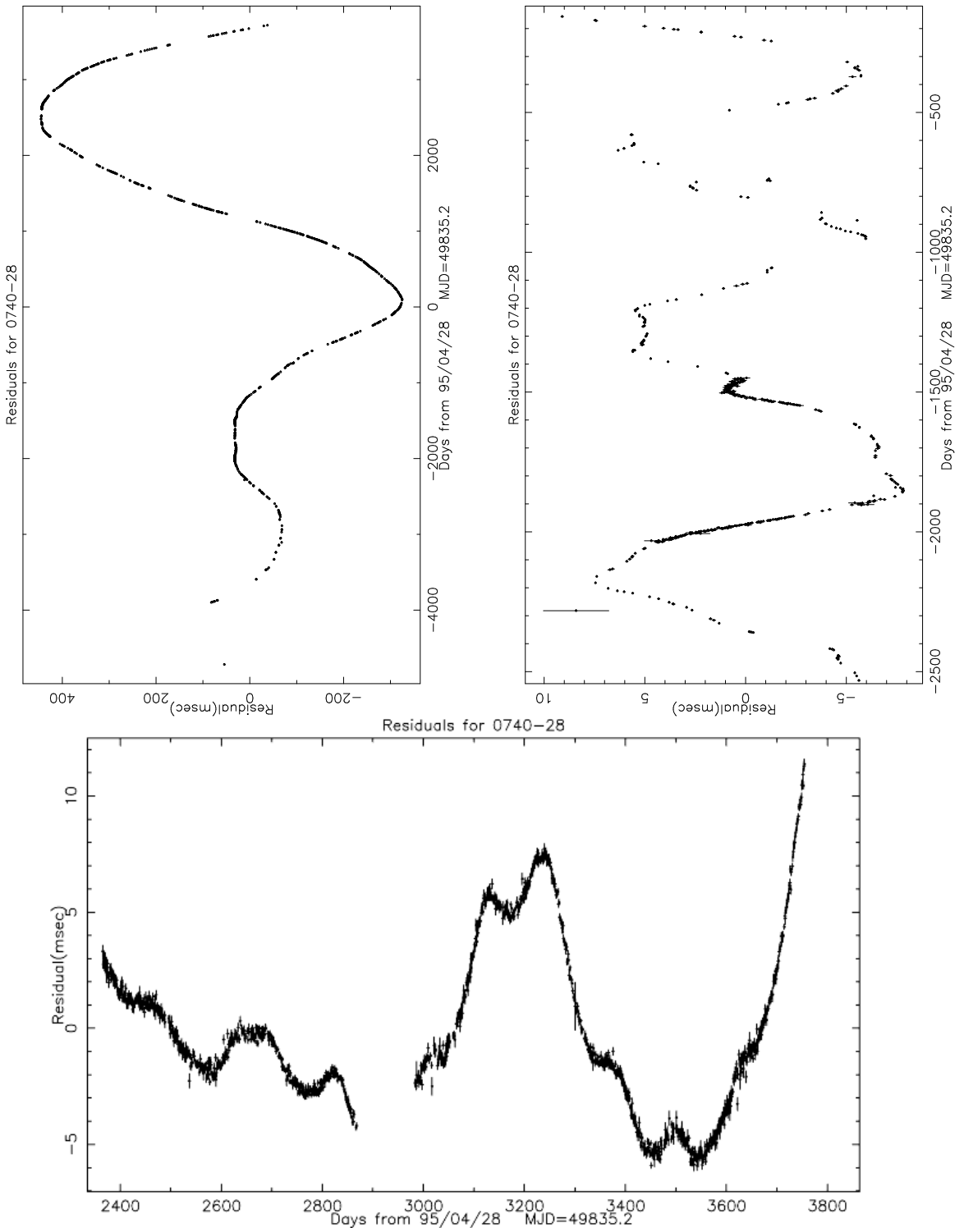

Figure 5.15: The timing residuals of B0740–28. The upper-left plot shows the residual data from the Lovell and Mark II telescopes with no fitting. A fit for the period and its first two derivatives (P, $\dot{P}$, and $\ddot{P}$) has been made to the left-hand maximum and is shown in the upper-right frame. The lower frame is a fit to the data after the right-hand maximum of the upper-left plot, but this time using data from the 42-foot telescope, which has a better sampling frequency. Periodicities are seen in both fitted plots at around 125 days and 700 days, plus a possible 4000 day periodicity in the unfitted plot.

up with periodicities determined from the Lovell data.

In summary, this pulsar shows many, if not all of the classic signs of precession. While it has been difficult to determine periodicities exactly, the Lomb-Scargle test, the timing residuals and possibly also the P.C.A. test all show variations on a period of between 115 and 125 days. Shape changes may also be visible on timescales of 160 days and 330–360 days. The proximity of the proposed 360-day periodicity to an annual periodicity is of concern, but recognised profile shape changes and a high ecliptic latitude (-49 degrees) suggest that this is not a terrestrial or solar system induced effect. This period may also tie in as a harmonic of the 700-day periodicity in the timing residuals. It appears possible that this pulsar could be undergoing precession, although which of the components are varying and how is impossible to tell without higher-resolution data.

5.7 B1830–08

B1830–08 is a relatively short-period pulsar, with a rotation period of 85 ms (Hobbs et al. 2004b). It also has a high DM (411 cm^{-3} pc).

Examination of our Lomb-Scargle results (Figure 5.16 [left]) shows that there is a periodic variation detected with a period of 5700 days. A slightly weaker peak is also seen at 7120 days. The same beating effect that has been seen in B1828$-$11 and B0740$-$28 may be present here, but the resolution of our data is not sufficient to detect it. It is most likely that, in this case, a fundamental frequency lies somewhere within this range. The plot also shows us that the variations are largely in the width of the main component.

If we examine our P.C.A. results (Figure 5.17), we see what appears to be either a bimodal or long-period wave-like structure in the first eigenvector evolution (left frame), which is borne out by either a bimodal or linear plot in the

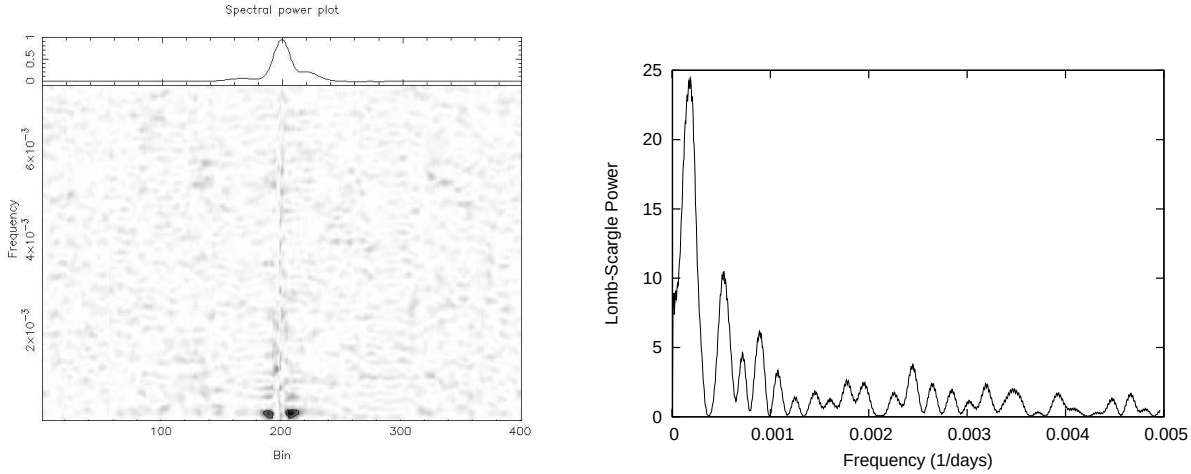

Figure 5.16: Periodicities found in data for B1830–08. The left panel shows the phase-binned Lomb-Scargle result (see Figure 5.1 for explanation), and the right panel shows the periodicity analysis of the P.C.A. data (see Figure 5.2). In both cases, periodicities are visible at 5500–7500 days and, more weakly, at around 1900 days.

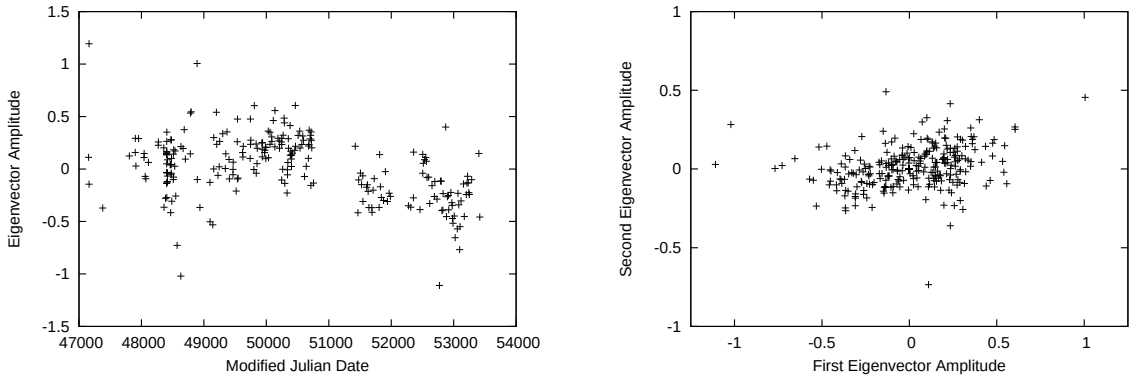

Figure 5.17: The variation of the principal components (eigenvectors) from Principal Component Analysis for B1830–08. The panels are as described in Figure 5.6. The evolution over time of the first eigenvector shows apparent trends — a slight increase towards MJD 51000 and a decrease to a minimum around MJD 53000 — the cause of which could be inherent behaviour on approximately a 7000-day scale, or, more likely, instrumental variations due to the filterbank change. The outlying profiles contain RFI contamination.

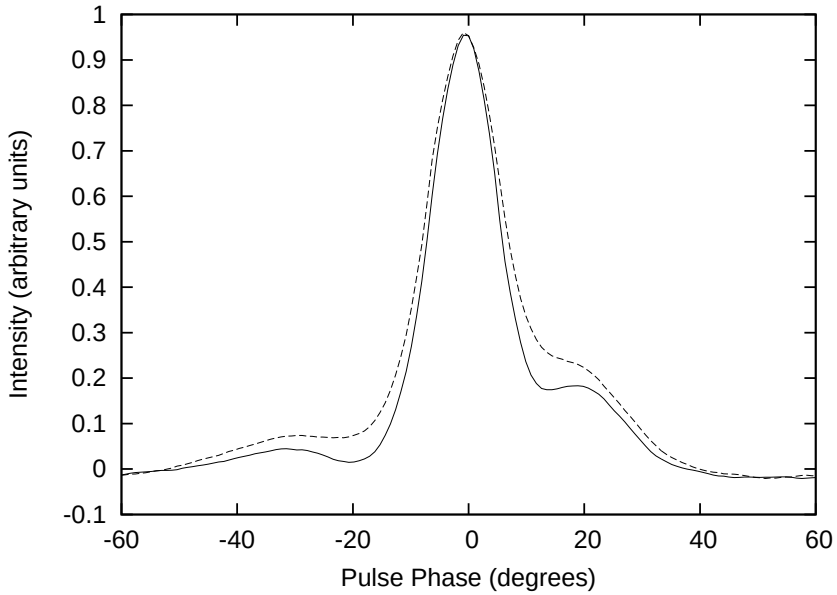

Figure 5.18: Possible profile changes from Principal Component Analysis of B1830–08, showing profile extrema reconstructed from a mean profile and the two principal eigenvectors. This plot shows the average profile, plus the first two components at an amplitude of 0.2 and 0.05, respectively, for the solid profile, and at -0.3 and -0.05 for the dashed profile (c.f. Figure 5.17).

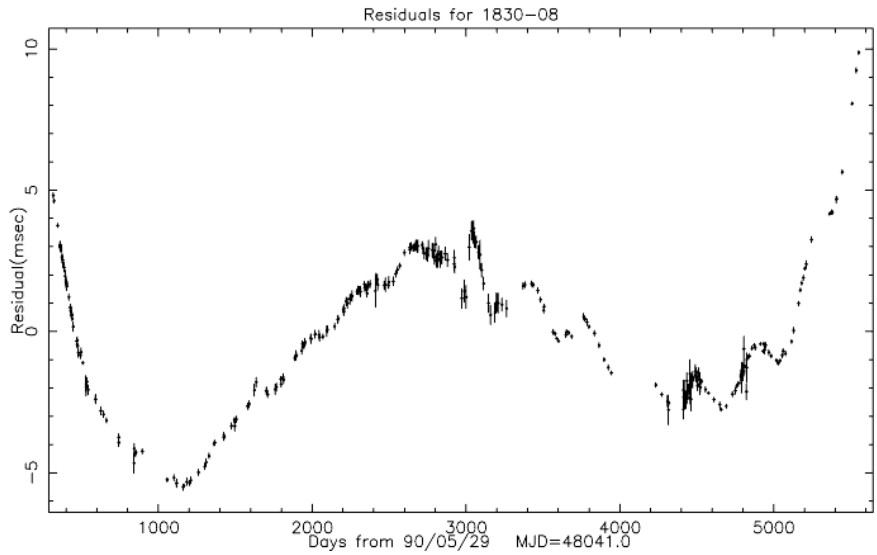

Figure 5.19: Timing residuals observed for B1830–08 over the last 15 years following a fit to the pulse period (P) and its first two derivatives ($\dot{P}$, $\ddot{P}$). A major glitch was observed around MJD 48041, and only the data following this is shown. A sinusoidal variation with a period of around 3000 days is present, along with a weaker periodicity at 304 ± 5 days.

first/second eigenvector plot (right frame). A Lomb-Scargle analysis of the first eigenvector produces a strong peak at a periodicity of 5340 days, which appears to correspond with the 5700 period from the original phase-binned Lomb-Scargle analysis. We can also pick up a slight beating effect here. A less significant peak in the power spectrum is also picked up at 1890 days, which corresponds very closely to a fainter 1900-day periodicity in the phase-binned Lomb-Scargle analysis. The profile changes here correspond to an increase in flux from the outlying components, as can be seen in Figure 5.18, in contrast to the change found using Lomb-Scargle analysis above.

Examining the timing residuals (Figure 5.19), we find a more complex picture. A glitch with a short recovery period can be seen around MJD 48040 (Shemar & Lyne 1996a). It is possible to fit a wave to the timing residuals with a period of roughly 3000 days, which would be roughly double that found using shape change tests. This suggests that there may be a real change going on in the pulsar, with effects similar to those provided by precession. Determining, with any certainty, if this is actually precession on a 3000- or 7000-day timescale would require a much longer dataset. Another possibility is the movement of the polar cap as a result of the glitch and later changes that mimic precession.

Several shorter periodicities also appear to be present in the timing residuals. A smaller wave present at 304 $\pm$ 9 days, is also present with strong periodicities at 636 $\pm$ 20 days, 1230 $\pm$ 130 and 1750 $\pm$ 140 days, all above a null probability level of 10^{-4}. Whether this has any relation to a weak periodicity (below our imposed cut-off threshold) in our Lomb-Scargle data at 50 and 59 days at 20% probability is open to debate. Independent analysis by Hobbs *et al.* (*private communication*) confirms periodicities at 53.0 $\pm$ 0.3 days, 651 $\pm$ 18 days and 1340 $\pm$ 150 days, and also detects periodicities at 715 $\pm$ 27 days, 857 $\pm$ 62 days and 1023 $\pm$ 47 days, again above a null probability level of 10^{-4}.

To summarise, B1830−08 may to show some evidence for aperiodic profile variations which could be consistent with precession of a tri-axially asymmetric pulsar. However, corroboration with the timing residuals is complicated by a glitch. We put forward that it is possible that B1830−08 is undergoing real variations, but these would be very small and our detection of them is complicated by problems arising from hardware changes at Jodrell Bank, specifically changes in the filterbank used.

5.8 B0144+59

B0144+59 is a moderately fast rotator, at 196 ms, though with a fairly low spin-down rate of 2.57×10^{-16} (Hobbs et al. 2004b). It is of fairly low luminosity, at 7.66 mJy kpc^2 at 1400 MHz (compared to a median for our sample of 34.2 mJy kpc^2). High resolution data (Seiradakis et al. 1995) show the main component, unresolved in the Lovell data, to be comprised of two distinct peaks, and at low frequencies von Hoensbroech et al. (1998) showed there to be three resolved components. Von Hoensbroech *et al.* pointed out that the pulsar has a high degree of circular polarisation (see also Gould & Lyne 1998), which increases with frequency, in contrast to expected depolarisation towards higher frequencies. They also show that this pulsar has a significant amount of linear polarisation and find a strong frequency development. It is therefore possible that the profile of this pulsar will change significantly over the bandwidth used in this study.

Looking at our data, our phase-binned Lomb-Scargle periodogram picks up a very definite 310-day periodicity in the data (Figure 5.20), which is reflected in a periodogram (Figure 5.22) of the first eigenvector of our P.C.A. data. The variation of the first eigenvector in Figure 5.21 shows rapid increases, then a decay towards a negative contribution. This decay reflects a change in the pulse profile, corresponding to an decrease in both the width of the profile and the

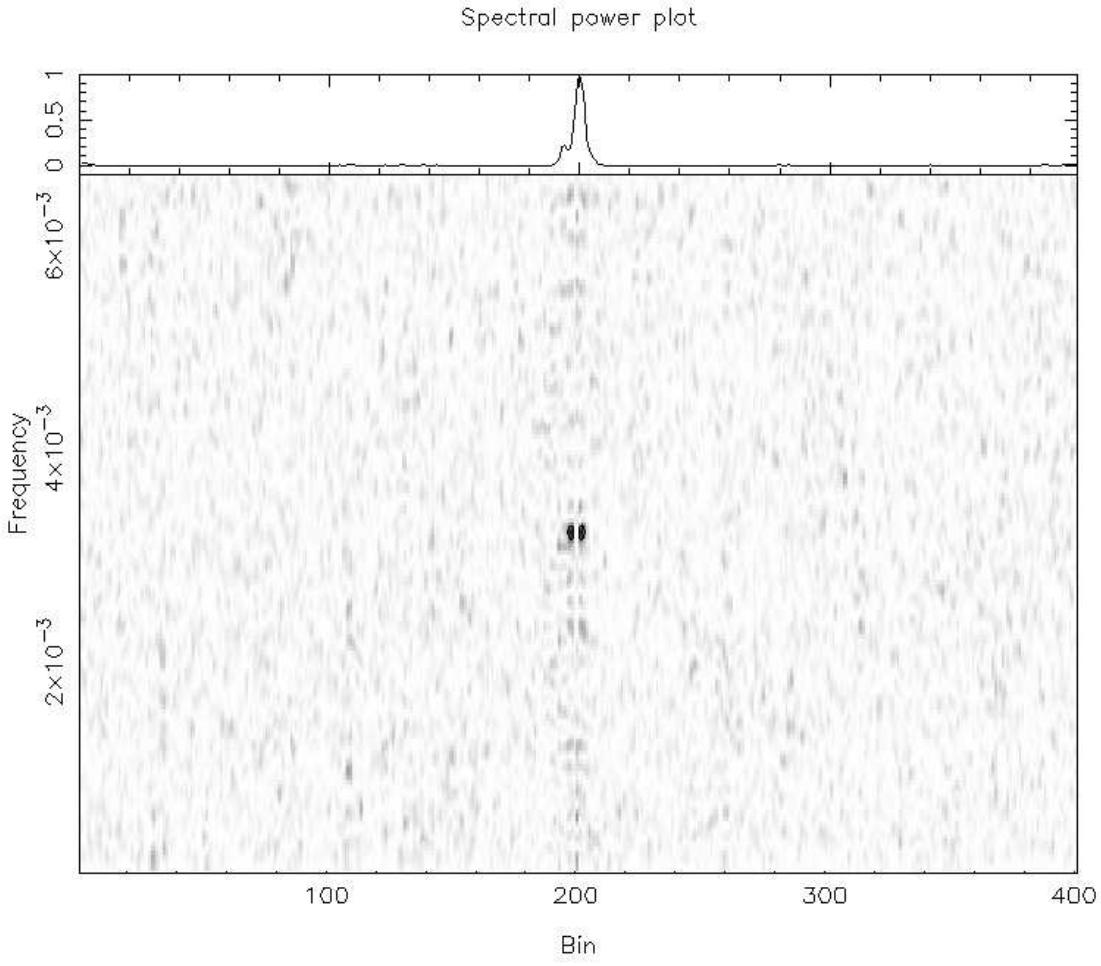

Figure 5.20: Signal strength for B0144+59 from Lomb-Scargle periodogram analysis. For an explanation of this plot, see Figure 5.1. A clear periodicity can be seen at 310 days.

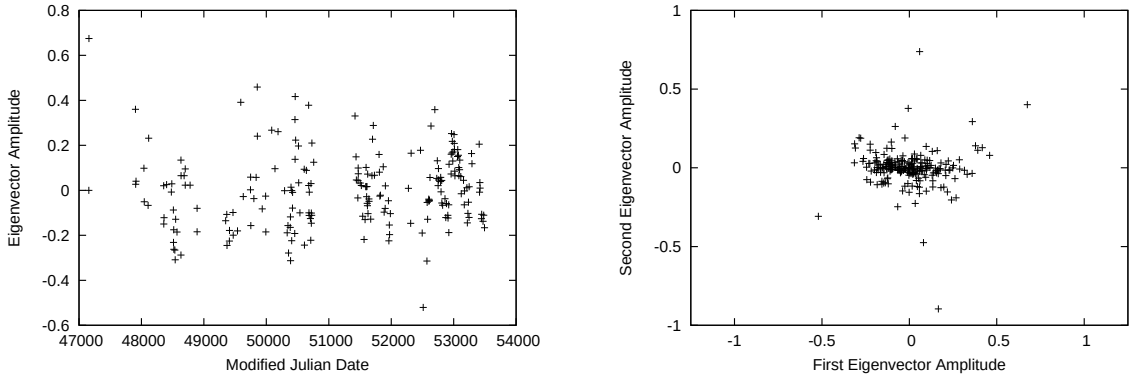

Figure 5.21: The variation of the principal components (eigenvectors) from Principal Component Analysis for B0144+59. The panels are as described in Figure 5.6. The first eigenvector (left panel) shows a variation on a timescale of around 300 days, particularly in the later data which, although not readily visible, is found to a high significance in a Lomb-Scargle periodogram of the data, as shown in Figure 5.22. A periodogram of this is presented in Figure 5.22. The first/second eigenvector plot (right panel) shows a linear structure around the first eigenvector, with the second eigenvector being mostly random, suggesting the first eigenvector accounts entirely for the observed changes.

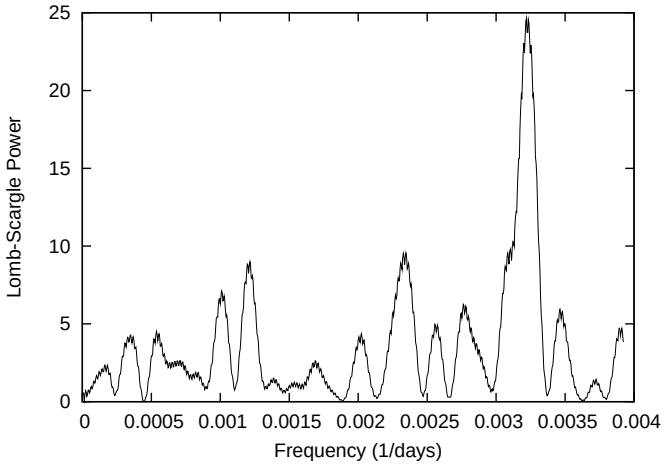

Figure 5.22: Periodicities from a Lomb-Scargle analysis of the Principal Component Analysis (see Figure 5.21) of B0144+59. Higher powers represent stronger periodicities. A strong periodicity can be seen at a period of 310 days.

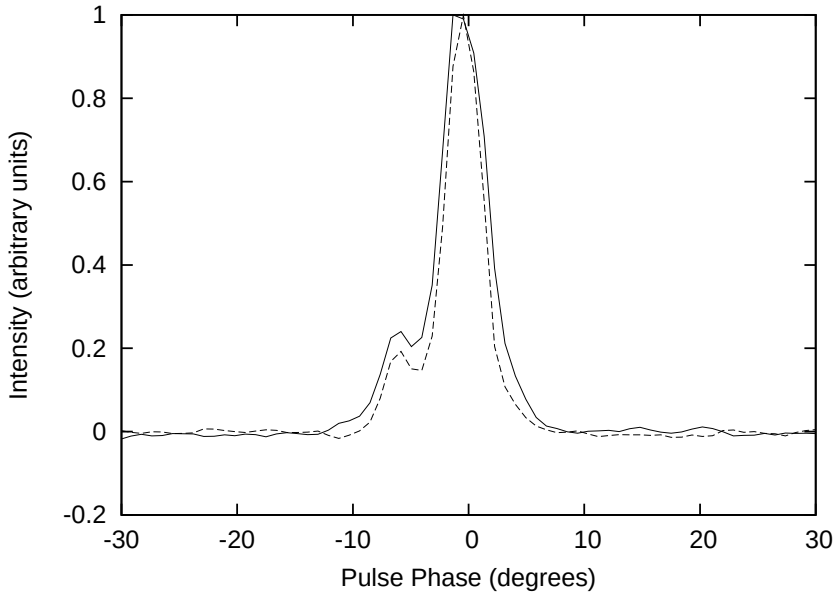

Figure 5.23: Possible profile changes from Principal Component Analysis of B0144+59, showing profile extrema reconstructed from a mean profile and the two principal eigenvectors. This plot shows the average profile, plus the first two components at an amplitude of 0.25 and -0.05, respectively, for the solid profile, at -0.2 and 0 for the dashed profile and at 0 and 0.2 for the dotted profile (c.f. Figure 5.21).

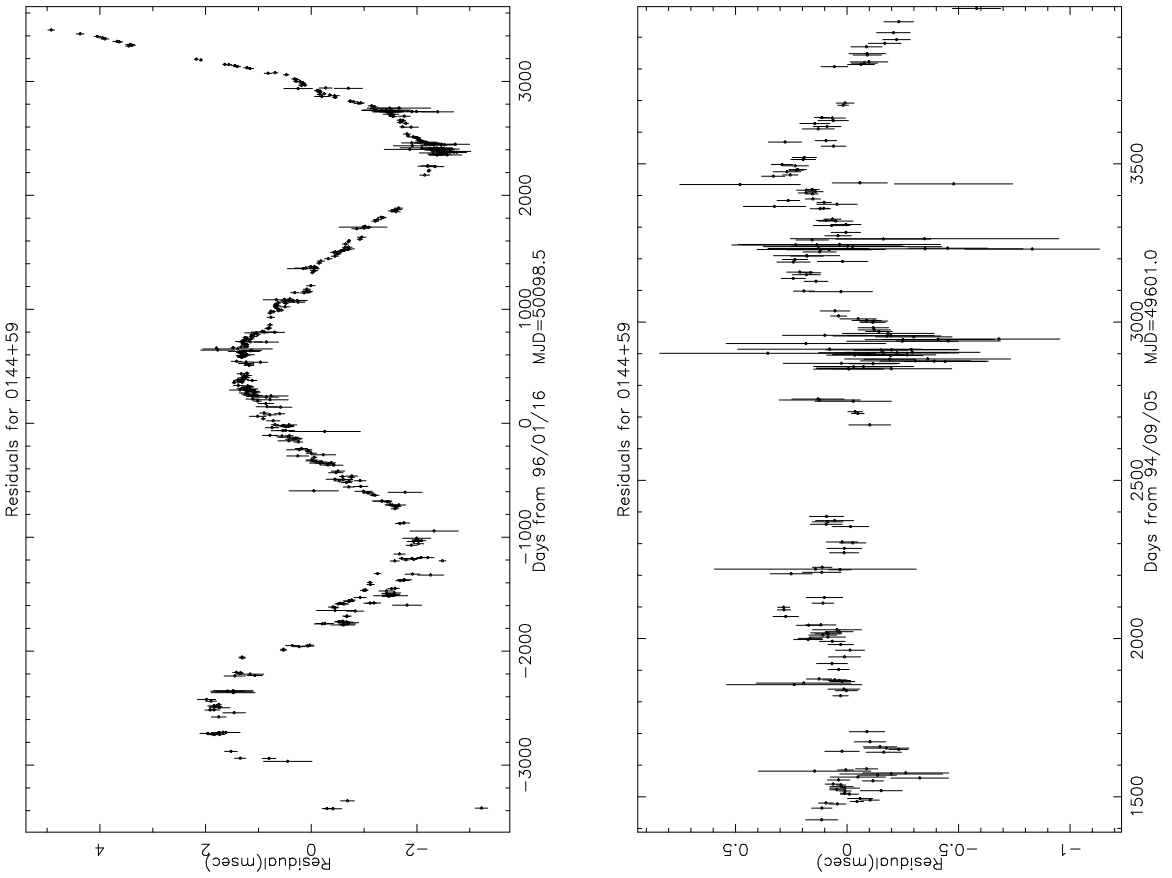

Figure 5.24: The timing residuals of B0144+59 from the Lovell database. The right plot shows an enlargement of the right-hand (latter) minimum, fitted for period (P) and the first two period derivatives ($\dot{P}$ and $\ddot{P}$). The timing residuals show a wave-like structure with a possible periodicity of around 5000 days, with a 330-day period superimposed on top of this, at an amplitude of around 200 μs. A fit for position and proper motion does not remove this wave.

amplitude of the leading (left-hand) component (see Figure 5.23). The changes seem entirely described by the first eigenvector (also Figure 5.21), as the second eigenvector shows a Gaussian distribution, while the first does not.

Examination of the timing data (Figure 5.24) shows a very strongly-varying structure, possibly exhibiting a periodicity of around 3500 days. In our fitted data, we find strong periodicities at 330 ± 11 days and at 1280 ± 150 days, although the latter may be an artifact of the fitting process. Other periodicities may also be present in the data, including one at 54 ± 2 days. It should be stressed that the amplitude of all these variations is very small compared to the $\sim$ 4 ms FWHM of the pulsar peak (**?**)seiradakisetal:0144+59). Amplitudes on this timescale could well be due to inaccuracies in the timing method caused by template matching to profiles of a changing shape, or could be due to timing noise, but we believe that the profile changes are small enough and the timing variations regular enough that this is not the case.

Independent analysis of the timing residuals (Hobbs *et al.*, *private communication*) confirms these periodicities as 329.5 ± 2.7 days and 1214 ± 27 days, and also other strong detections at the following periods: 196.7 ± 0.6 days, 224.1 ± 1.1 days, 342 ± 2.1 days, 377.3 ± 4.1 days, 442.6 ± 5.6 days, 463.7 ± 4.7 days and 613.5 ± 7.2 days, all with null probabilities below 10^{-6}. It should be noted, however, that these periodicities were only found when the *hifac* ratio (see Chapter 3 and Press et al. 1992) in the Lomb-Scargle period search was increased to 50 to give sufficient time resolution.

With all our methods for detecting precession apparently pointing to a 310- to 330-day periodicity in the data, we must conclude that it is possible that precession is taking place. Two things, however, are remarkable. The first is the very small amplitude of the variations in the timing data — only around 200 μs for B0144+59 against several to tens of milliseconds for our other cases. The

second is the lack of harmonics in the data. There appear to be no harmonics, nor subharmonics, above the noise level. The only possibilities are a 70-day (fifth harmonic) periodicity and a 1820-day (sixth sub-harmonic) periodicity in the Lomb-Scargle results, but these are both well below our imposed noise limit. A further point of note is that the 310-day periodicity is consistent and well-defined enough and far enough away from a 365-day periodicity for us to conclude that it is unlikely to be either due to filterbank or receiver changes, or due to errors in the pulsar position.

To summarise, there appears to be a real change in the pulse width of B0144+59 over a period of 310 days, which could be reflected in the timing residuals. However, this could be affected by variation of the pulse profile over the observed bandwidth. For this reason, we suggest that it is possible that B0144+59 is undergoing precession, but we cannot prove this conclusively at this point in time.

5.9 J0631+1036

J0631+1036 is a moderate period pulsar (288 ms — Hobbs et al. 2004b) and displays a pulse with four clearly-resolved peaks. We find good evidence for changes in the second (both in phase and brightness) of these components. Whether these changes are periodic, or constitute a precessional effect, we have not resolved.

Figure 5.25 shows the variation of the first eigenvector from our P.C.A. data with respect to time (left) and with respect to the second eigenvector (right). The right-hand panel of Figure 5.26 shows the power spectrum of the first eigenvector with respect to time. Numerous peaks appear visible, in particular representing the first six harmonics of a 3500-day period. The strongest of these appears to be an 880-day period, which would represent the fourth harmonic, and may be visible around MJD 53000 in Figure 5.25.

The periodicities determined here are also reflected in our phase-binned Lomb-Scargle results (left panel of Figure 5.26). These results show variations mainly in the second component with some changes in the fourth components. This corroborates with the profile changes from our P.C.A. data (Figure 5.27) — the changes here seem largely confined to the second component with the first and fourth components varying to a lesser extent. That we do not find any changes in pulse width from any of the four components suggests that it is not a filterbank issue. This change could be polarisation-related, but could well be real.

Analysis of the timing residuals (Figure 5.28) provide further clues. The pulsar shows four glitches prior to MJD 50730 (*Jodrell Bank Observatory Pulsar Glitch Database (unpublished)*), which are not shown on the plot for clarity. What is interesting is the remaining data. Several arcs and a large glitch can be seen (there are also two smaller glitches present, but they are not easily visible on the scale shown). We speculate that the arcs may form part of a 3500-day period wave which may have been occasionally interrupted. A power spectrum of the timing residuals shows several weak (sub-millisecond amplitudes), yet statistically significant periodicities at 249 ± 8 days, 137 ± 3 days, and 67.5 ± 0.8 days. Other peaks exist at 384 ± 27 days, 620 ± 50 days and 1150 ± 160 days, but some or all of these are likely present due to the glitches.

There appears to be substantial evidence that shape changes are occurring in J0631+1036. Whether these are due to precession, glitch-related behaviour or some other mechanism, we cannot determine.

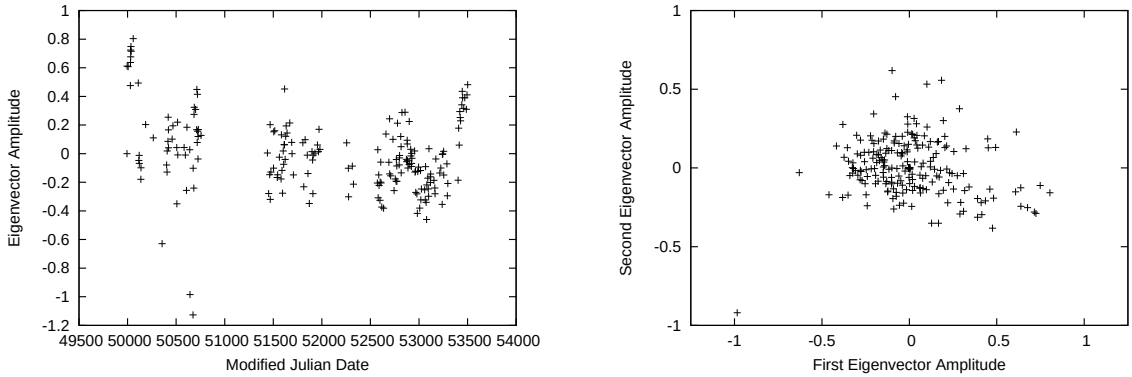

Figure 5.25: The variation of the principal components (eigenvectors) from Principal Component Analysis for J0631+1036. The panels are as described in Figure 5.6. The evolution of the first eigenvector (left panel) shows a distinct downward trend which could be independent of filterbank changes. A possible 880-day periodicity exists, especially around MJD 53000. The first/second eigenvector plot (right panel) shows a fairly Gaussian-like appearance, apart from a 'tail' to the lower-right, which represents the most recent few profiles, and a slight linear tendency about the x-axis (first eigenvector). The direction of this tail shows that both the first and second eigenvector are significant.

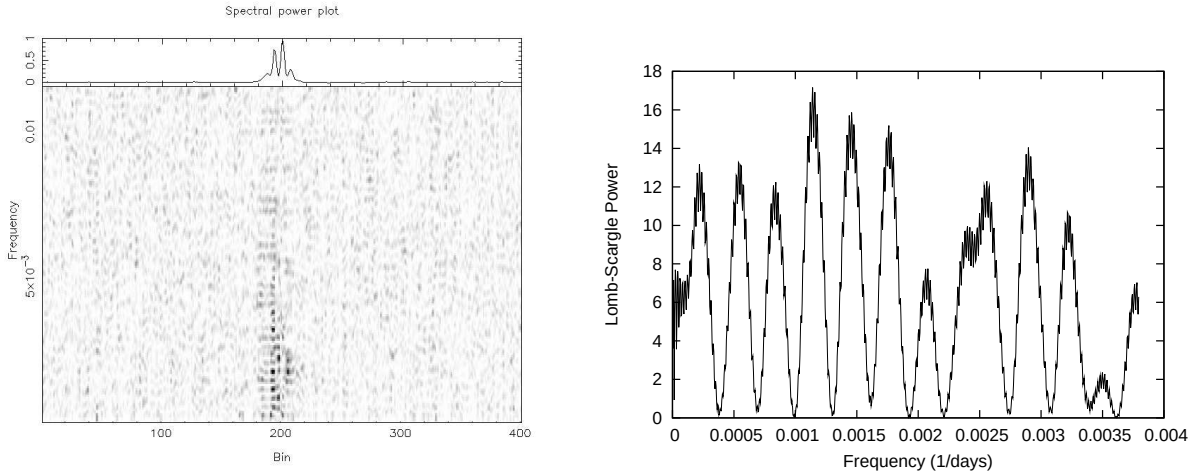

Figure 5.26: Periodicities found in data for J0631+1036. See Figure 5.16 for an explanation of the plots. A large number of periodicities have been found in this data, both in the phase-binned Lomb-Scargle results and the P.C.A. periodogram. Note also the 'beating' effect present.

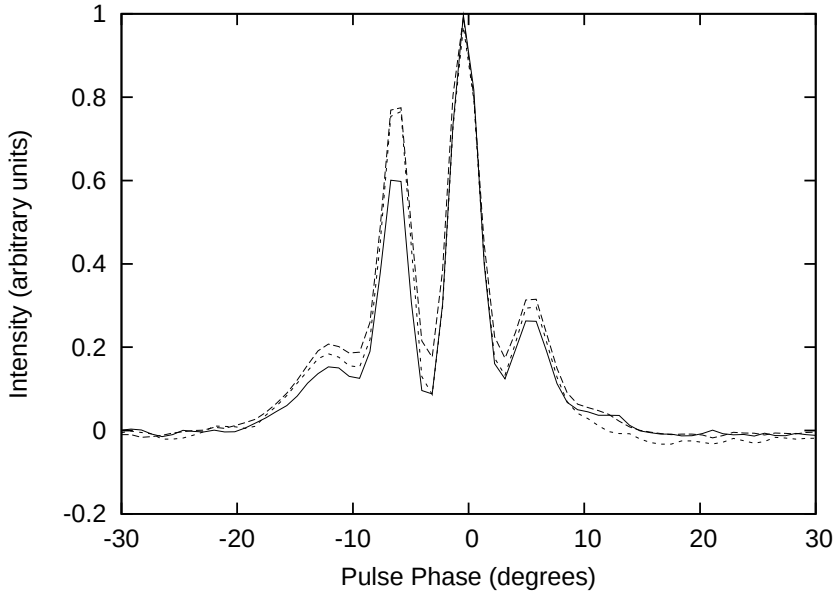

Figure 5.27: Possible profile changes from Principal Component Analysis of B0631+1036, showing profile extrema reconstructed from a mean profile and the two principal eigenvectors. This plot shows the average profile, plus the first two components at an amplitude of 0.3 and −0.2, respectively, for the solid profile, at −0.3 and 0 for the dashed profile and at 0 and 0.2 for the dotted profile (c.f. Figure 5.25).
5.25

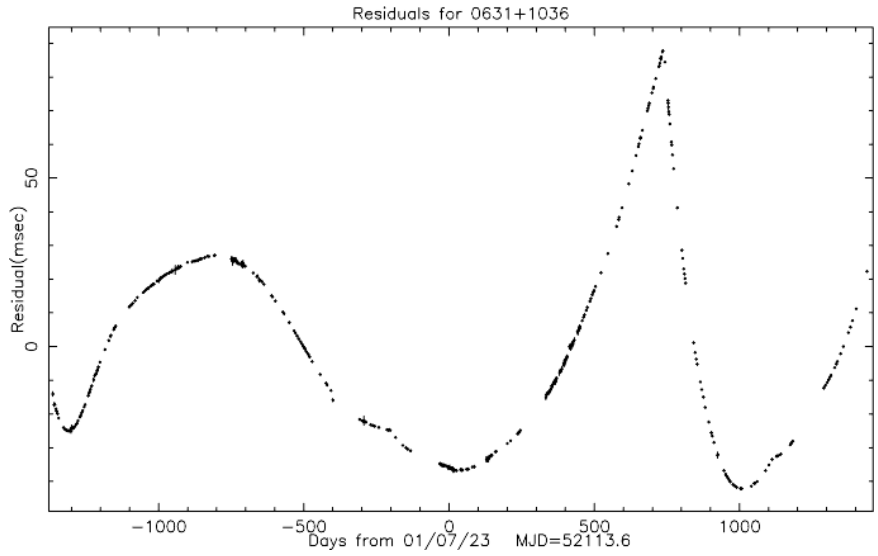

Figure 5.28: Timing residuals observed for J0631+1036. These data are for the period of coherent timing only. Note a pseudo-sinusoidal period of around 1800 days which can be seen in several places and the (comparatively) small period change at MJD 52740.

5.10 B0329+54

5.10.1 Literature

B0329+54 is a long-studied pulsar that has been speculated to harbour a planetary system (e.g. Demianski & Proszynski 1979). It is the brightest pulsar in our dataset, hence one where we have the greatest signal-to-noise. It is moderately close, with a parallactic distance of 1060 pc (Taylor & Cordes 1993) and has a fairly long period (715 ms – Hobbs et al. 2004b). With a characteristic age of 5.53 Myr (Manchester et al. 2005), it is one of the older pulsars in our study, hence if precession is occurring here, it should provide insight into the strengths and abilities of any damping mechanisms present.

The first relevant study on B0329+54 was by Demianski & Proszynski (1979). In this study, they made a claim for a periodicity in the timing residuals of the pulsar with a period of 1105 ± 30 days. This was followed by a study by Bailes et al. (1993) which confirmed a 1101-day period and found another 2370-day period, despite having not been seen in other studies. A further periodicity at 6160 ± 60 days was reported by Shabanova (1995), along with a confirmation of the 1105-day period. Most recently, Konacki et al. (1999) ruled out a reproduction of the 3-year orbit in more recent data taken from the Effelsberg and Torun databases.

B0329+54 is also known to mode-switch between four distinct modes (Rankin 1986). These manifest themselves predominantly in changes in amplitude of the outlying components and a slight 'shift' of the main pulse from the beam centre.

5.10.2 Timing Residuals

We now present our own timing residuals from the Jodrell Bank database. Periodicities can easily be seen by eye in the data. Figure 5.29 shows recent timing

residuals from the Lovell, Mark II and 42-foot telescopes. Both appear to show a periodicity on a timescale of around 375 days — the Lovell/Mark II data at 377 ± 3 and the 42-foot data at 374 ± 28. Interestingly, this shows up in the work of Konacki *et al.* in their Torun data. It is also confirmed by Hobbs *et al.* (*private communication*), who show a strong periodicity at 377.4 ± 3.9 days, as well as strong periodicities at 443 ± 5 days and 1212 ± 28 days. As with B0144+59, these latest periodicities only become present when increasing the *hifac* ratio on the Lomb-Scargle period analysis (see also Chapter 3 and Press et al. 1992).

Our 377-day periodicity is very close to an annual variation, although a fit to the data for position and proper motion cannot remove the wave successfully. We therefore have concurrent data from four telescopes using two separate reduction methods. Interestingly, the periodicity we find is almost exactly a third of that found by Demianski & Proszynski.

With the apparent departure from the suggested 6160-day periodicity, the loss of the 1105-day periodicity and now an apparent 375-day periodicity, it is tempting to suggest that at least the latter two modes represent different modes of precession that are being excited. However, it would be premature to suggest this without presenting evidence for corresponding shape changes in the profile.

5.10.3 Principal Component Analysis Results

Unfortunately, our P.C.A. tests fail to reproduce any substantial periodicities. It may be that the strength of the variations is not strong enough to be detectable by our tests, or it may be that the variations are not there at all. Another possibility is that P.C.A. picks up the mode-switching more readily than longer-term changes. Examination of the eigenvector profiles shows that the first eigenvector does appear to show longer-term changes not associated with moding, but that the second and third eigenvectors represent moding changes.

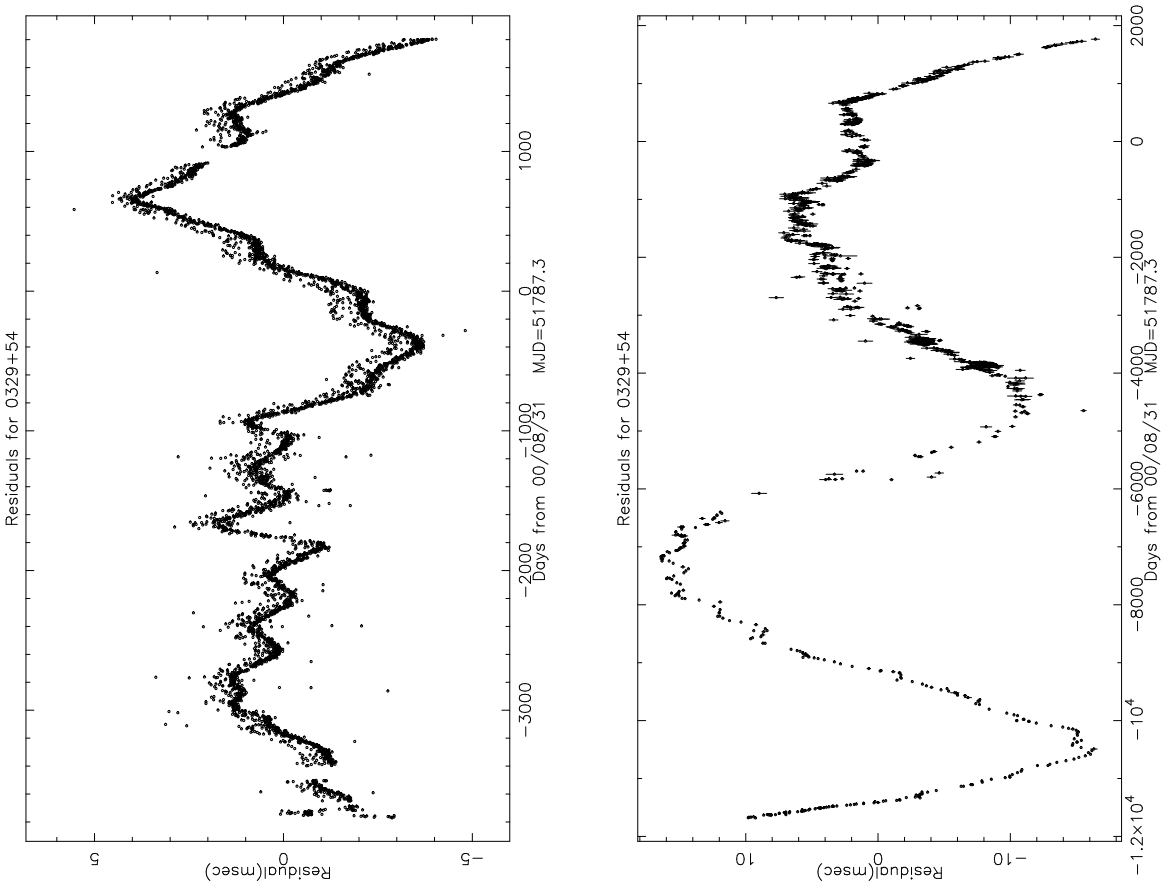

Figure 5.29: A section of the timing residuals observed for B0329+54 from the Jodrell Bank pulsar database. Data from the 42-foot telescope (left — for clarity shown without error bars) and Lovell/Mark II telescopes (right) are shown. These have been fitted for the pulsar period and its first two derivatives (P, $\dot{P}$, $\ddot{P}$). Periodicities of around 375 days and 1500 days are seen in both sets of data, with a 6000-day periodicity also seen in the Lovell/Mark II data.

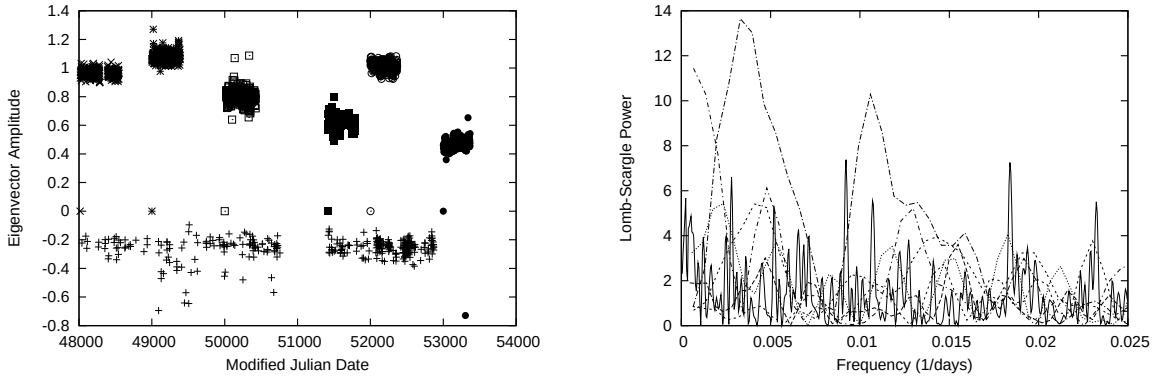

Figure 5.30: The variation of the principal components (eigenvectors) from Principal Component Analysis for B0329+54. The left-hand panel shows the evolution of the first eigenvector over time, similar to that of Figure 5.7 and the right-hand panel shows a power spectrum of these data, similar to Figure 5.2. As with Figure 5.7, the discontinuities between the 1000-day segments are due to different principal components being assigned in different segments. Data from the Lovell/Mark II telescopes are shown as "plus" signs on the left-hand plot and a continuous line on the right hand plot. The 1000-day segments from the 42-foot telescope data are shown in other styles. Various tentative periodicities were found using a period search on this data, including several around 380 days, but nothing of sufficient significance to be above our noise threshold.

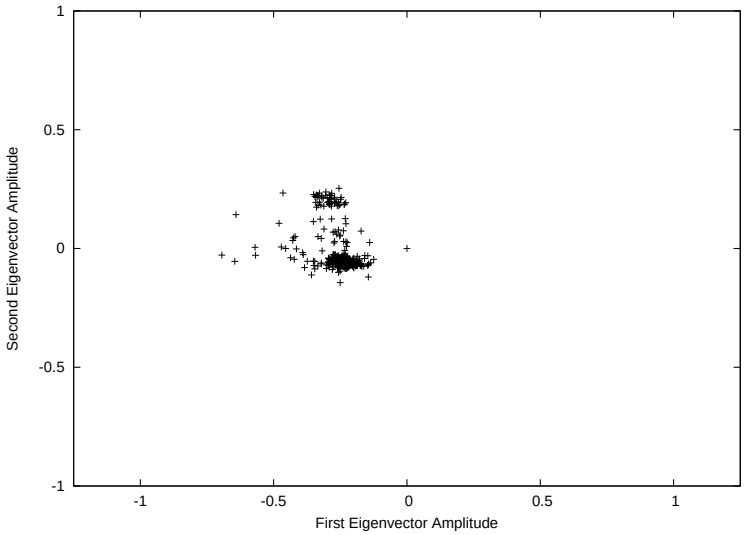

Figure 5.31: The variation of the first and second components (eigenvectors) from Principal Component Analysis over time for B0329+54, as in Figure 5.3 and other Figures. The bimodal distribution of this plot reflects two distinct modes of emission, corresponding to a change in the second eigenvector. A third mode, corresponding to a change in the first eigenvector is present, but is not clearly visible. This is distinct from the continuous variation seen in B1828–11 (Figure 5.3).

Tentative periodicities can be seen in the data by eye (see Figure 5.30), especially around MJD 51000 in the 42-foot data and MJD 52500 in the Lovell data, both at a period approaching 380 days, but they are not strong enough to register in our data with sufficient significance.

It is worth noting that, at these timescales, the resolution of the 42-foot data periodogram may be insufficient to find periodicities of several hundred days (i.e. 40% of the length of the dataset). A 308-day periodicity was found in the MJD 51000–51999 segment, which may correspond to a weak 356-day periodicity found in the Lovell data, which could in turn correspond to the 380-day periodicity found in the timing residuals. However, this is highly speculative and far from conclusive evidence at this point.

Table 5.1: Possible harmonics and resonances from phase-binned Lomb-Scargle Analysis of B0329+54, based on a 380-day fundamental period. The asterisked entry marks the Lovell/Mark II data, the remainder are from the 42-foot telescope data.

Date (MJD) '000s	Detected Periods (days)				Harmonic Number				Percentage Departure			
48	47.5	44.3	45.3	64.6	8			6	0.8%			11.4%
49	80.0	125.0	88.9	97.6		3		4		3.9%		10.6%
50	276.0	112.4	178.6	758.9	4/3		2	1/2	5.8%		12.8%	0.1%
51	291.7	583.4	89.8	86.4	4/3	2/3			4.1%	2.3%		
52	74.1	363.7	571.6	190.5	5	1	2/3	2	12.9%	4.5%	0.3%	0.6%
53	199.5	498.6	51.1	199.5	2			2	9.5%			9.5%
$\star$	54.3	127.9	123.1	325.3	7	3	3		0.7%	2.9%	8.7%	

5.10.4 Lomb-Scargle Results

Our phase-binned Lomb-Scargle data produce strong periodicities for all periods for the 42-foot data, and marginally significant periodicities in the Lovell data. Although not shown here, all these strong periodicities occur close to the main pulse peak, which would be concordant with shifting due to mode-switching, but could also be indicative of other changes.

Table 5.1 shows the periodicities returned by our Lomb-Scargle tests for the 42-foot and Lovell(/Mark II) data. Many of these periodicities are very strong (see Table 4.2), rivalling those found in B1828–11. The pattern here, however, appears to be more complex. Following the 380-day periodicity in the timing residuals, we also give possible harmonics in the data which may correspond to this, and the percentage departure of the periodicities from them. Table 5.1 shows that a number of periodicities fit the data very well, both for harmonics of this period and sub-harmonics.

5.10.5 Conclusions

It appears clear that periodic timing irregularities are present in B0329+54 — this has been noted for decades. We find that a new periodicity may be present, with several harmonics of this period possibly visible in our Lomb-Scargle analysis of the data. This is highly suggestive of precession, although our P.C.A. results cannot confirm this. If this were the case, the sub-harmonics suggest that the 380-day periodicity is not the fundamental period. More likely, the original 1105-day periodicity found by Demianski & Proszynski is the true fundamental period — i.e. three times the 380-day periodicity found. Without fully concordant results from P.C.A. data, it is far from certain that precession is happening in B0329+54, but it may be a possible explanation for the behaviour of this source.

5.11 Other Possible Detections

The 39 pulsars deemed to be 'significant' in Chapter 4 were all studied in considerable detail, including the nine examined above. The remainder of these 'significant' pulsars were subsequently found either not to be likely candidates for precession, or are sources where the evidence is inconclusive. Table 5.2 states reasons why individual cases were rejected. In cases of insufficient data, the repetition period of the possible shape changes was deemed too long for us to be certain of its presence. For cases of lack of consistency between the results of different techniques, we find periodicities in shape changes using only one method (usually our phase-binned Lomb-Scargle technique), which are not present in the timing residuals. More detailed information is available on specific cases to the interested reader in the Appendix.

Table 5.2: The remaining significant pulsars not analysed in this Chapter, along with reasons for their rejection as candidates for precession in this study. More information on individual pulsars in presented in the Appendix.

Pulsar	Reason for Rejection
B1737–30	Insufficient data, timing disrupted by glitches
B1821–19	Insufficient data
B1933+16	No consistency between techniques, filterbank changes
B1930+22	Filterbank changes mimicking periodicities
B1913+10	Insufficient data, possible effects of filterbank changes
B1859+03	Filterbank changes mimicking periodicities
B1834–10	Filterbank changes mimicking periodicities
B1742–30	Filterbank changes mimicking periodicities
B0834+06	Timing disrupted by glitches, filterbank changes
B1838–04	No consistency between techniques, glitches, noise from sampling
B0919+06	Insufficient data
B0535+21	Insufficient data, timing disrupted by glitches
B1826–17	Insufficient data, possible periodic timing variations
B1822–09	Possible template matching errors, filterbank changes
J2043+2740	Data unclear, probably due to filterbank changes
B1620–26	Insufficient data
B1756–22	No consistency between techniques, filterbank changes
B1931+24	Lack of consistency, probably a sampling effect
B1929+10	Insufficient data
J1835–1031	Data sampling artifact
B0621–04	Insufficient data
B1133+16	No consistency between techniques
B0818–13	Insufficient data, probably due to filterbank changes
B2255+58	Filterbank changes mimicking periodicities, RFI
B2053+21	Filterbank changes mimicking periodicities
B1732–07	No consistency between techniques
B2020+28	Filterbank changes mimicking periodicities
B2045–16	Insufficient data, probably due to filterbank changes
B2035+36	Insufficient data
B0355+54	Possible template matching errors, no consistency between techniques

Chapter 6

Discussion and Conclusions

6.1 Summary of Possible Detections

A summary of our investigation into individual cases is presented in Table 6.1, with their properties presented in Table 6.2.

Naïvely, we would be surprised to find evidence of precession in only six out of the 281 pulsars we have studied, disregarding the results from previous studies. However, we only find weak evidence of precession in all cases except B1828–11. This suggests that what we are seeing is only the pulsars with the strongest precession, and that other pulsars may also show precession, but below our detection limit.

6.2 Statistics of Possible Detections

Table 6.3 contains a list of statistics relating to the possible detections with relation to those of the candidate sample. The immediately noticeable disparity between the two datasets is the characteristic age of the pulsars. This in turn leads to a typically shorter period, higher period derivative ($\dot{P}$), shorter pulse full-width half-maximum and higher rate of energy loss than the rest of the dataset.

Table 6.1: List of pulsars in which precession may have been detected by this study.

Pulsar	Precession detected?	Precessional Period(s) (days)
B1828–11	Yes	1000 (fundamental), 500, 250 possibly also 667, 400, 220, 157–169, 118
B0740–28	Probably	360, 160, 120, possibly also 60
B0144+59	Possibly	310
B0329+54	Possibly	1105 (fundamental), 380, many other harmonics
B1830–08	Unlikely	5500–7500, 1890–1900 possibly also 300, 50 and 59
J1022+1001	Unlikely	
J1713+0747	Unlikely	
B1642–03	No	
All other pulsars	No	

Interestingly enough, however, the magnetic field of the two sets is identical.

6.3 Comparisons with Theory

6.3.1 Damping

Perhaps one of the most crucial differences between pulsar precession theory and observations is the timescales on which precession would be damped. This damping depends on the nature of the coupling between the pulsar's superfluid core and its solid crust, the strength of this coupling and the timescale on which it occurs. While the details of this coupling remain unclear, much work has been done with pulsar glitches in an attempt to investigate this coupling.

While there have been several studies into the possible damping effects of precession, one of the most interesting studies (in that it allows precession to exist on timescale sufficiently long for us to observe it, which we appear to do) is that of Link & Epstein (2001) which states (after Sedrakian et al. 1999b) that

Table 6.2: Properties of the pulsars in which precession may have been detected by this study from the ATNF website (http://www.atnf.csiro.au/research/pulsar/psrcat) (Manchester et al. 2005). Figures in brackets show errors in the last digits where available. *Ec. — Ecliptic; Gal. — Galactic; Long. — Longitude; Lat. — Latitude; DM — Dispersion Measure; RM — Rotation Measure; S_f, L_f — Flux/Luminosity at f MHz; Est. — Estimated; B_surf — Surface Magnetic Field; v_trans — Transverse Velocity to Line-of-Sight. * Accuracy abbreviated for this table.* Note that J1713+0747 is in a binary orbit and would be undergoing *geodetic* not free precession.

Pulsar	B1828-11	B0740-28	J1713+0747	B0144+59	B0329+54
Ec. Long. (deg)	277.73303(4)	125.33	256.67	50.651904(4)	65.19
Ec. Lat. (deg)	12.24178(15)	-48.71	30.7	44.237818(5)	34.26
Gal. Long. (deg)	20.81	243.77	28.75	130.06	145
Gal. Lat. (deg)	-0.48	-2.44	25.22	-2.72	-1.22
Period (s) *	0.405043	0.166762	0.004570	0.196321	0.714520
$\dot{P}$ *	6.003×10^{-14}	1.682×10^{-14}	8.529×10^{-21}	2.568×10^{-16}	2.048×10^{-15}
DM (cm^{-3} pc)	161.50(20)	73.758(8)	15.9899(6)	40.111(3)	26.833(10)
RM (rad m^{-2})	47(5)	156(5)	—	19(5)	-63.7(4)
FWHM (ms)	3.2	5.4	0.218	7	6.6
S_{400} (mJy)	2.1	296(14)	36	6.6(0.5)	1500(200)
S_{1400} (mJy)	1.40(0.15)	15.0(1.5)	3	2.1(0.3)	203(57)
Distance (kpc)	3.58	1.89	1.12	1.91	1.06
L_{1400} (mJy kpc^2)	17.94	53.58	3.79	7.66	229.74
Est. Age (Myr)	0.107	0.157	8490	12.1	5.53
B_surf (GG)	4990	1690	0.2	227	1220
$\dot{E}$ (ergs/s)	3.6×10^{34}	1.4×10^{35}	3.5×10^{33}	1.3×10^{33}	2.2×10^{32}
v_trans (km/s)	—	262.31	34.03	—	98.22

Table 6.3: Statistics of pulsars in which precession may have been detected by this study compared to those of the sample set. (*St. Dev. — standard deviation,* $\dot{P}$ *— period derivative, DM — dispersion measure, FWHM — pulse full-width half-maximum,* S_{1400}/L_{1400} *— flux/luminosity at 1400 MHz,* B_{surf} *— surface magnetic field*). ⋆Excluding J1713+0747, which is not thought to be undergoing *free* precession. Data taken from the ATNF pulsar catalogue (Manchester et al. 2005).

Property	Median (st. dev.) of set of possible detections⋆	Median (st. dev.) of candidate set
Period (ms)	196 (253)	476 (598)
log(Period [s])	-0.707 (0.357)	-0.223 (0.523)
log($\dot{P}$)	-14.04 (0.91)	-14.60 (1.34)
log(DM [cm$^-$3] pc)	1.87 (0.48)	1.85 (0.50)
FWHM (ms)	5.4 (1.5)	10.6 (28.5)
log (FWHM [ms])	0.73 (0.13)	1.09 (0.44)
log (S_{1400} [mJy])	0.56 (0.88)	0.32 (0.47)
log (L_{1400} [mJy kpc^2])	1.73 (0.60)	1.37 (0.74)
log (Age [yr])	5.19 (0.99)	6.61 (1.10)
log (B_{surf} [G])	12.08 (0.49)	12.10 (0.86)
log ($\dot{E}$ [ergs/s])	34.6 (1.4)	32.7 (1.3)

precession should be damped on timescales of:

$$\tau_D \approx \frac{2\pi\tau_f}{P}, \tag{6.1}$$

for a damping time τ_D in precessional periods, period P in seconds and a crust-core coupling time of τ_f, also in seconds.

The uncertainty in this value is entirely down to the uncertainty in τ_f. This has been estimated as being anywhere from $\lesssim 10$ seconds (Abney et al. 1996) (based on the Vela Pulsar's 'Christmas' glitch), through $60P$ (Epstein & Baym 1992) to 400–10^4P (Alpar & Saulis 1988). All studies thus far give $\tau_f \gg P$, hence, to first order, we can assume that the crust remains uncoupled to the core, allowing the crust to precess freely without influence from the liquid interior (at least on short timescales).

Using these values, we can estimate a damping time for our pulsars. These are presented in Table 6.4. We can see that only in the uppermost limit of the values given in Alpar & Sauls is the damping period sufficiently long to allow precession

on timescales near the characteristic age. From this, we can draw one of four conclusions. Firstly, the estimated values of τ_f could be too low, the problem being that this would then not tie in with the observations — if anything the more modern values tend towards a lower value of τ_f; another possibility being that τ_f varies significantly between pulsars. Secondly, that damping occurs on much longer timescales or does not occur at all, for some reason such as a longer interval between crust-core coupling periods (glitches). In this case, why do we not see precession in all pulsars below a certain age? Perhaps if the period of precession was an order of magnitude or more shorter on average, this would damp out more quickly. A third possibility could be that some kick mechanism is present to excite precession, which raises the question of what this might be. It is also possible that free precession is present in many more pulsars, but at a level below our threshold sensitivity — this is a view substantiated by Cordes (1993) (also Cordes, *private communication*), who suggests that much of the timing noise observed in pulsars could be due to precessional effects too small to be detected in pulse shape changes. Finally, we must also suggest may not be detectable at all, and that what we have found is evidence of some other process.

6.3.2 Consistency with Models

Jones & Andersson (2001) formulate a free precession model against which we can test our observations. In this model, we expect that:

$$\epsilon_0 > \epsilon_{fluid} \tag{6.2}$$

must be true for the neutron star to be precessing, where ϵ_0 is the 'reference' or zero-strain oblateness and ϵ_{fluid} is the fluid oblateness. If this criterion does not hold, it implies that the crust has 'frozen' during a period where the star was spinning more slowly than present.

Table 6.4: Estimated damping times using Equation 6.1 from Link & Epstein (2001), for a variety of core-crust coupling times.

Pulsar	Fundamental Period (days)	Characteristic Age (kyr)	Damping Period (kyr)			
			Abney *et al.* (upper limit)	Epstein & Baym	Alpar & Sauls	
					Lower Limit	Upper Limit
B1828−11	1000	107	0.425	1.03	6.88	172
B0740-28	360	157	0.371	0.372	2.48	61.9
B0144+59	310	12100	0.271	0.320	2.13	53.3
B0329+54	380	5530	0.091	0.392	2.61	65.4
	1105		0.266	1.14	7.60	190

Table 6.5: Estimated oblatenesses from Jones & Andersson (2001), given a neutron star mass of 1.4 $M_\odot$ and radius of 10 km.

Pulsar	Observed Fundamental period (days)	Spin Period (seconds)	Effective Eccentricity ϵ_{eff} $\times 10^9$	Reference Oblateness ϵ_0 $\times 10^6$	Fluid Oblateness ϵ_{fluid} $\times 10^6$	$\frac{I_{SF}}{I_{star}}$ $\times 10^9$
B1828–11	1000	0.405	4.69	2.81	0.518	0.543
B0740–28	360	0.167	5.36	3.22	3.06	0.621
B0144+59	310	0.196	7.33	4.40	2.21	0.848
B0329+54	380	0.715	21.8	13.1	0.166	2.52
B0329+54	1105		74.8	4.49	0.166	0.866

In the limit where the superfluid interior pinned to the crust has zero moment of inertia, the reference oblateness can be calculated as follows (Jones & Andersson 2001, equation 69):

$$\epsilon_0 = 10^3 \epsilon_{eff} \frac{M_{1.4}}{R_6}, \tag{6.3}$$

where $M_{1.4}$ and R_6 are the mass and radius at 1.4 $M_\odot$ and 6 km, and ϵ_{eff} is the effective deformation, given by the ratio of the spin and precessional periods (their equation 67).

The fluid oblateness can be calculated using the pulsar's spin frequency (in the absence of precession) ω_0:

$$\epsilon_{fluid} = I\omega_0^2 \left(\frac{GM^2}{R}\right)^{-1}, \tag{6.4}$$

for total moment of inertia $I \approx \frac{2}{5}MR^2$, pulsar mass M and radius R (Lyne & Graham-Smith 1990).

In addition to the above, we can also find a limit to the fraction of the moment of inertia associated with any pinned superfluid I_{SF}/I_{star}, using the equation 71 from Jones & Andersson (2001) which states that, in the limit that $\epsilon_0 = 0$:

$$\frac{I_{SF}}{I_{star}} = 1.5 \times 10^{-2} \epsilon_{eff} \frac{R_6^4}{M_{1.4}^2}. \tag{6.5}$$

The ellipticity for our candidates, based on the above equations, are shown in Table 6.5. In all cases, Equation 6.2 is satisfied for masses of 1.4 $M_\odot$ and radii

of 10 km. Thus, if the model of Jones & Andersson (2001) is correct, all our positive candidates satisfy the criterion for free precession. It is worth noting that ϵ_0 scales linearly with mass and inversely with radius, whereas ϵ_{fluid} scales non-linearly with both mass and radius. If B0740–28 is of lower mass or larger radius than our estimate, Equation 6.2 may no longer hold.

6.4 Conclusion

In this thesis, we have produced a software package able to detect precession amongst pulsars. We have used this package on the Jodrell Bank pulse profile database and have confirmed precession in B1828–11 and put forward tentative evidence of precession in a number of other pulsars.

While there is no clear evidence that precession is certainly taking place in any of these, there is some evidence to suggest that B1828–11 is not the only pulsar we know of that is precessing. We suggest that precession has not previously been detected in other pulsars not because it is not present, but because it is too weak to be detectable in most cases.

6.5 Future Work

In this study, the focus has been on finding periodic shape changes in the pulsar profiles. However, the software developed for use in this project has uses beyond what could be accomplished in an MSc thesis. A better study of the timing residuals could be made, with particular attention being paid to the period derivative, $\dot{P}$. Changes in this parameter are not easily mimicked by artificial effects, such as matching templates to profiles. Of particular important are pulsars highlighted in this study, namely B0740–28, B0144+59, B0329+54 and B1830–08.

A more thorough investigation of links between timing residual changes and

profile shape changes should be made, focussing on correspondences between maxima and minima in each. Also of interest is whether any profile shape changes occur during glitches.

Other work could also be done using the Principal Component Analysis software developed here, focussed on aperiodic changes or more complex periodicities, which could result from complex or chaotic rotation in tri-axially asymmetric pulsars, which could, in turn, be linked to timing residuals as well.

As always, better data could be found from continual recording of high-resolution profiles from both today's instruments, and future instruments, such as the Square Kilometre Array (SKA), which should enable us to better determine whether or not precession is taking place, both in our candidates and in other pulsars.

Appendix A

Other Possible Detections

The pulsars contained in this section are those previously identified in Chapter 4 as having detections of shape changes that were considered 'significant'. However, upon further analysis, it is thought that the evidence there is for precession is either anomalous or inconclusive enough that support for their detection as precessing pulsars cannot be presented.

A.1 B1737–30

The main evidence for candidacy for precession for this pulsar has been the very strong 7214-day period found by phase-binned Lomb-Scargle analysis. Coincidentally enough, this is the exact same length as the length of the dataset used in the analysis. Compounding this with the fact that the periodicity found using P.C.A. is particularly low (71.4% chance of null detection), this strongly suggests that there is no strong variation at all. Examination of the timing residuals shows a long series of glitches (McKenna & Lyne (1990), Shemar & Lyne (1996b), D'Allesandro & McCulloch (1997), Krawczyk et al. (2003b), Urama (2002), *Jodrell Bank Observatory Pulsar Glitch Database (unpublished)*), meaning any periodicities are likely lost and that the mechanisms generating them may

well have been disturbed.

A.2 B1821–19

Pulsar B1821–19 shows a strong detection in both Lomb-Scargle and the power spectrum of its P.C.A. data, both at a period of around 5000 days. In addition to this, there is also a very clear 2300–2500 day periodicity in the timing residuals. The combination of these would normally make it an ideal candidate for precession. However, closer inspection of the Principal Component (first eigenvector) from the P.C.A. data shows a distinct difference between data before MJD 51000 and after. This is presumably due to the filterbank change that has also affected J1022+1001 and J1713+0747. Negating this abrupt change, the profile appears to be stable in the first eigenvector, and subsequent eigenvectors appear to consist only of noise. Taking this into account, we are forced to accept that, at best, our analysis of B1821–19 is incomplete due to changes in the filterbank, and that there is no evidence for precession in this pulsar.

A.3 B1933+16

Pulsar B1933+16 is the most intrinsically luminous pulsar in our dataset based on its DM distance and 1400 MHz flux density (Manchester et al. 2005). As such, this pulsar is covered extensively in both the Lovell/Mark II and 42-foot databases.

The strong periodicities to come from the phase-binned Lomb-Scargle results are at extremely long periods. There is insufficient resolution to fully test these periodicities in either a periodogram of the P.C.A. data or the 42-foot data, but on this timescale, even if they are real, there is no evidence that they are periodic.

A periodogram of our P.C.A. data does produce two weak peaks at 245 days

and 1100 days for the Lovell data, but both of these are below our imposed noise detection limit. There is little or no correlation between these peaks and the data obtained from the 42-foot data, which appears to be entirely aperiodic.

Statistically significant peaks are also seen in our phase-binned Lomb-Scargle analysis at periods of 5550, 4750, 144, 154 and 1280 days, but all of these fail to be picked up using P.C.A. The first two eigenvectors in the P.C.A. appear to be correlated, but periodicities on these levels do not appear to be present. The third eigenvector appears to represent a complex broadening term, and has a bimodal distribution in time around MJD 51000 as seen previously, suggesting this is due to the filterbank change that occurred at this time, which would explain the 4750 and 5500 day periods found.

The timing residuals for B1933+16 show a very triangular structure, with a possible 8000-day wave. Superimposed on top of this appears to be a wave with a period of just over 1000 days and an amplitude of half a millisecond, visible in both the Lovell/Mark II and 42-foot data.

While there do appear to be profile changes going on in B1933+16, there is insufficient evidence to find any periodicity in them. Were it to be found, from our data, we would expect it to be on a timescale of several years — either three or 20 years — but there is insufficient evidence to imply it exists now.

A.4 B1930+22

Pulsar B1930+22 is another young pulsar, with a characteristic age of only 40 kyr ((Manchester et al. 2005)). Our periodicity data for this pulsar are very similar to those of B0144+59: there is a single, very strong periodicity in both the phase-binned Lomb-Scargle results and the periodogram of the P.C.A. results; however, it is somewhat longer, less powerful, and less well constrained at 5310 and 4650 days, respectively, and the P.C.A. periodicity is only slightly above our

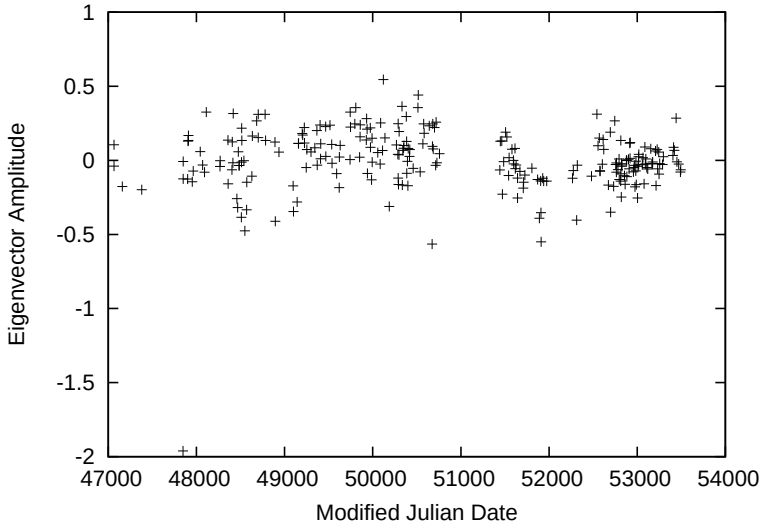

Figure A.1: The variation of the first (principal) component (eigenvector) from Principal Component Analysis over time for B1930+22, as in Figure 5.3 and other Figures. Lomb-Scargle analysis of this data shows a possible variation on a 5000-day timescale. A suggested peak is around MJD 50000.

imposed detection threshold.

It is possible that the trends are due to changes in instrumentation, particularly in the filterbank around MJD 51000, as has been seen in other pulsars. The data do seem to represent a more general trend apart from this — showing an increase from MJD 48000 to 51000, as can be seen in Figure A.1, but this may be due to changes in receiver setup as well, particularly the use of the multibeam receiver.

As usual, we must also consider the timing data from this pulsar, which shows a large aperiodic variation, with a major glitch at MJD 50264 ± 20 (Krawczyk et al. 2003b), followed by 2500 days of very noisy (possibly incoherent) timing ending with one or two glitches (*Jodrell Bank Observatory Pulsar Glitch Database (unpublished)*). There is, however, no evidence of any periodicities on a 5000-day timescale, although multiple periodicities do seem to be present on timescales of 150 to 400 days in more recent, coherently-timed data.

The data suggest that some shape changes may be ongoing in B1930+22.

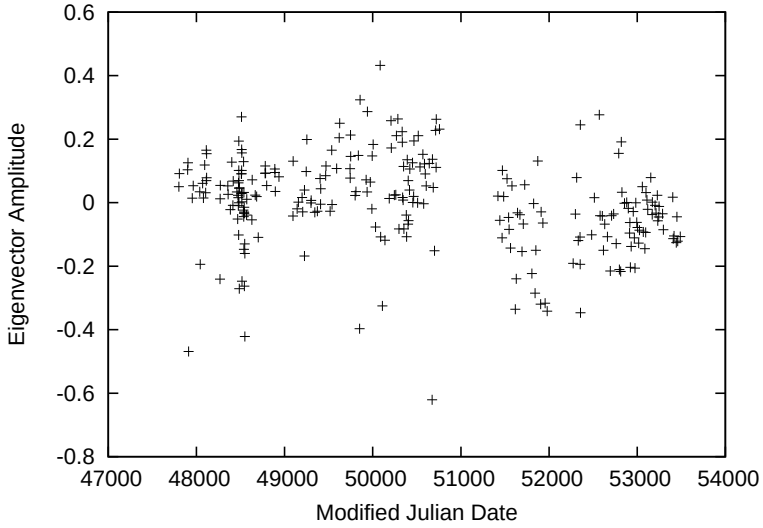

Figure A.2: The variation of the first (principal) component (eigenvector) from Principal Component Analysis over time for B1913+10, as in Figure 5.3 and other Figures. A possible variation is present on a 5000-day timescale, showing a peak around MJD 50000.

However, this variation is close to our detection limit in our P.C.A. and there is a good chance that they are entirely due to the changes in filterbanks. Without any evidence of corresponding timing variations, we suggest that it is unlikely that precession is occurring in B1930+22.

A.5 B1913+10

Pulsar B1913+10 is a fairly average pulsar, with a moderate period, inferred luminosity and DM (405 ms, 36.79 mJy kpc^2 at 1400MHz and 242 cm^{-3} pc, respectively — Manchester et al. 2005). Our shape tests yield very concordant periodicities: 5380 days for phase-binned Lomb-Scargle and 5350 days for our P.C.A. periodogram. Once again, the P.C.A. detection is only marginally above our threshold for noise. In fact, the eigenvector data for B1913+10 bears a striking resemblance to that of B1930+22, showing the broader peaks and troughs in identical places (see Figure A.2).

The timing residuals for B1913+10 show similar changes to B1930+22, showing changes in the rotation period on timescales of around 200 days, followed by long periods with no period change. These are also aperiodic, although they do exhibit more of a wave-like structure. Without any concordance between the shape-changing results and the timing residuals, we cannot support any evidence of precession in B1913+10.

A.6 B1859+03

Pulsar B1859+03 was labelled as significant due to its relatively strong periodicities of 5070 and 6340 days picked up by phase-binned Lomb-Scargle results at 'null probabilities' (see Chapter 4) of 4×10^{-9} and 5×10^{-8}, respectively — significantly lower than our cutoff of around 3×10^{-4}. However, this periodicity is not supported by our P.C.A. results, which show the data to be aperiodic to a 99.999% confidence level. The timing residuals show some evidence of periodicities on a 700-day timescale, but they are dominated by changes such as those seen in B1913+10 and B1930+22. Thus, we cannot support evidence for precession in this case.

A.7 B1834–10

Pulsar B1834–10 experiences a similar problem to B1859+03. A strong periodicity was found at 6540 days by our phase-binned Lomb-Scargle test, which is very close to the length of the dataset at 6583 days. Again, there is no periodicity in the P.C.A. results to a 97.7% confidence level. The timing solutions are very similar to those of B1859+03 in negative. Once again, there is no evidence to support precession.

A.8 B1742–30

Pulsar B1742–30 has an average period, DM and luminosity (367 ms, 88.4 cm^{-3} pc and 56.2 mJy kpc^2 at 1400 MHz, respectively). Its profile consists of two main components, the major one of which consists of at least two unresolved Gaussians (Seiradakis et al. 1995). Our Lomb-Scargle results appear to show a significant variation in the left-hand side of the major component at a period of 6355 days. Once again, this is the exact same period as the length of the dataset, suggesting this is a processing artifact.

The P.C.A. analysis shows a residual profile consisting entirely of noise for all of the first three eigenvectors. From this, we deduce that the profile is actually stable to changes over a timescale of years. The timing solution shows a familiar 'bump' in an otherwise smooth acceleration term, such as has been seen in B1859+03 and B1934–10. Interestingly, there seems to be no evidence for an underlying short-period wave within this data, as with other pulsars described here, with the smallest variation times appearing to be around 2000 days. Without consensus between the methods, and particularly with our main evidence being the 6355-day periodicity, we conclude that detectable precession is unlikely to be taking place here.

A.9 B0834+06

Pulsar B0834+06 was identified as significant due to its strong Lomb-Scargle periodicities at 5050 and 6050 days, which can be identified using both the phase-binning as occurring on the rise and fall of both of the components. Examination of the P.C.A. results show them to be aperiodic to a 99.93% confidence level. The same can be said of the timing data, which show remarkably low residuals, with a 870 μs r.m.s. value over 22 years. We therefore suggest that this periodicity is

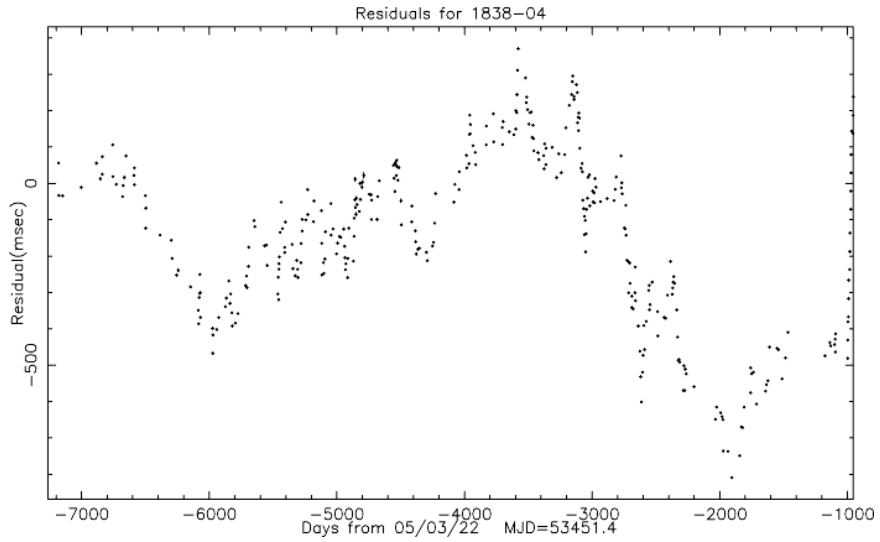

Figure A.3: Timing residuals observed for B1838–04. This data is for the only the time span before the sharp period changes. Possible periodicities of about 200 days can be seen around MJD 48000 and of around 400 days near MJD 50000.

due to a 'smoothing' term caused by differences in the temporal resolution (either through interpolation or smearing) between the old and new filterbanks.

A.10 B1838–04

Pulsar B1838–04 was picked up for the same reasons as B0834+06 with periodicities of 4800 and 5760 days in Lomb-Scargle. Our P.C.A. results are aperiodic to a 97.5% confidence level. The timing residuals, however, are far from stable, and show very noisy behaviour with two glitches at MJD 52000 and 53356 (*Jodrell Bank Observatory Pulsar Glitch Database (unpublished)*). This behaviour does show signs of being periodic, with 200-day and 400-day periodicities visible, as can be seen in Figure A.3. 40- and 50-day periodicities are present in the phase-binned Lomb-Scargle data, but these are below our significance threshold, so can probably be attributed to noise. In short, we do not find substantial enough evidence to support precession in this case.

A.11 B0919+06

Pulsar B0919+06 is a fairly close, moderately bright pulsar with a moderate period (1200 pc, 6.1 mJy kpc^2 at 1400 MHz and 431 ms, respectively), and was again picked up due to a strong Lomb-Scargle periodicity, in this case of 15000 days. While the P.C.A. data is again entirely aperiodic and all other periodicities are below the noise thresholds, the timing residuals show a strong periodicity of around 600 to 630 days at an amplitude of around 10 ms on top of a seemingly more random, long-period variation. This is a similar situation to B1642–03, which shows a variation in timing residuals, but no significant changes in profile shape. We conclude that this change is unlikely to be due to precession without evidence of shape changes and that the periodicity found by Lomb-Scargle is an artifact due to a period being fitted to a non-repeating trend.

A.12 B0525+21

Pulsar B0525+21 provides a similar situation to B0919+06, with an 11300-day and a 17000-day periodicity. Once again, the P.C.A. data is entirely aperiodic. The timing data is also quasi-stable, the only major features being two large glitches at MJD 42057 and 52298.2 (*Jodrell Bank Observatory Pulsar Glitch Database (unpublished)*). A 1600-day periodicity is possible, but it is only at a 3 ms level, which is only $\frac{1}{60}$ of the profile FWHM (Lorimer et al. 1995). Again, it is likely that the periodicities found are caused by over-extrapolation of data.

A.13 B1826–17

Pulsar B1826–17 shows periodicities in both the Lomb-Scargle and P.C.A. data, at 6308 days and 5778 days, respectively. Examination of the first eigenvector

evolution shows a trend similar to that observed in B1930+22 and B1913+10. The co-incidence of all of these results is likely to mean they are due to receiver changes, rather than changes in the actual pulsar. B1826–17 shows a triple-component profile and changes are observed over all three components, which would not necessarily be expected for precession — we would expect a transition more like that seen in J0631+1037.

The timing residuals for B1826–17 show a very distinct periodicity, with a period of between 1050 and 1100 days and an amplitude of around 10 ms. However, we find no link between this change and shape changes in the pulsar, so conclude that this pulsar belongs in the category of B1642–03 and B0919+06, and is not precessing, but is producing periodic timing irregularities.

A.14 B1822–09

Pulsar B1822–09 is a known moding pulsar (Fowler et al. 1981) and as such any periodicities we find are more likely to be periodicities in the moding than precession, due to the amplitude of the changes involved. Our phase-binned Lomb-Scargle analysis shows a strong periodicity at 6700 and at 16700 days, which we would normally attribute to over-extrapolation of data or filterbank changes. However, it is worth noting that the strong periodicity is not present in the main pulse, but in the interpulse region. Fowler et al. (1981) and Dyks et al. (2005) note that the interpulse region is involved in the mode switching, but comparative changes in the left-hand component of the main pulse (which plays the dominant rle in the mode-switching) are not seen. Given the broad range of possible precession periods (the periodicity is also strong between the 6700 and 16700 days) it could be that the interpulse region is slowly changing over a timescale of several years in a largely aperiodic fashion.

Analysis of the P.C.A. eigenvector variations show a very noisy structure,

with the first eigenvector connected to the left-hand component (and hence the mode-switching) and the other eigenvectors due to noise terms. A periodicity is found at 431 days, although it is has a 23% null probability and hence is well below our noise threshold of 3×10^{-4} null probability. Interestingly enough, a 434-day periodicity is also found in phase-binned Lomb-Scargle at the interpulse, although it is well below our noise threshold. In addition to this, as can be seen in Figure A.4, there appears to be a corresponding periodicity in the timing data. It seems to be present throughout the entire data at around the 5 ms level, but is most easily visible in the stable region around MJD 50200. This is obviously very small in comparison to the period of the pulsar (769 ms — Hobbs et al. 2004b) and even the FWHM of the profile (12 ms — Hobbs et al. 2004a) and could well be due to problems with matching a template to the pulse due to the changing profile.

Pulsar B1822–09 provides an interesting case where all our detection methods agree, although they are all below the expected detection thresholds. Compounding this with the moding known to be present in the pulsar, we must conclude there is insufficient evidence to determine whether precession is occurring or not. It seems more likely that these phenomenon are all related due to changes imposed upon the data in collection (whether through template matching, filterbank de-dispersion or otherwise) rather than real periodic changes.

A.15 J2043+2740

Pulsar J2043+2740 was also picked up due to its high periodicity in the phase-binned Lomb-Scargle data, with a 6520-day period at a null probability level of 1.5×10^{-6}. Other periodicities at 1086 and 2173 days were found near our detection limit. However, only 63 profiles passed the required frequency and signal-to-noise tests to warrant inclusion in our data.

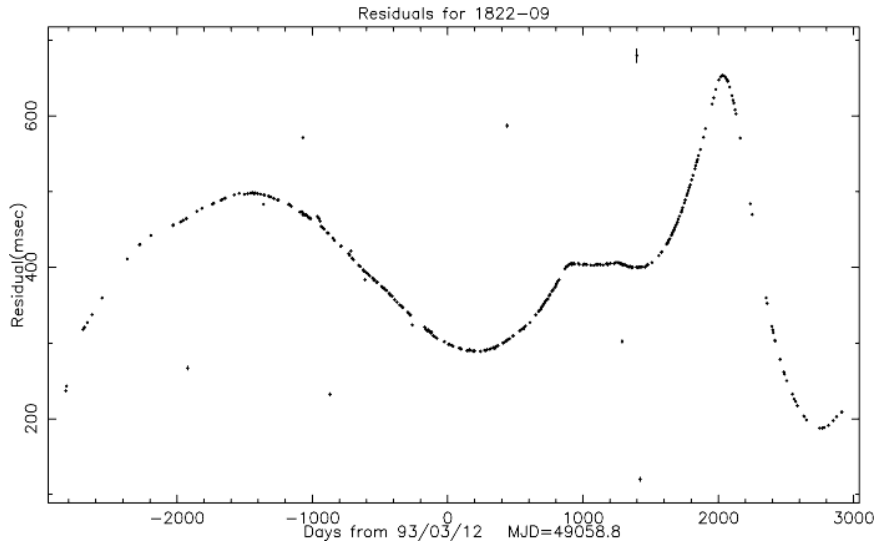

Figure A.4: Timing residuals observed for B1822–09. This data is for a subset of the data only. Possible periodicities of about 430 days can be seen, most clearly around MJD 50200.

Examination of our P.C.A. data shows a consistent change in the first eigenvector, which represents a widening of the pulse peak, around MJD 53000. This is well away from any major filterbank changes. A corresponding change in the pulse period can also be ascertained from the timing residuals. There do not, however, appear to be any periodic changes in either of these, so we suggest that, while shape changes could well be taking place, it seems unlikely that they are connected with precession.

A.16 B1620–26

Pulsar B1620–26 is another case of periodicity being picked up at the length of the dataset (in this case 5594 days). A further 2000-day periodicity found in the P.C.A. tests at a 29% null probability level is most likely a combination of noise, intermittent sampling, poor phase sampling (this is a millisecond pulsar) and filterbank changes. A 4000-day periodicity may exist in the timing residuals with a 5 ms amplitude, but there is insufficient data to determine whether its is

a true periodicity or just a quasi-periodic variation.

A.17 B1756–22

The case of B1756–22 is similar to that of B1620–26, although here the periodicity is slightly shorter than the observations at 5077 days. The P.C.A. eigenvector data appears entirely aperiodic, yet the timing residuals also show a 2400-day periodicity at 20 ms amplitude. Shorter periods may also be visible in the timing data on periods of around 200 days, but neither periodicity appears to manifest itself in changes in the pulsars shape.

A.18 B1931+24

Pulsar B1931+24 is one of the "new class" of pulsars, showing distinct 'on' and 'off' periods. For the purposes of our study, it appears to exhibit much the same effects as B1822–09. It shows a reasonably long-period variability in the anti-pulse region (opposite the main pulse) in the phase-binned Lomb-Scargle analysis (920 days), which is probably due to coherent noise. It shows very little evidence of periodicity in the P.C.A. results (99.92% null probability) and the timing results vary widely in an aperiodic fashion. We do not find any apparent periodicities in the data, and suggest that the periodicity found by Lomb-Scargle is unlikely to be real, especially given there is nothing in the timing residuals to back it up.

A.19 B1929+10

Pulsar B1929+10 has also been noted due to a long-period result from our Lomb-Scargle analysis. Significant peaks at 8450 and 11270 days were found corresponding to changes near the pulse peak, which consists of two partially-resolved

components. Our P.C.A. shows no evidence for any substantial periodicities, nor does the timing data, which only shows smooth changes in period over timescales of years. This pulsar is also covered by the 42-foot telescope, which failed to find any significant periodicity in any of the 1000-day segments, with the exception of one (at 979 days), which can be put down to an artifact due to a finite dataset. We therefore discount this pulsar from our list of candidates as well.

A.20 J1835–1031

Pulsar J1835–1031 has a small data sample compared to the other pulsars in this study: only 53 profiles were included in our dataset, over a period of 1935.5 days. Coincidentally enough, the strong periodicities found by our Lomb-Scargle analysis are at 1935 and 968 days, so we can immediately discount those as being irrelevant. A significant 2077-day periodicity found in our P.C.A. tests is also likely to be due to a combination of this and changes in the filterbank, which occurred shortly after the first observations in our data. The timing solution is very stable, with only a 365-day period present (presumably due to the inaccuracy of the pulsar's position, required for timing data).

A.21 B0621–04

Pulsar B0621–04 shows similar effects to J1835–1031, exhibiting a strong periodicity at 11200 days — twice the length of the observation set. A further significant periodicity is found at 3200 days and a weaker one at 1600 days, but these are very close to the main peak of the pulsar, which shows a complex pulse, and are likely due to errors in the cross-correlation process, which manifests itself as spikes in the first eigenvector evolution plot. The P.C.A. shows no periodicities of any significance whatsoever, and the timing solution is extremely stable to within

a millisecond, hence we can safely remove this object from our candidate list also.

A.22 B1133+16

Pulsar B1133+16 is a long-period pulsar (1.188 s — Hobbs et al. 2004b). It is also very bright: not because it is luminous, but because it is so close to us, only 360 pc away (Manchester et al. 2005). As a result of this brightness, it is observed not only by the Lovell and Mark II telescopes, but by the 42-foot telescope as well. This gives us two independent datasets with which to work.

Four 'significant' periodicities were found from the Lovell(/Mark II) data using our Lomb-Scargle tests, at periodicities of 56.5, 3776, 68.7 and 128 days and null probabilities of between 8.3×10^{-6} and 4.3×10^{-5} (c.f. our imposed cutoff at 3.2×10^{-4}). There is no significant result observed for our P.C.A. data, but, judging from our Monte Carlo tests described in Chapter 4, periodicities at this power should be found by our phase-binned Lomb-Scargle test and not by our P.C.A. test.

Examining our 42-foot data, we find the same thing — strong periodicities using Lomb-Scargle, but none using P.C.A. above a 20% null probability level (the value is almost certainly attributable to noise because if its period anyway). Several strong periodicities were found here: a periodicity between 350 and 380 days was visible in three of the seven 1000-day segments; a possible sub-harmonic 726-day periodicity was also found, as well as a $\frac{3}{2}$ resonance at 571 days; further periodicities were also found at 46.5 days, 59.2 days, 68.4 days, 77.8 days, 86.3 days, 97.2 days, 129.6 days and 145.9 days, all of which were found between MJD 41000 and 42999, with the exception of the 46.5 day periodicity, found from MJD 43000 onwards. It would seem sensible that some of these periodicities are (sub-)harmonics of each other. It is also interesting to note that there are particularly close matches for a 68.5 day and 129 day periodicity between the two datasets,

as well as a possible 56–59 day periodicity.

Looking at the timing data for both the Lovell and 42-foot observations, there is no evidence of any periodicity in the residuals. The Lovell data show no departures from a noise pattern in the short term and only a possibly periodic 7000-day variation in the long term. The 42-foot data provides more frequent observations and does not show any periodic variation above a millisecond (with noise r.m.s. of around 800 μs).

While it seems possible that shape changes may be occurring, without corresponding P.C.A. data, we cannot tell exactly what the profile changes represent. Phase-binning on our Lomb-Scargle data shows that they involve the main peak, but no more information is obtainable. With very good timing observations that show no sign of periodic variation on timescales close to those observed in the possible shape changes. Therefore, we must conclude that, even if the profile shape is changing periodically, we cannot support a case for precession taking place in B1133+16.

A.23 B0818–13

Pulsar B0818–13 is another long-period pulsar (1.238 s — Hobbs et al. 2004b). Strong periodicities were found by our Lomb-Scargle routine at 15130 days. Regrettably, this is exactly twice the length of the dataset and no similar periodicities were detected using P.C.A. We once again put forward that this is a processing error and that precession is not taking place. The timing residuals confirm this, showing a possible 4000- to 4500-day periodicity at an amplitude of only around 2 ms, but no evidence of anything on either longer or shorter periods.

A.24 B2255+58

Pulsar B2255+58 appears to be another false detection. The profile consists of two equal-intensity, partially-resolved components. Moderate, but significant periodicities were found at 8481 and 3635 days in the region between the two components. No evidence for any variation can be found in either the P.C.A. data, which appears to be noisy and contains several spikes from poorly-matching profiles, nor the timing residuals, which appear constant on the millisecond level, apart from the occasional small change in period. We therefore conclude that it is unlikely that precession is occurring in this pulsar.

A.25 B2053+21

Moderately strong periodicities have been found for B2053+21 in our phase-binned Lomb-Scargle data at periods of 619, 8454, 85.7 and 259 days. The 86-day period is almost certainly due to noise as it is found in a blank region of the profile. The 259- and 619-day periods are found at the anti-pulse region of the profile (i.e. the region of a possible interpulse, opposite the main pulse), yet no interpulse appears to exist. The 8454-day period represents a 'smoothing' term and is likely connected with the change in filterbanks. The P.C.A. data is entirely aperiodic and the timing residuals show no periodicity and are constant over the last 10 years to a level of around 500 μs. Therefore, we suggest that this result is due mostly to noise and that precession is not taking place.

A.26 B1732–07

Pulsar B1732–07 also records moderately strong periodicities from phased-binned Lomb-Scargle tests at 122, 82.2, 224 and 54.8 days. These results are not reproduced by our P.C.A. tests, which show no periodicities present. The timing residuals show a seemingly aperiodic long-term variation with an amplitude of a few milliseconds. Limits of a millisecond can easily be placed on finding further periodicities in the data. Thus, we cannot support precession in this case either.

A.27 B2020+28

Pulsar B2020+28 was labelled as significant due to moderately strong periodicities found at three phases, all at a period of 10000 days, backed up by a weak 8600-day periodicity in the P.C.A. data. Closer examination of the latter found that this is again likely to be due to filterbank changes. Comparison with the timing residuals shows no evidence for a period of anywhere near this length. Hence, we claim that precession has not been detected in this pulsar.

A.28 B2045–16

The case of B2045–16 shows a similar situation to B2020+28. Here, a 3774-day periodicity was found by Lomb-Scargle, along with further short periodicities which are almost certainly noise. A periodogram of our P.C.A. data shows no periodicities present and while timing residuals do show very weak evidence for a complex 4000-day periodicity, it is deemed unlikely that precession is taking place here.

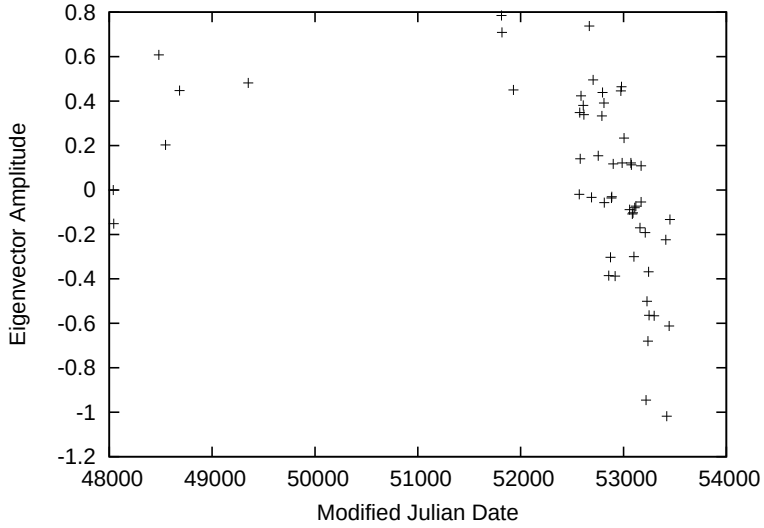

Figure A.5: The variation of the first (principal) component (eigenvector) from Principal Component Analysis over time for B2035+36, as in Figure 5.3 and other Figures. A clear decrease in the amplitude of the eigenvector can be seen from the start of the major part of our data (around MJD 52500) onwards.

A.29 B2035+36

Pulsar B2035+36 is interesting in that it supports a weak 3100-day periodicity in our phase-binned Lomb-Scargle results and also a 3200-day periodicity in a periodogram of our P.C.A. results. While this is not borne out in the timing residuals (they show apparently random fluctuations), we do have some evidence for changes taking place.

Figure A.5 shows the evolution of the first eigenvector from our P.C.A. analysis. While this does not support any periodicity, it does appear to be changing on a gradual basis, which is not in line with any likely variations imposed by filterbanks. The eigenvector itself seems to represent a 'spreading' or 'blurring' in the profile. Closer analysis of our phase-binned Lomb-Scargle results show that the periodicities found are spread out widely in frequency space, suggesting low-frequency noise on the timescale of years, although as can be seen from Figure A.5, there is little data before MJD 52500. This suggests that, at least from MJD

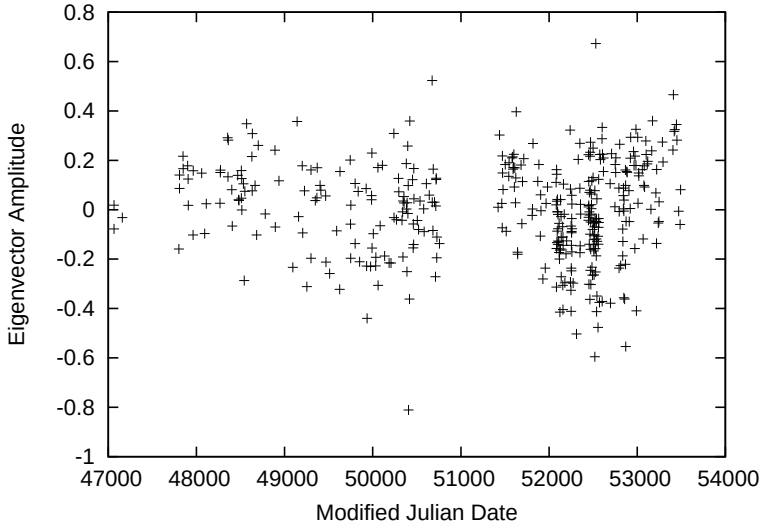

Figure A.6: The variation of the first (principal) component (eigenvector) from Principal Component Analysis over time for B0355+54, as in Figure 5.3 and other Figures. Lomb-Scargle analysis produces a 2460-day periodicity. We suggest peaks are present around MJD 48500, 51000 and 53500.

52500 onwards, a gradual, yet distinct change in profile shape has been taking place. While this does not appear to be connected to precession, it nevertheless seems likely to be a real change.

A.30 B0355+54

Our final case is that of B0355+54, which has been noted here not because of its phase-binned Lomb-Scargle results, but from its P.C.A. data, which show a moderate periodicity at 2460 days. Our Lomb-Scargle results also pick out this periodicity, but it is very weak and below our threshold; however, it does appear to be periodic over the entire pulse region. A further, slightly stronger periodicity was determined by Lomb-Scargle at 310 days on the right side of the leftmost of the two partially-resolved components of the pulse.

Figure A.6 shows the evolution of the first eigenvector of our P.C.A. over time, with the 2460-day periodicity apparently present, though not easily visible to the

eye. With this periodicity confirmed exactly by Lomb-Scargle, if rather weakly (at a null probability of 5.3×10^{-4}, compared to our 3×10^{-4} noise threshold), we conclude that shape changes may well be occurring in the profile of B0355+54 on a timescale of 2460 days.

Unfortunately, this is not borne out by the timing residuals, which show a smoothly varying structure with no periodicities visible to the eye. A full analysis would be required to determine whether any periodicity exists on this timescale in the timing data at all, but we can probably conclude that although periodic shape changes are possibly taking place (this is a known moding pulsar (Rankin 1986)), they are unlikely to be associatable with precession without a more rigorous study of the timing data.

References

Abney M., Epstein R. I., Olinto A. V., 1996, Ap. J. Lett., 466, L91+

Alpar M. A., Saulis J. A., 1988, Ap. J., 327, 723

Baade W., Zwicky F., 1934, Proc. Natl. Acad. Sci., USA, 20, 254

Backer D. C., 1970, Nature, 228, 42

Bailes M., Lyne A. G., Shemar S. L., 1993, in ASP Conf. Ser. 36: Planets Around Pulsars. p. 19

Barker B. M., O'Connell R. F., 1975, Phys. Rev. D, 12, 329

Bertotti B., Carr B. J., Rees M. J., 1983, Mon. Not. R. Astron. Soc., 203, 945

Blaskiewicz M., 1991, PhD thesis, Cornell University

Boerner G., Ehlers J., Rudolph E., 1975, Astron. & Astroid., 44, 417

Brecher K., 1975, Nature, 257, 203

Burrows A., Lattimer J. M., 1986, Ap. J., 307, 178

Camilo F., Nice D. J., Shrauner J. A., Taylor J. H., 1996, Ap. J., 469, 819

Cordes J. M., Helfand D. J., 1980, Ap. J., 239, 640

Cordes J. M., 1993, in ASP Conf. Ser. 36: Planets Around Pulsars. p. 43

Cutler C., Ushomirsky G., Link B., 2003, Ap. J., 588, 975

D'Allesandro F., McCulloch P. M., 1997, Mon. Not. R. Astron. Sob., 292, 879

Davis M. M., Taylor J. H., Weisberg J. M., Backer D. C., 1985, Nature, 315, 547

Demianski M., Proszynski M., 1979, Nature, 282, 383

Durney B. R., Faulkner J., Gribbin J. R., Roxburgh I. W., 1968, Nature, 219, 20

Dyks J., Zhang B., Gil J., 2005, Ap. J. Lett., 626, L45

Epstein R. I., Baym G., 1992, Ap. J., 387, 276

Fowler L. A., Morris D., Wright G. A. E., 1981, Astron. & Astroid., 93, 54

Giacconi R., Gursky H., Paolini F. R., Rossi B. B., 1962, Phys. Rev. Lett., 9, 439

Gil J. A., Kijak J., Seiradakis J. H., 1993, Astron. & Astroph., 272, 286

Gold T., 1968, Nature, 218, 731

Gould D. M., Lyne A. G., 1998, Mon. Not. R. Astron. Sob., 301, 235

Gullahorn G. E., Rankin J. M., 1982, Ap. J., 260, 520

Hayakawa S., Matsouka M., 1964, Prog. Theor. Phys. Suppl., 30, 204

Helfand D. J., Manchester R. N., Taylor J. H., 1975, Ap. J., 198, 661

Helfand D. J., Taylor J. H., Backus P. R., Cordes J. M., 1980, Ap. J., 237, 206

Hesse K. H., Wielebinski R., 1974, Astron. & Astroph., 31, 409

Hewish A., Bell S. J., Pilkington J. D., Scott P. F., Collins R. A., 1968, Nature, 217, 709

Hills J. G., 1983, Ap. J., 267, 322

Hobbs G. et al., 2004, Mon. Not. R. Astron. Sob., 352, 1439

Hobbs G., Lyne A. G., Kramer M., Martin C. E., Jordan C. A., 2004b, Mon. Not. R. Astron. Sob., 353, 1311

Hobbs G., 2002, PhD thesis, Jodrell Bank Observatory, University of Manchester

Hobbs G., in ANITA Gravity 2004

Hotan A. W., Bailes M., Ord S. M., 2004, Mon. Not. R. Astron. Sob., 355, 941

Jones D. I., Andersson N., 2001, Mon. Not. R. Astron. Sob., 324, 811

Kaspi V. M., Taylor J. H., Ryba M. F., 1994, Ap. J., 428, 713

Kaspi V. M., 1995, in IAU Symp. 166: Astronomical and Astrophysical Objectives of Sub-Milliarcsecond Optical Astrometry. p. 163

Konacki M., Lewandowski W., Wolszczan A., Doroshenko O., Kramer M., 1999, Ap. J. Lett., 519, L81

Kramer M. et al., 1999, Ap. J., 520, 324

Kramer M., 1994, Astron. & Astroid. Supple., 107, 527

Krawczyk A., Lyne A. G., Gil J. A., Joshi B. C., 2003a, Mon. Not. R. Astron. Soc., 340, 1087

Krawczyk A., Lyne A. G., Gil J. A., Joshi B. C., 2003, Mon. Not. R. Astron. Sob., 340, 1087

Large M. I., Vaughan A. F., Mills B. Y., 1968, Nature, 220, 340

Lawrence G. M., Ostriker J. P., Hesser J. E., 1967, Astron. Jour., 72, 81

Link B., Epstein R. I., 2001, Ap. J., 556, 392

Lorimer D., Kramer M., 2004, Handbook of Pulsar Astronomy. Cambridge University Press

Lorimer D. R., Yates J. A., Lyne A. G., Gould D. M., 1995, Mon. Not. R. Astron. Sob., 273, 411

Lorimer D. R. et al., 1998, Astron. & Astroid. Supple., 128, 541

Lyne A. G., Graham-Smith F., 1990, Pulsar Astronomy. Cambridge University

Press

Lyne A. G., Manchester R. N., 1988, Mon. Not. R. Astron. Sob., 234, 477

Manchester R. N., Hobbs G. B., Teoh A., Hobbs M., 2005, Astron. Jour., 129, 1993

McKenna J., Lyne A. G., 1990, Nature, 343, 349

Melrose D. B., 1979, Australian Journal of Physics, 32, 61

Melzer D. W., Thorne K. S., 1966, Ap. J., 145, 514

Mitra D., Rankin J. M., 2002, Ap. J., 577, 322

Oppenheimer J., Volkoff G. M., 1939, Phys. Rev., 55, 374

Ostriker J. P., Tassoul J. L., 1968, Nature, 219, 577

Pacini F., 1968, Nature, 219, 145

Pasachoff J., 1977, Contemporary Astronomy. Saunders

Phillips J. A., Wolszczan A., 1992, Ap. J., 385, 273

Press W. H., Teukolsky S. A., Vetterling W. T., Flannery B. P., 1992, Numerical recipes in FORTRAN. The art of scientific computing. Cambridge: University Press, —c1992, 2nd ed.

Qiao G. J., Xue Y. Q., Xu R. X., Wang H. G., Xiao B. W., 2003, Astron. & Astroid., 407, L25

Radhakrishnan V., Cooke D. J., 1969, Astrophys. Lett., 3, 225

Radhakrishnan V., Manchester R. N., 1969, Nature, 222, 228

Ramachandran R., Kramer M., 2003, Astron. & Astroid., 407, 1085

Rankin J. M., 1983, Ap. J., 274, 333

Rankin J. M., 1983, Ap. J., 274, 359

Rankin J. M., 1986, Ap. J., 301, 901

Rankin J. M., 1993, Ap. J., 405, 285

Rasio F. A., Nicholson P. D., Shapiro S. L., Teukolsy S. A., 1992, Nature, 355, 325

Reichley P. E., Downs G. S., 1969, Nature, 222, 229

Rezania V., 2003, Astron. & Astroid., 399, 653

Rezania V., 2003, Astron. & Astroid., 399, 659

Ritchings R. T., 1976, Mon. Not. R. Astron. Soc., 176, 249

Schilling G., 1996, Science., 273, 429

Sedrakian A., Wasserman I., Cordes J. M., 1999a, Ap. J., 524, 341

Sedrakian A., Wasserman I., Cordes J. M., 1999, Ap. J., 524, 341

Seiradakis J. H., Gil J. A., Graham D. A., Jessner A., Kramer M., Malofeev V. M., Sieber W., Wielebinski R., 1995, Astron. & Astroid. Supple., 111, 205

Shabanova T. V., Urama J. O., 2000, in ASP Conf. Ser. 202: IAU Colloq. 177: Pulsar Astronomy - 2000 and Beyond. p. 99

Shabanova T. V., Lyne A. G., Urama J. O., 2001, Ap. J., 552, 321

Shabanova T. V., 1995, Ap. J., 453, 779

Shaham J., 1977, Ap. J., 214, 251

Shemar S. L., Lyne A. G., 1996, Mon. Not. R. Astron. Sob., 282, 677

Shemar S. L., Lyne A. G., 1996, Mon. Not. R. Astron. Sob., 282, 677

Splaver E. M., Nice D. J., Stairs I. H., Lommen A. N., Backer D. C., 2005, Ap. J., 620, 405

Staelin D. H., Reifenstein E. C., 1968, Science, 162, 1481

Stairs I. H., Thorsett S. E., Camilo F., 1999, Astrophys. J. Suppl., 123, 627

Stairs I. H., Lyne A. G., Shemar S. L., 2000, Nature, 406, 484

Stairs I. H., 2003, Living Reviews in Relativity, 6, 5

Taylor J. H., Cordes J. M., 1993, Ap. J., 411, 674

Taylor J. H., 1992, Philosophical Transactions of the Royal Society of London, 341, 117-134 (1992), 341, 117

Tkachenko K., 1966, Sov. Phys. JEPT, 23, 1049

Urama J. O., 2002, Mon. Not. R. Astron. Sob., 330, 58

von Hoensbroech A., Xilouris K. M., 1997, Astron. & Astroid. Supple., 126, 121

von Hoensbroech A., Kijak J., Krawczyk A., 1998, Astron. & Astroid., 334, 571

Wasserman I., 2003, Mon. Not. R. Astron. Sob., 341, 1020

Weisberg J. M., Taylor J. H., 1984, Phys. Rev. Lett., 52, 1348

Wolszczan A., Frail D. A., 1992, Nature, 355, 145

Wolszczan A., 1994, Science, 264, 538

Zel'dovich Y. B., Guseynov O. K., 1964, Ap. J., 144, 840